POWER EFFICIENCY AND DIVERSITY ISSUES FOR PEAK POWER CONSTRAINED WIRELESS COMMUNICATIONS

A Thesis
Presented to
The Academic Faculty

by

Qijia Liu

In Partial Fulfillment
of the Requirements for the Degree
Doctor of Philosophy in the
School of Electrical and Computer Engineering

Georgia Institute of Technology
August 2010

POWER EFFICIENCY AND DIVERSITY ISSUES FOR PEAK POWER CONSTRAINED WIRELESS COMMUNICATIONS

Approved by:

Professor G. Tong Zhou, Advisor
School of Electrical and Computer Engineering
Georgia Institute of Technology

Professor Ye (Geoffrey) Li
School of Electrical and Computer Engineering
Georgia Institute of Technology

Professor Robert D. Foley
School of Industrial & Systems Engineering
Georgia Institute of Technology

Professor Xiaoli Ma
School of Electrical and Computer Engineering
Georgia Institute of Technology

Professor James Stevenson Kenney
School of Electrical and Computer Engineering
Georgia Institute of Technology

Date Approved: April 22, 2010

To my wife,

Siyang Peng,

the one better than I deserve.

ACKNOWLEDGEMENTS

I would like to express my sincere gratitude to my advisor, Dr. G. Tong Zhou, for offering me the opportunity to pursue my Ph.D. degree at Georgia Tech and shedding light on my path to any success. What I have learned from her is by no means limited to research techniques, but rather the zeal and high standards she has always demanded of herself.

I would like to thank my dissertation committee members, Professor Robert D. Foley, Professor James Stevenson Kenney, Professor Ye (Geoffrey) Li, and Professor Xiaoli Ma for taking the time to serve on my committee and for their helpful suggestions.

In particular, I would like to thank Dr. Xiaoli Ma for her support and close guidance throughout my Ph.D. study. Her tireless creativity and encouragement engined every collaboration we had. She is the ultimate tiger in my heart.

My sincere thanks also go to my group members, Dr. Robert J. Baxley, Dr. Chunming Zhao, Dr. Kun Shi, Dr. Wei Zhang, Dr. Thao Tran, Dr. Sungeun Lee, Vince A. Emanuele II, Benjamin R. Hamilton, Giwan Choi, Marie Shinotsuka, Jiaxi Xiao, Hayang Kim, Qi Zhou, and Jiaming Chen, for not only the insightful discussions, but, more importantly, their friendship.

Finally, I would like to express my deepest gratitude to my family. I would like to thank my grandma and my parents for their unconditional and eternal love. Without their unreserved support, all would not have been possible. Their encouragement is always with me and has given me the strength to complete this work.

A special appreciation to my wonderful wife, Siyang Peng, who enlightened every step in my life. Along with her, every day is full of joy and happiness.

TABLE OF CONTENTS

LIST OF TABLES

LIST OF FIGURES

SUMMARY

Along with the rapidly increasing demand for high data rate communications, orthogonal frequency division multiplexing (OFDM) has become a popular modulation in current and future communication standards. By distributing a high-speed data stream to many parallel low-rate data streams, OFDM is able to mitigate the detrimental effects of multipath fading using simple one-tap equalizers and achieve high spectral efficiency. However, the OFDM signal waveform suffers from large envelop variations, which are usually measured by the peak-to-average power ratio (PAR). In wireless transmitters, many RF components, especially the power amplifiers, are inherently nonlinear and peak power constrained. Therefore, low power efficiency and/or severe nonlinear distortions are the main shortcomings of OFDM systems.

In this dissertation, we develop algorithms and analyze performance bounds for peak power constrained wireless communications. To address the balance between power efficiency and nonlinear distortions, we model the peak power constrained OFDM systems in both statistical and deterministic manners. We first propose an error vector magnitude (EVM) optimization algorithm to strictly satisfy the distortion requirements in accordance with communication standards and provide the maximum power efficiency for OFDM transmitters without receiver-side cooperations. Moreover, we develop a multi-channel partial transmit sequence (MCPTS) PAR reduction method for OFDM-based frequency-division multiple access (OFDM-FDMA) multiuser systems, which can achieve significant power efficiency improvement without using side information. Joint MCPTS and power allocation schemes are also proposed to improve the error performance of OFDM-FDMA systems.

Furthermore, diversity-enabled communication systems have practical merits in combating channel fadings. Therefore, in the second part of this dissertation, peak power constrained diversity techniques are proposed. The error performance of peak power constrained single-input multiple-output (SIMO) OFDM is studied. Several low-complexity SIMO-OFDM transceiver designs are presented to collect full antenna diversity with respective performance and complexity tradeoffs.

The next major piece of work in this dissertation addresses the design of peak power constrained amplify-and-forward (AF) cooperative networks, which enable the cooperative diversity with single-antenna terminals. The effects of the availability of channel state information and the peak power constraint on the diversity performance are theoretically studied. Design criteria for general diversity-enabled AF relaying strategies are established and further applied to the designs in peak power constrained networks. In the end, a general theorem that relates the diversity gain function with the probability density function of instantaneous signal-to-noise ratio is derived and used to analyze the diversity performance of relay selection schemes.

CHAPTER I

INTRODUCTION

1.1 Motivations

Since Guglielmo Marconi conducted the first successful transatlantic experimental radio communication in 1901, wireless communications have quickly and comprehensively pervaded our daily life. Especially in the last two decades when information has become ubiquitously critical to individual and social development, wireless communications have become an indispensable technology that can provide easily accessible information, overcome geographic spans, and even save lives in disasters. Only in ancient movies could contemporary people imagine the life without communication technologies. Furthermore, consumers' rapidly growing demands for high data rates, high quality, and high mobility services are consistently pushing forward the development of future wireless communication systems. To cope with these diverse challenges, there have been tremendous efforts devoted to wireless technology innovations, for example, orthogonal frequency division multiplexing (OFDM), multi-antenna multi-input multi-output (MIMO), and multi-user code division multiple access (CDMA) systems.

The system performance of wireless communications, however, is inevitably confined by the intrinsic imperfections of radio frequency (RF) front-ends [91]. A wireless technique designed under the assumption of ideal and linear RF components may lose its projected merits in a practical system. Therefore, it is essential to analyze the effects of RF imperfections on transmission performance and design wireless communication systems to specifically address these practical issues. This problem is particularly critical for multi-carrier systems, e.g., the OFDM systems. The OFDM

modulation has been adopted by various modern communication standards and is a promising technique for future cellular systems because of its high spectral efficiency and low complexity in combating frequency-selective fading channels [1, 2, 3, 4, 28]. However, one of the primary disadvantages of OFDM is that the time-domain OFDM signals exhibit a large dynamic range, which is usually characterized by the peak-to-average power ratio (PAR) [35, 97, 100]. As a result, the performance of OFDM systems is liable to be affected by the RF imperfections and worth special attention [20].

For band-limited communication systems, RF imperfections may seriously deteriorate the error performance, arouse the inter-channel interference (ICI), and limit the power efficiency of wireless transceivers. For example, in-band distortions result from nonlinear RF characteristics and directly degrade the error performance [100]. To quantify and limit the amount of in-band distortions that occur at the transmitter, measurements are defined in communication standards, e.g., the error vector magnitude (EVM) for OFDM signals in the IEEE 802.16e standard [3]. The out-of-band spectral growth is another effect of nonlinear distortions [100]. It increases the ICI, which is detrimental to the reliable transmissions of other users. Communication standards always specify a spectral mask requirement to constrain the out-of-band power spectrum of the transmitted signals [2, 3]. In addition, distortions caused by RF imperfections may also affect the synchronization and channel estimation performance.

Typically, RF components have greater imperfections when they are working in a high power region [91]. Thus, to manage the nonlinear distortions to stay within the limits specified in communication standards, a common mechanism is to significantly back off (i.e., scale down) the signal power. The cost is a reduced efficiency of the RF-to-DC power conversion, which greatly wastes energy, limits capacity, and shortens the duration of single-charged mobile devices. Therefore, for modern communication

systems, power efficiency and nonlinear distortions are conflicting metrics that must be balanced.

It is important to acknowledge the existence of RF imperfections and design digital signal processing algorithms to suppress the negative impacts of RF imperfections on system performance. Extensive research has been conducted to compensate the imperfections, for instance, the digital predistortion (DPD) methods for reducing the RF nonlinearities and memory effects [7, 23, 51, 109], the compensations of the IQ imbalance and carrier phase offsets [98, 103, 113], etc.

Although some of the RF imperfections can be well moderated by using signal processing techniques and improving RF design and manufacturing skills, the peak power constraint is an intrinsic nonlinear characteristic that cannot be overcome. Many RF/analog components in the transmission chain are peak power constrained (PPC) devices, for instance, digital-to-analog converters (DACs), mixers, and particularly power amplifiers (PAs). In addition, the DC power consumption of PAs, which makes up of a large proportion of the total power consumption at transmitters, is generally determined by the peak power constraint. Thus, consideration of the peak power constraint is fundamental with respect to the balance between power efficiency and nonlinear distortions. Therefore, our research on PPC wireless communications is well motivated.

1.2 Objectives

In this dissertation, we focus on analyzing and designing power-efficient PPC wireless communication systems.

OFDM systems will be our major subject, for which the reduction of the dynamic range is essential for realizing a good trade-off between power efficiency and nonlinear distortions. Various algorithms have been proposed to achieve this goal

[35, 40], including the coding [24, 54], clipping and filtering [10, 12, 77], partial transmit sequence (PTS) [11], selected mapping (SLM) [13, 73], active constellation extension [44], tone reservation [100], and waveform optimization methods [6]. They can achieve respective tradeoffs among different metrics, including power efficiency, bandwidth efficiency, and nonlinear distortions. However, a few limitations remain among the existing methods. For instance, they generally cannot avoid large peak power spikes, which result in uncontrolled distortions. Additionally, receiver-side cooperation is required in some methods and makes them incompatible with existing systems. Therefore, the designs of PAR reduction methods that can be used in current OFDM and OFDM-FDMA systems are of particular interest.

Reliable transmission is also our objective. To quantify the error performance of different communication systems, two parameters are usually used: diversity order and coding gain (see for example, [83, 102]). The diversity order describes how fast the error probability decays with signal-to-noise ratio, while the coding gain measures the error performance gap among different schemes when they have the same diversity. Thus, diversity-enriched transceivers have well-appreciated merits. Various diversity techniques, e.g., antenna diversity and cooperative diversity, have been enabled by properly designed transceivers [48, 71, 92, 96, 102]. However, little work has investigated the diversity performance in PPC wireless systems. In this thesis, we will also study and design low-complexity, power-efficient, and diversity-enabled PPC systems.

1.3 Outline and Notations

The rest of the dissertation is organized as follows:

In Chapter 2, the mathematical models are established for general peak power constrained systems, the orthogonal frequency division multiplexing systems as well as the error performance measurements in wireless fading channels.

In Chapter 3, PAR reduction methods are proposed to improve the power efficiency in both OFDM and OFDM-FDMA systems. We focus on the methods that are compatible with existing standards and require no receiver-side modification. The performance is analyzed for the proposed methods, which are also combined with parameter optimization and power allocation schemes to improve relevant performance metrics.

In Chapter 4, the antenna diversity enabled by multiple receiving antennas is studied for peak power constrained OFDM systems. Several full-diversity transceiver designs are presented for the PPC SIMO-OFDM systems.

In Chapter 5, amplify-and-forward cooperative networks are studied. Practical and simple cooperative network designs, which also achieve full cooperative diversity, are of particular concern. Besides, general design criteria for full-diversity amplify-and-forward relaying strategies and a general theorem on diversity gain function are given.

In the end, Chapter 6 summarizes the main contributions of this dissertation and offers a few suggestions for future research.

Before all, let us introduce the following notations that are used throughout the dissertation unless indicated otherwise:

Superscript * denotes conjugate, ^{T} transpose, and ^{H} Hermitian. For a complex number a, $\Re(a)$ and $\Im(a)$ stand for its real and imaginary parts. Bold face letters are used for vectors and matrices, whose elements are indexed by subscripts. Specifically, $\mathbf{0}_l$ is an l-by-1 vector with all zero entries and $\mathbf{I}_{l\times l}$ is an l-by-l identity matrix. In addition, diag($\mathbf{x}$) denotes a diagonal matrix with vector $\mathbf{x}$ on its diagonal and $tr(\cdot)$ stands for the trace of a matrix. We denote $|a|$ as the magnitude of scalar a and $\|\mathbf{x}\|_\ell$ for the ℓth norm of vector $\mathbf{x}$. As usual, the empty set is represented by $\emptyset$.

Moreover, we use $f_x(a)$ and $F_x(a)$ to denote the probability density function (PDF) and the cumulative density function (CDF) of a random variable x evaluated at a,

respectively. We also reserve $E_x[\cdot]$ as the expectation over x. $\mathcal{CN}(0, \sigma^2)$ stands for the complex Gaussian distribution with zero mean and variance σ^2.

The Q-function is defined as $Q(a) = (1/\sqrt{2\pi}) \int_a^\infty e^{-\frac{t^2}{2}} dt$. In addition, we use $f(a) \doteq g(a)$ to represent the asymptotic exponential equality, i.e., $\lim_{a\to\infty} \ln f(a)/\ln a = \lim_{a\to\infty} \ln g(a)/\ln a$. Similarly, "$\dot{\leq}$" and "$\dot{\geq}$" are also defined. Moreover, $x \to a^+$ (a^-) indicates that x tends to a from above (below) and $o(x)$ represents $\lim_{x\to 0^+} o(x)/x = 0$.

CHAPTER II

BACKGROUND

In this chapter, a review of the peak power constrained (PPC) wireless communication systems is presented. With respect to the PPC components of wireless transmitters, a generic system model is introduced. The rest of this chapter is dedicated to establish the signal models for orthogonal frequency division multiplexing (OFDM) and diversity-enabled systems.

2.1 Peak Power Constrained System Model

The diagram for general wireless transmitters is illustrated in Figure 2.1. The RF devices, especially the power amplifiers (PAs), are indispensable components in a communication system. However, the PAs are inherently nonlinear and peak power constrained. As motivated in Chapter 1, although scaling down PA input signals can restrain nonlinear distortions, the price is the low RF-to-DC power efficiency. Thus, it is necessary to linearize PAs so that the in-band distortions and spectral broadening effects can be surpassed without a substantial sacrifice of power efficiency at the first place.

The PA linearization problem is well under study and a number of techniques have been adopted for commercial use [7, 21, 23, 26, 51, 109]. From the implementation aspect, digital baseband predistortion is among the most cost-effective techniques. A digital predistorter is a functional block that precedes the PA and processes the baseband PA input signal accordingly. It generally creates an expanding nonlinearity to neutralize the compressing characteristic of the PA. In addition, by adopting a memory polynomial model, the predistorter can also well compensate PA memory effects which cannot be ignored for wideband systems. To adaptively identify the

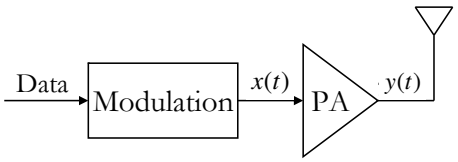

Figure 2.1: A generic wireless transmitter model.

polynomial model for the predistorter, the indirect learning structure can be used and its diagram is shown in Figure 2.2. The details of the digital predistorters are not the focus in this dissertation, but can be found in [26] and the references therein.

For the PAs that exhibit mild nonlinearities prior to saturation, existing predistortion techniques are capable of producing a linearized PA that is well approximated by an ideal soft-limit (SL) model, whose input-output characteristic is illustrated in Figure 2.3 [7, 23, 26]. Denoting the input signal of the PA as $x(t)$ with the average power of $\sigma_x^2 = E[|x(t)|^2]$, the output signal of the soft-limit model is [100]

$$y(t) = \begin{cases} G \cdot x(t), & |x(t)|^2 \leq \frac{P_{\text{peak}}}{G^2}, \quad (2.1) \\ \sqrt{P_{\text{peak}}} e^{j\angle x(t)}, & |x(t)|^2 > \frac{P_{\text{peak}}}{G^2}, \quad (2.2) \end{cases}$$

where P_{peak} is the peak power constraint for the PA output signal, G is the gain of the linearized PA, and $\angle a$ denotes the phase of a complex variable a. Within the SL model, nonlinear distortions occur only when clipping (i.e., PA saturation) happens, i.e., $|x(t)|^2 > P_{\text{peak}}/G^2$.

The input back-off (IBO) is defined as the ratio between the peak power constraint and the average power of the input signal, namely,

$$\text{IBO} = \frac{P_{\text{peak}}}{G^2 \sigma_x^2}. \quad (2.3)$$

A class-A PA is considered in this dissertation, where the DC power consumption is twice the peak power of the PA output, i.e., $P_{\text{dc}} = 2P_{\text{peak}}$. Admittedly, other types of PAs, e.g., class-B and class-AB PAs, are more power efficient than the class-A PA in nature. The ratio between P_{peak} and P_{dc} is greater than 0.5 for class-B and class-AB PAs [21]. Nevertheless, the consideration of only class-A PAs in this dissertation does

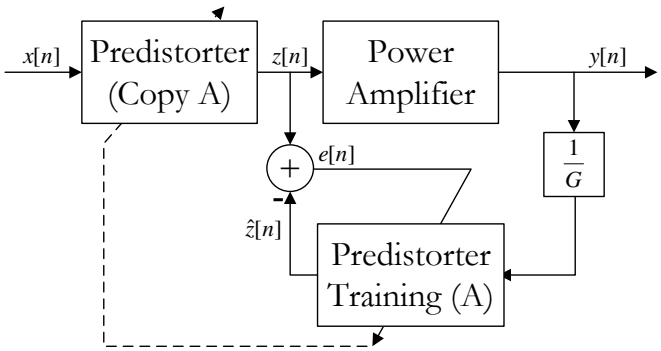

Figure 2.2: The digital predistorter of the indirect learning structure.

not lose the generality of the discussion, and the analysis can be extended to other types of PAs accordingly.

Because $|y(t)|^2 \leq G^2|x(t)|^2$, the average transmit power has $\sigma_y^2 = E[|y(t)|^2] \leq G^2\sigma_x^2$. In other words, $\sigma_y^2 \in S_y$ as illustrated in Figure 2.3. For the class-A PA, the power efficiency ρ is thus given by [110]

$$\rho = \frac{\sigma_y^2}{P_{\text{dc}}} \leq \frac{1}{2\text{IBO}}. \tag{2.4}$$

The equality in (2.4) holds if no saturation occurs at the PA, i.e., $|x(t)| \leq \sqrt{P_{\text{peak}}}/G$. However, for IBOs that are not too small, $\rho \approx (2\text{IBO})^{-1}$ is a good approximation.

To characterize the signal power level with respect to the channel condition, the signal-to-noise ratio (SNR) is usually used in ideal linear transmissions. For the PPC systems, however, since the power consumption P_{dc} relies on the peak power constraint P_{peak}, it is the peak-signal-to-noise ratio (PSNR), which compares the PA power consumption with the channel noise level, a relevant measurement, i.e.,

$$\text{PSNR} = \frac{P_{\text{peak}}}{N_0} \approx \text{IBO} \cdot \frac{\sigma_y^2}{N_0}, \tag{2.5}$$

where N_0 denotes the additive white Gaussian channel noise power. It is worth noting that the use of PSNR is not conflicting with SNR. In fact, as given in Eq. (2.5), we have $\text{PSNR} \approx \text{IBO} \cdot \text{SNR}$.

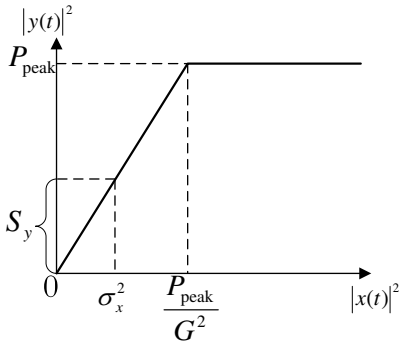

Figure 2.3: The soft-limit characteristic of peak power constrained PAs.

2.2 Orthogonal Frequency Division Multiplexing Systems

The invention of the orthogonal frequency division multiplexing (OFDM) modulation should be dated back to the 1960s. The basic principles of OFDM have already been proposed in several publications as early as 1966 [17, 89, 111]. The idea of OFDM is to distribute the high-rate data stream to many low-rate data streams that are transmitted in a large number of parallel and closely-spaced orthogonal subcarriers. It breaks a wideband spectrum into orthogonal narrowbands and thus simplifies the equalization at the receivers. However, this idea could not be implemented efficiently at that time.

Today, attributed to the efficient OFDM implementation with fast Fourier transform (FFT) and the spring of powerful semiconductor devices in the last decade, even relatively complex and high-rate OFDM transmission systems are technically feasible [19, 108]. Due to its high spectral efficiency and low complexity in combating frequency-selective fading effects, the OFDM technique has been widely adopted by wireless communication standards, e.g., from the DVT-B broadcasting standard, to wireless local area networks (WLAN) such as the IEEE 802.11a and the IEEE 802.16 standards, and even future cellular systems like the Long Term Evolution (LTE) under the consideration by the Third Generation Partnership Project (3GPP), etc [1, 2, 3, 4, 28].

However, OFDM experiences certain implementation challenges due to the large dynamic range of its time-domain waveforms, which is usually measured by the peak-to-average power ratio (PAR) [100]. It forces the OFDM system vulnerable to the PA nonlinearity, yielding significant distortions on the signals and/or highly inefficient power consumption at the PA.

In this section, the signal model of the OFDM modulation will be presented. The PAR and other performance metrics in OFDM systems will be discussed consequently.

2.2.1 Signal Model

OFDM is a block-wise modulation, whose system diagram is given in Figure 2.4.

For an uncoded OFDM system, data are transmitted on N orthogonal subcarriers. For each frequency-domain OFDM symbol, an N-point inverse fast Fourier transform (IFFT) operation can be used to generate the time-domain signal. After parallel-to-serial conversion (P/S), the cyclic prefix (CP), whose length L_{cp} should be greater than the longest channel delay, is appended to each OFDM symbol. The symbol is then oversampled by L times and converted to analog signals. After up-converting it to radio frequency, it is amplified by the PA and sent to the receivers through the wireless channel. On the other hand, the OFDM demodulation is exactly the same process but in reverse order. The receivers are assumed to achieve ideal channel estimation by the help of training symbols or pilot subcarriers [52, 53]. The estimated channel gains are subsequently used in the one-tap equalizer succeeding the N-point FFT operation. Additionally, rather than power amplifiers, low-noise amplifiers (LNAs) are adopted to amplify weak signals at the receivers [104].

Denote the frequency-domain OFDM symbol as $\mathbf{X} = [X_0, \cdots, X_{N-1}]^T$. Due to the property of FFT, the oversampled OFDM signal can be efficiently generated by zero-padding. Thus, for each OFDM symbol, the L-times oversampled time-domain

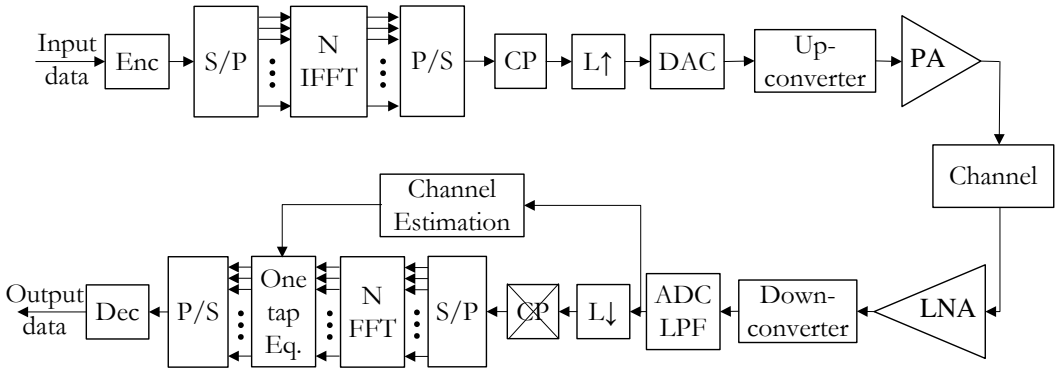

Figure 2.4: The system diagram for OFDM transceivers.

signal can be obtained from the LN-point IFFT operation, i.e.,

$$\mathbf{x} = [x[0], \cdots, x[LN-1]]^T = \mathbf{F}^H \mathbf{X}, \tag{2.6}$$

where $\mathbf{F}$ is the $N \times LN$ oversampling FFT matrix formed by retaining only the first N rows of a full $LN \times LN$ FFT matrix whose $(m+1, n+1)$st entry is $\frac{1}{\sqrt{LN}} e^{-j2\pi mn/(LN)}$.

According to the standards [2, 3], the OFDM subcarriers are usually categorized into three non-overlapping sets: pilot subcarriers, free subcarriers and data subcarriers, denoted by sets of indices $\mathcal{K}_p$, $\mathcal{K}_f$ and $\mathcal{K}_d$, respectively. They have the cardinalities $|\mathcal{K}_p| = p$, $|\mathcal{K}_f| = f$ and $|\mathcal{K}_d| = d$ so that $p + f + d = N$. For instance, the subcarrier categorization in IEEE 802.11a is illustrated in Figure 2.5, where $p = 4$, $f = 12$ and $d = 48$ [2].

The signal transmitted over the pilot subcarriers is prescribed and known *a priori* to the receivers, denoted as $X_k = \mathcal{P}_k$ $(k \in \mathcal{K}_p)$. It is supposed to help receivers estimate the channel response. For example, the pilot signals are defined as $\mathcal{P}_k \in \{\pm 1\}$ $(k \in \mathcal{K}_p)$ in the IEEE 802.11a standard [2]. In order not to interfere with the channel estimation, transmitters are not allowed to modify these pilot signals.

On the free subcarriers, any complex values can be transmitted as long as they comply with the spectral mask constraint as specified in communication standards and discussed in Section 2.2.3.

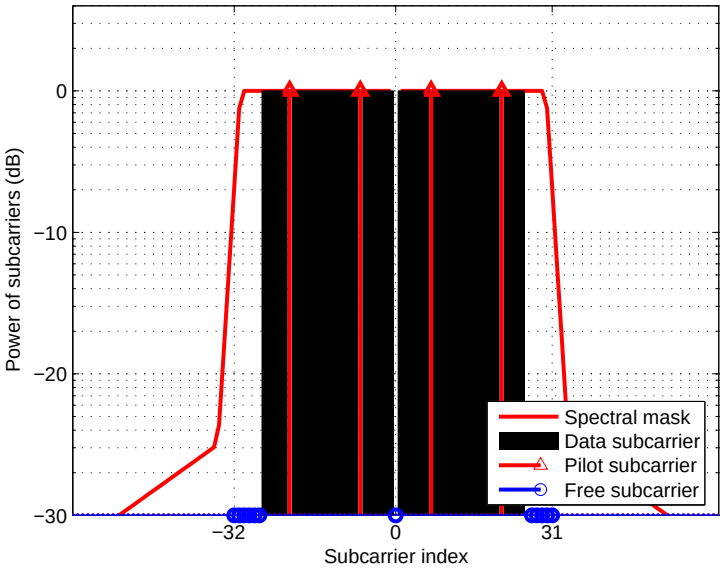

Figure 2.5: The OFDM subcarrier categorization in IEEE 802.11a.

On the data subcarriers, the information bits are mapped into an ideal constellation Ω of the adopted modulation schemes, namely $X_k \in \Omega$ ($k \in \mathcal{K}_d$). The average power of data subcarriers (i.e., the constellation itself) is denoted as $P_0 = E[|X_k|^2]$ ($k \in \mathcal{K}_d$).

2.2.2 Peak-to-Average Power Ratio

The peak-to-average power ratio (PAR) is usually used to quantify the dynamic range of OFDM signals. Since the cyclic prefix does not impact the dynamic range, it is ignored in the analysis and $\mathbf{x}$ in Eq. (2.6) is taken as the RF input signal [100].

Denote the ensemble mean power of the OFDM samples $x[n]$ as $\sigma_x^2 = E[|x[n]|^2]$, which is equal to the infinite-time average power because $\mathbf{x}$ is ergodic. PAR of the symbol-wise OFDM signal is defined as

$$\mathrm{PAR}(\mathbf{x}) = \max_{n \in \{0, \cdots, LN-1\}} \frac{|x[n]|^2}{\sigma_x^2}. \tag{2.7}$$

Although PAR is based on sampled OFDM signals, it has been shown to well approximate the dynamic range of continuous waveform when the oversampling rate $L \geq 4$

[100].

According to the Central Limit Theorem, the time-domain sample $x[n]$ exhibits an approximate complex Gaussian distribution when N is reasonably large [100]. For example, the power of the samples of one OFDM symbol is demonstrated in Figure 2.6. Therefore, OFDM symbols can have very large PAR values with non-zero probabilities. The curves of the complimentary cumulative distribution function (CCDF) of the PAR values are plotted in Figure 2.7 for the OFDM with different numbers of subcarriers ($N = 64$, 256, 512 and 1024). As shown in Figure 2.7, when the OFDM has $N = 1024$ subcarriers, about 1 percent symbols still experience clipping distortions when IBO = 11dB and the PA power efficiency is only $\rho \approx 4\%$.

When the PAR values exceed the IBO, clipping will occur and generate the in-band error vector magnitude and spectral broadening effects that may exceed the distortion limits imposed by standards or that are difficult to predict and control. Thus, IBO needs to be made large enough to accommodate the large, albeit occasional, peaks [20, 76]. Large IBO, however, diminishes the PA power efficiency.

Therefore, PAR reduction methods become essential in an efficient OFDM system. By modifying the OFDM signal in a certain way, the PAR reduction methods cancel the large peaks before passing the signals into the linearized PA. The diagram for such an OFDM system with PAR reduction is drawn in Figure 2.8.

2.2.3 Performance Metrics

Before studying the PAR reduction methods in Chapter 3, the performance metrics of the PPC OFDM systems are discussed in thus subsection.

2.2.3.1 Power Efficiency

As discussed in Section 2.1, power efficiency characterizes the proportion of the total PA power consumption that is turned into effective signal power.

For a class-A PA, the power efficiency is mainly determined by the input back-off

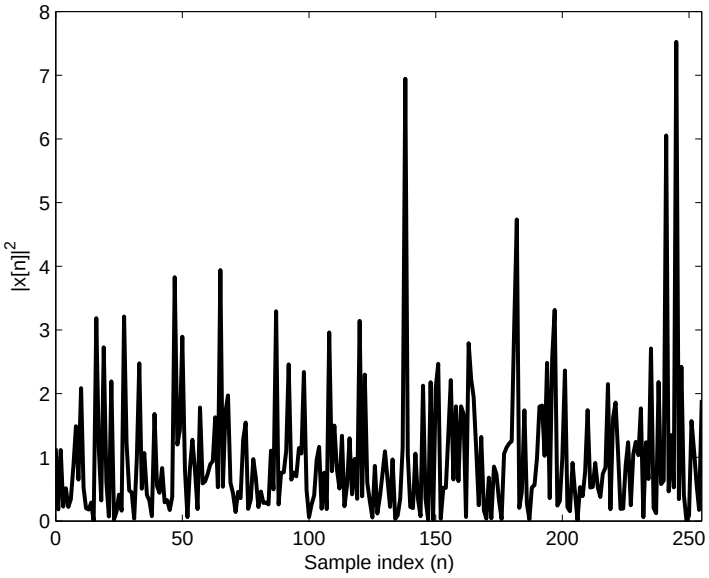

Figure 2.6: The power of the samples of an OFDM symbol; $N = 256$ and $L = 1$.

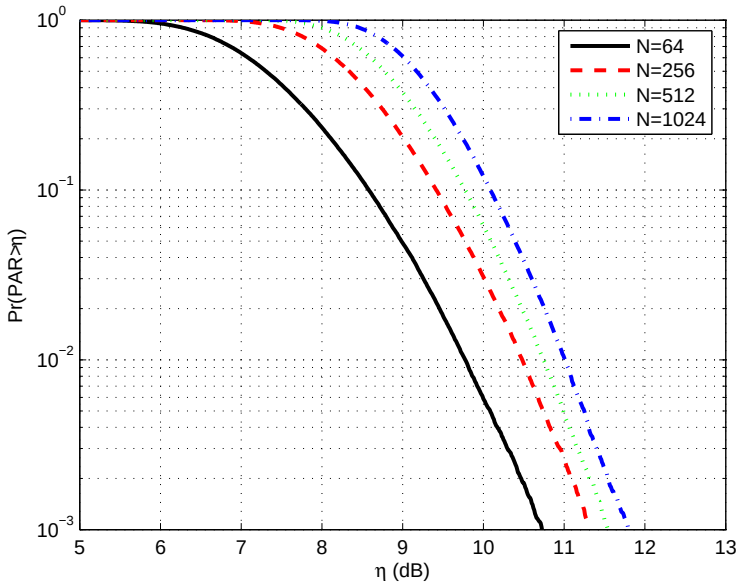

Figure 2.7: CCDF curves of the PAR of OFDM signals with the number of subcarriers $N = 64$, 256, 512 and 1024; $L = 4$.

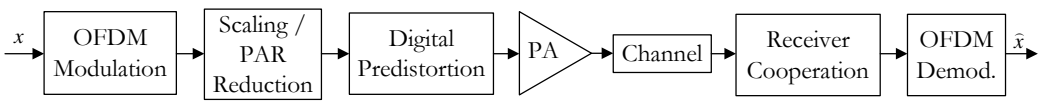

Figure 2.8: The system diagram for the OFDM transceivers aided by PAR reduction methods.

and is defined as

$$\rho = \frac{\sigma_y^2}{P_{\text{dc}}} \leq \frac{1}{2\text{IBO}}. \tag{2.8}$$

2.2.3.2 Error Vector Magnitude

Error vector magnitude (EVM) is widely adopted to quantify the amount of in-band distortion that occurs at OFDM transmitters [2, 3]. It directly affects the error performance, e.g., bit error rate. EVM can be caused by any number of non-ideal components in the transmission chain, including the PA, the DAC, the up-converter, etc. A distortion-based PAR reduction algorithm increases the EVM as well. As an example, in Figure 2.9, the constellations of one OFDM symbol are compared with those after the PA clipping. EVM is meant to characterize the constellation error exhibited on the clipped signal.

Denote $\tilde{\mathbf{Y}}$ as the frequency-domain symbol actually transmitted by the PA, and $\tilde{\mathbf{X}} = \tilde{\mathbf{Y}}/G$ as the corresponding PA input symbol. For each OFDM symbol, the (symbol-wise) EVM is defined as

$$\epsilon(\mathbf{X}, \tilde{\mathbf{X}}) = \sqrt{\frac{\sum_{k \in \mathcal{K}_d} |X_k - \tilde{X}_k|^2}{d \cdot P_0}}. \tag{2.9}$$

Notice that the EVM definitions may be presented in different forms among standards. The definition in Eq. (2.9) is in accordance with the IEEE 802.11a standard, while P_0 should be replaced by the maximum power of the constellation in IEEE 802.16 [2, 3].

In communication standards, the in-band distortion is constrained in terms of the root mean-square (RMS) EVM. That is, the RMS EVM value must be no greater than the threshold ε which is set forth in the standards, i.e.,

$$\text{RMS EVM} = \sqrt{E[\epsilon(\mathbf{X}, \tilde{\mathbf{X}})^2]} \leq \varepsilon. \tag{2.10}$$

For example, the RMS EVM thresholds for phase-shift keying (PSK) and quadrature amplitude modulation (QAM) constellations defined in the IEEE 802.11a standard are summarized in Table 2.1.

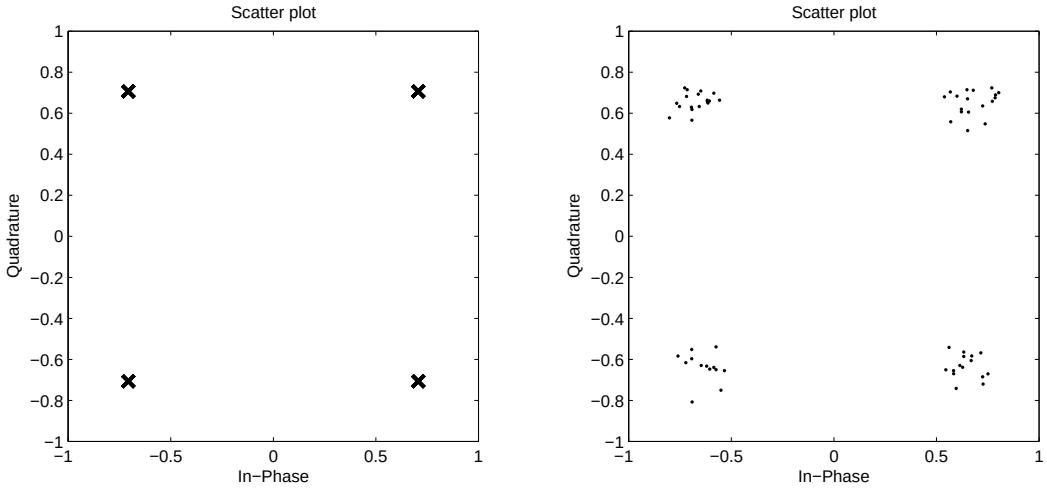

(a) Original OFDM.

(b) Clipped OFDM (IBO = 3dB).

Figure 2.9: The constellation comparison of the original and clipped OFDM; QPSK; $N = 256$ and $L = 4$; EVM $\epsilon = 0.18$.

Table 2.1: The RMS EVM thresholds for different constellations with the coding rate of 1/2 in the IEEE 802.11a standard.

Constellation	RMS EVM threshold (dB)
BPSK	-5
QPSK	-10
16-QAM	-16
64-QAM	-22

2.2.3.3 Spectral Mask

Another negative effect of nonlinear distortions is spectral broadening. It will not only diminish the orthogonality of in-band subcarriers, but also generate out-of-band spectral growth which behaves as inter-channel interference to other users. Figure 2.10 gives an example of the spectral density of clipped OFDM signals. When the IBO is small, the distortions become prominent that the out-of-band spectral components and RMS EVM values are not ignorable.

To avoid severely interfering other channels, communication standards define the spectral mask requirements for the transmitted power on both the in-band subcarriers

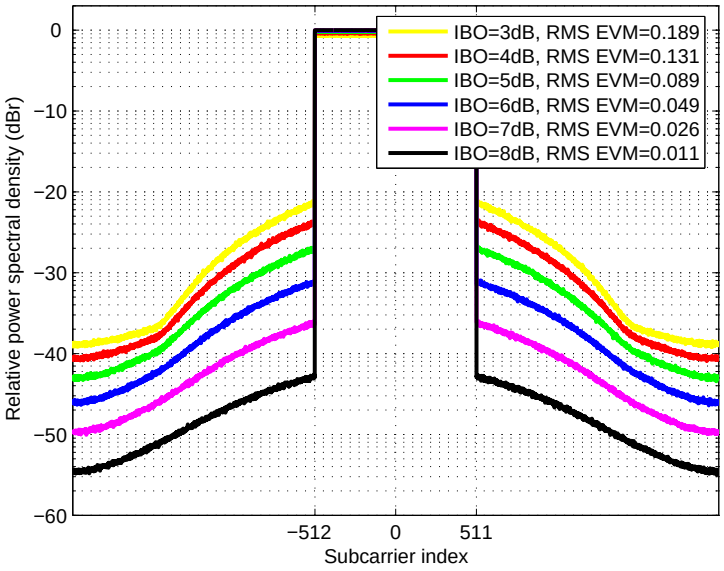

Figure 2.10: The spectral broadening effect of PA clipping; IBO = 3 ∼ 8dB.

and the out-of-band spectral components. For instance, the IEEE 802.11a spectral mask has been plotted in Figure 2.5. Denote $\mathcal{M}_k$ as the spectral mask constraints relative to the average power P_0 of data subcarriers. The signals transmitted on free subcarriers should also satisfy

$$E[|\tilde{X}_k|^2] \leq \mathcal{M}_k \cdot P_0, \ k \in \mathcal{K}_f. \tag{2.11}$$

2.3 Diversity-Enabled Systems in Fading Channels

In the wireless environment, random fading channels are detrimental to the transmission because they convert an exponential decay of the symbol error rate (SER) or bit error rate (BER) on the average SNR into a linear one [99, 107].

Denote the instantaneous SNR in a fading channel as

$$\gamma = \beta\bar{\gamma}, \tag{2.12}$$

where β is a channel-dependent random variable and the average transmit SNR $\bar{\gamma}$ is defined as the ratio between the average transmit power σ_x^2 and the channel noise power N_0, i.e., $\bar{\gamma} = \sigma_x^2/N_0$.

Without loss of generality, additive white Gaussian channel noise is assumed so that the instantaneous SER is in the form of

$$P_E(\gamma) = \kappa_1 Q(\sqrt{\kappa_2 \gamma}), \tag{2.13}$$

where κ_1 and κ_2 are constellation-specific constants, e.g., $\kappa_1 = 4(1 - M^{-\frac{1}{2}})$ and $\kappa_2 = \frac{3}{M-1}$ for M-ary QAM modulations [83, p. 278]. By averaging over the channel variable β, the average SER in fading channels is thus given by

$$P_e = E_\beta[P_E(\gamma)], \tag{2.14}$$

which is the function of the average SNR $\bar{\gamma}$.

The asymptotic SER is of particular interest because it describes how much the error rate can benefit by increasing the transmit power.

As a unified way to quantify the error performance in fading channels at high SNR, the average SER P_e of an uncoded system is usually approximated by [99, 107]

$$P_e \approx (G_c \cdot \bar{\gamma})^{-G_d}, \text{ for } \bar{\gamma} \to \infty, \tag{2.15}$$

where G_c and G_d are referred to as the *coding gain* and the *diversity order*, respectively [107]. Specifically, the diversity order of the average SER is defined as (see also [99]):

Definition 2.1 (Diversity order) *Suppose that P_e is the average SER as a function of the average SNR $\bar{\gamma}$. The diversity order G_d is defined as*

$$G_d = \lim_{\bar{\gamma} \to \infty} -\frac{\log P_e}{\log \bar{\gamma}}. \tag{2.16}$$

In other words, $P_e \doteq \bar{\gamma}^{-G_d}$.

The diversity order G_d describes how fast the error rate decreases with SNR, while the coding gain G_c measures the shift in SNR of the SER curves relative to the benchmark curve of $\bar{\gamma}^{-G_d}$.

The greater the diversity order, the better the asymptotic SER performance. Therefore, diversity-enabled systems have well-appreciated virtues. The basic principle of the diversity techniques is to provide the receiver multiple faded replicas of the same information bearing signal. A variety of diversity techniques have been proposed in literature and adopted in practical implementations, e.g., space, time, frequency, angle, polarization, and cooperative diversity techniques [48, 67, 82, 94, 97]. Particularly, in this dissertation, the space (i.e., multi-antenna systems) and cooperative (i.e., cooperative networks) diversities will be investigated in Chapters 4 and 5.

With the instantaneous receive SNR $\gamma = \beta\bar{\gamma}$, if the PDF of β (i.e., $f_\beta(\beta)$) can be approximated by polynomial series around the origin, the relationship between the diversity order and the PDF of β has been revealed [107].

In many communication systems, e.g., in wireless cooperative networks, however, recently it has been observed that the average SER could not be accurately characterized by an exponential function of the SNR [27, 41]. The average SER generally involves the logarithm function of the average SNR and can be approximated by

$$P_e \approx G_c \cdot G_f(\bar{\gamma}), \text{ for } \bar{\gamma} \to \infty, \tag{2.17}$$

where $G_f(\bar{\gamma}) = \bar{\gamma}^{-m}(\ln \bar{\gamma})^n$ $(m, n \geq 0)$. To distinguish from the diversity order, the following definition is introduced (see also [27]):

Definition 2.2 (Diversity gain function) *The diversity gain function $G_f(\bar{\gamma})$ is defined as a function of the average SNR $\bar{\gamma}$*

$$G_f(\bar{\gamma}) = \bar{\gamma}^{-m}(\ln \bar{\gamma})^n, \ m, n \geq 0. \tag{2.18}$$

If the asymptotic SER achieves $G_f(\bar{\gamma})$, it also collects the diversity order of $G_d = m$ gradually. In other words, diversity gain function not only describes the asymptotic diversity order, but also depicts how fast it is approached. Thus, the diversity gain function can fully characterize the diversity behavior of the concerned communication systems and is a more accurate extension of G_d.

CHAPTER III

PAR REDUCTION IN OFDM SYSTEMS

Several PAR reduction methods are proposed in this chapter for OFDM and OFDM-based frequency-division multiple access (OFDM-FDMA) systems. Significant performance improvements, in terms of power efficiency, throughput and error rate, can be achieved by the proposed methods. In addition, the presented approaches require no receiver-side modification and are thus compatible with existing systems.

3.1 Introduction

Many methods have been proposed to reduce the PAR of OFDM signals. A complete literature review can be found in [35, 40] and the references therein.

Any PAR reduction method has to modify the signal waveform in some fashion, and is usually categorized into distortionless and distortion-based approaches. With the soft-limit PA, distortionless PAR reduction techniques aim at avoiding any nonlinear distortion in the transmitted signal. For example, the piece-wise linear scaling (PWLS) [76], selected mapping (SLM) [11], partial transmit sequences (PTS) [73], and coding schemes [54] all belong to the distortionless PAR reduction methods. In this case, however, some sort of reverse operation should usually be done at the receiver and thus requiring receiver-side modifications. On the other hand, the distortion-based PAR reduction approaches can reduce the dynamic range of the transmitted signal by carefully managing the distortions so that we stay within the limits as specified in the communication standards. A number of distortion-based PAR reduction algorithms have been investigated in literature, e.g., in [6, 12, 13, 35, 40, 44, 45, 50, 64, 77, 100]. Some methods operate by constraining the distortion energy on data subcarriers [12, 44, 77]; some by projecting the distortion

energy onto the free subcarriers [45, 50, 100].

To be compatible with existing systems is important for a practical PAR reduction method. Therefore, the PAR reduction methods that require no receiver-side cooperation will be particularly focused in this chapter.

3.2 EVM Optimization with a Deterministic PAR Constraint

As introduced in Section 2.2.3, EVM is widely adopted to quantify the amount of in-band distortion in communication standards. In the presence of digital predistorter, it is reasonable to assume that there is sufficient EVM "headroom" left from the analog devices to allow for a distortion-based PAR reduction algorithm.

In the recent literature [6, 64], PAR reduction has been cast as a convex optimization problem where the symbol-wise PAR is minimized by deliberately introducing free subcarrier signals and in-band distortions subject to the spectral mask constraint in (2.11) and a symbol-wise EVM constraint. By exploiting the IFFT structure of OFDM modulation, an interior-point method (IPM) can be devised to solve the convex optimization problem efficiently thus providing good PAR reduction performance with relatively low complexity.

However, the PAR-minimization method possesses two main shortcomings. First, minimizing the symbol-wise PAR does not automatically yield power efficiency improvements, unless one implements adaptive biasing or piece-wise scaling [76] to boost the average transmit power of PAR-reduced symbols. Otherwise, if the PAR has non-zero probability of exceeding the prescribed IBO, the signal still will be clipped, in which case the standard's requirements (e.g., RMS EVM and spectral mask) may be violated. Therefore, it is desirable to have an algorithm which guarantees that the PAR of the modified OFDM signal will never exceed a given threshold so that no PA clipping may be encountered.

Moreover, in communication standards, the RMS EVM constraint in (2.10) is

typically given [2, 3]. Therefore, the symbol-wise EVM can fluctuate from symbol to symbol and does not have to be as tightly constrained as in [6] and [64]. This degree of freedom in the symbol-wise EVM can thus be taken advantage of to boost the PAR reduction performance.

To address the above problems, in this section, an EVM optimization task is formulated subject to the spectral mask constraint and a deterministic (as opposed to probabilistic) PAR constraint

$$\text{PAR} \leq \gamma, \tag{3.1}$$

where $\gamma > 0$ represents a deterministic PAR constraint in this section. A low-complexity IPM algorithm will also be derived to efficiently solve the EVM optimization problem [61, 62].

Our proposed method differs from existing approaches in the following ways: (i) We target the RMS EVM rather than the symbol-wise EVM. This is not only standard-oriented, but also results in better PAR reduction performance. When the RMS EVM constraint is used, certain large PAR symbols can be allocated greater symbol-wise EVM budget to permit significant PAR reduction. If an OFDM symbol has a small PAR value to start with, very little symbol-wise EVM allowance may be needed in order to reach the PAR threshold. It is easier to achieve a RMS EVM goal than to achieve a symbol-wise EVM goal of the same magnitude. Therefore, when the RMS EVM metric is used, there is more room for the PAR reduction algorithm to do its work. (ii) A deterministic PAR constraint is used. In other words, we are interested in a fixed PAR threshold for all signal blocks rather than optimum but variable PAR values from block to block. Once the PAR threshold is judiciously chosen, the PA's size, bias, and/or IBO can be determined corresponding to the threshold. Consequently, the peak power constrained symbols achieved by the proposed algorithm avoid any PA clipping, thus eliminating the possibility of uncontrolled in-band distortion, out-of-band spectral regrowth and average power reduction.

3.2.1 Framework

Denote $\tilde{\mathbf{X}}$ as the modified symbol generated by the PAR reduction method, whose time-domain counterpart $\tilde{\mathbf{x}} = \mathbf{F}^H\tilde{\mathbf{X}}$ has a lower PAR than the original waveform $\mathbf{x}$.

We formulate the EVM optimization algorithm that minimizes the symbol-wise EVM while simultaneously satisfying the deterministic PAR constraint (3.1) and the spectral mask constraint (2.11) as follows:

$$\min_{\tilde{\mathbf{X}}} \quad e \tag{3.2}$$

$$\text{s.t.} \quad \sqrt{dP_0}\cdot\epsilon(\mathbf{X},\tilde{\mathbf{X}}) \le e \tag{3.3}$$

$$\tilde{X}_k = X_k,\ k\in\mathcal{K}_p \tag{3.4}$$

$$|\tilde{X}_k|^2 \le \mathcal{M}_k\cdot P_0,\ k\in\mathcal{K}_f \tag{3.5}$$

$$\sum_{k\in\mathcal{K}_d}\Re(X_k^*(\tilde{X}_k - X_k)) \ge -\frac{e^2}{2} \tag{3.6}$$

$$\tilde{\mathbf{x}} = \mathbf{F}^H\tilde{\mathbf{X}} \tag{3.7}$$

$$|\tilde{x}[n]| \le \sqrt{\gamma}\sigma_x,\ n = 0,\cdots,LN-1. \tag{3.8}$$

In particular, (3.2) and (3.3) set the symbol-wise EVM, $\epsilon(\mathbf{X},\tilde{\mathbf{X}})$, as the objective of minimization. Eq. (3.4) keeps the pilot subcarriers unchanged (see Section 2.2.1). (3.5) constrains the instantaneous power of the free subcarriers to satisfy the spectral mask requirement. Although (3.5) provides a stricter constraint than (2.11), it is easier to solve symbol-wise. Additionally, since directly constraining the PAR leads to a complicated non-convex problem, we follow the derivation in [6] and separately restrict the peak power as in (3.8) and the average power on data subcarriers according to (3.6). Eq. (3.6) is a convex inequality constraint and is equivalent to

$$\sum_{k\in\mathcal{K}_d}|\tilde{X}_k|^2 \ge \sum_{k\in\mathcal{K}_d}|X_k|^2, \tag{3.9}$$

when the constraint of (3.3) is active (i.e., $\sqrt{dP_0}\cdot\epsilon(\mathbf{X},\tilde{\mathbf{X}}) = e$), which always holds in optimality. Eqs. (3.6) and (3.8) guarantee that the PAR of the optimized signal $\tilde{\mathbf{x}}$ will never exceed the threshold γ.

In summary, while strictly upper bounding the PAR of modified OFDM symbols, the convex EVM optimization framework minimizes the symbol-wise EVM and meets all the constraints on free and pilot subcarriers. The tradeoff between the optimized in-band distortion (in terms of RMS EVM) and power efficiency (in terms of the PAR threshold γ) can be subsequently determined. The minimum PAR threshold is then ready to be chosen to comply with the RMS EVM constraint laid by standards.

3.2.2 Customized Interior-Point Method

The iterative log-barrier interior-point method can be customized to efficiently solve the symbol-wise EVM optimization in (3.2)-(3.8) [16, Chap. 11]. The derivation and the customized IPM algorithm are introduced in this subsection.

Let us use an $N \times N$ matrix $\mathbf{S}$ to indicate the locations of the data subcarriers, whose (m,n)-th element is given by

$$S_{m,n} = \begin{cases} 1, & m = n \in \mathcal{K}_d, \quad (3.10) \\ 0, & m \notin \mathcal{K}_d, \text{ or } n \notin \mathcal{K}_d, \text{ or } m \neq n. \quad (3.11) \end{cases}$$

Thus, $\mathbf{S}$ consists of block identity and zero matrices. The symbol-wise EVM in Eq. (2.9) can be re-written as

$$\epsilon(\mathbf{X}, \tilde{\mathbf{X}}) = \frac{1}{\sqrt{dP_0}} \|\mathbf{S}(\mathbf{X} - \tilde{\mathbf{X}})\|_2. \quad (3.12)$$

Using the indicator matrix notation $\mathbf{S}$, the constraint in (3.3) becomes

$$\|\mathbf{S}(\mathbf{X} - \tilde{\mathbf{X}})\|_2 \leq e. \quad (3.13)$$

Moreover, the average power constraint (3.6) can also be expressed as

$$\Re(\mathbf{X}^H \mathbf{S}(\tilde{\mathbf{X}} - \mathbf{X})) \geq -\frac{e^2}{2}. \quad (3.14)$$

Therefore, the inequality constrained optimization problem in (3.2)-(3.8) can be approximately formulated as an equality constrained problem with the inequality

constraints implicit in the objective function [16, Chap. 11]:

$$\min_{\tilde{\mathbf{x}}} \quad f_o(\mathbf{X}, \mathcal{M}_k, \mathcal{K}_f, \mathcal{K}_p, e, \gamma, \mathbf{S}) \tag{3.15}$$

$$\text{s.t.} \quad \tilde{\mathbf{x}} = \text{IFFT}_L(\tilde{\mathbf{X}}), \tag{3.16}$$

where

$$f_o(\mathbf{X}, \mathcal{M}_k, \mathcal{K}_f, \mathcal{K}_p, e, \gamma, \mathbf{S}) = e + \text{I}_-\left[-\delta_a\right] + \text{I}_-\left[-\delta_e\right] + \sum_{n=0}^{LN-1} \text{I}_-\left[-\delta_n\right] + \sum_{k \in \mathcal{K}_f} \text{I}_-\left[-\phi_k\right], \tag{3.17}$$

$\text{I}_-[\cdot]$ is the indicator function for the nonpositive reals,

$$\text{I}_-[u] = \begin{cases} 0, & u \leq 0, \end{cases} \tag{3.18}$$

$$\begin{cases} \infty, & u > 0. \end{cases} \tag{3.19}$$

Let us denote

$$\delta_a = \frac{e^2}{2} + \Re(\mathbf{X}^H \mathbf{S}(\tilde{\mathbf{X}} - \mathbf{X})), \tag{3.20}$$

$$\delta_e = e^2 - \|\mathbf{S}(\mathbf{X} - \tilde{\mathbf{X}})\|_2^2, \tag{3.21}$$

$$\delta_n = \gamma\sigma_x^2 - |\tilde{x}[n]|^2, \ n \in \{0, \cdots, LN-1\}, \tag{3.22}$$

$$\phi_k = \begin{cases} \mathcal{M}_k \cdot P_0 - |\tilde{X}_k|^2, & k \in \mathcal{K}_f, \end{cases} \tag{3.23}$$

$$\begin{cases} 0, & \text{otherwise}, \end{cases} \tag{3.24}$$

all of which should be positive as required by the inequality constraints. The only equality constraint Eq. (3.4) sets the pilot subcarriers unchanged and not to be optimized over.

By using the log-barrier interior-point method as described in [16, Chap. 11], an iterative algorithm can be constructed to efficiently solve the equivalent symbol-wise EVM optimization problem in (3.15)-(3.16) as shown below.

Because the standard IPM optimization technique can only deal with real numbers, let us define the real-imaginary forms of an N-by-1 complex vector $\mathbf{X}$ and an

m-by-n complex matrix $\mathbf{A}$ as

$$\mathbb{X} = \left[\Re(X_0), \Im(X_0), \cdots, \Re(X_{N-1}), \Im(X_{N-1})\right]^T, \tag{3.25}$$

$$\mathbb{A}_{2m\times 2n} = \begin{bmatrix} \ddots & & & \\ & \Re(A_{ij}) & -\Im(A_{ij}) & \\ & \Im(A_{ij}) & \Re(A_{ij}) & \\ & & & \ddots \end{bmatrix}_{2m\times 2n}. \tag{3.26}$$

At each iteration, the actually transmitted OFDM symbol and its EVM are updated as

$$\tilde{\mathbf{X}}_{\text{new}} = \tilde{\mathbf{X}} + \beta\mathbf{V}, \tag{3.27}$$

$$e_{\text{new}} = e - \beta, \tag{3.28}$$

where β is the step size which will be discussed later and $\mathbf{V}$ is the updating vector. Then, the real-imaginary form $\mathbb{V}$ of the updating vector $\mathbf{V}$ should be calculated by solving the following linear model

$$\mathbb{H}\mathbb{V} = -\mathbb{G}, \tag{3.29}$$

where $\mathbb{G}$ and $\mathbb{H}$ are the gradient vector and Hessian matrix, respectively. $\mathbb{G} = -\frac{\partial^2 \hat{f}}{\partial\tilde{\mathbb{X}}\partial e}$ and $\mathbb{H} = \frac{\partial^2 \hat{f}}{\partial\tilde{\mathbb{X}}\partial(\tilde{\mathbb{X}})^T}$ where $\hat{f}$ is the log-barrier approximation of the objective function Eq. (3.17) by replacing $\mathrm{I}_-[\cdot]$ with the logarithmic barrier function [16]

$$\hat{\mathrm{I}}_-[u] = -\frac{1}{t}\log(-u),\ u \in \mathcal{R}^-, \tag{3.30}$$

where $t > 0$ is a parameter that sets the accuracy of the approximation. By implicitly choosing

$$t = \frac{\partial^2 \hat{f}}{\partial e^2} - \left(\frac{\partial^2 \hat{f}}{\partial\tilde{\mathbb{X}}\partial e}\right)^T \left(\frac{\partial^2 \hat{f}}{\partial\tilde{\mathbb{X}}\partial(\tilde{\mathbb{X}})^T}\right)^{-1} \left(\frac{\partial^2 \hat{f}}{\partial\tilde{\mathbb{X}}\partial e}\right), \tag{3.31}$$

Eq. (3.29) holds for the Newton's method [75, Chap. 6].

After some derivations, the gradient vector can be shown as

$$\mathbb{G} = \frac{4e}{\delta_e^2}\mathbb{S}(\tilde{\mathbb{X}} - \mathbb{X}) - \frac{e}{\delta_a^2}\mathbb{S}\mathbb{X}, \tag{3.32}$$

and the Hessian matrix becomes

$$\mathbb{H} = -(\mathbb{A} + \mathbb{E} + \mathbb{M} + \mathbb{Q}^T\mathbb{P}\mathbb{Q}). \tag{3.33}$$

In Eq. (3.33), we have

$$\mathbb{A} = -\frac{1}{\delta_a^2}(\mathbb{S}\mathbb{X})(\mathbb{S}\mathbb{X})^T, \tag{3.34}$$

$$\mathbb{E} = -\frac{2}{\delta_e}\mathbb{S} - \frac{4}{\delta_e^2}\mathbb{S}(\tilde{\mathbb{X}} - \mathbb{X})(\tilde{\mathbb{X}} - \mathbb{X})^T\mathbb{S}^T, \tag{3.35}$$

$$\mathbb{M} = \text{blkdiag}(\mathbb{M}_0, \cdots, \mathbb{M}_{N-1}), \tag{3.36}$$

$$\mathbb{P} = \text{blkdiag}(\mathbb{P}_0, \cdots, \mathbb{P}_{LN-1}), \tag{3.37}$$

where blkdiag() denotes the block-diagonal structure and $\mathbb{M}_k$ is

$$\mathbb{M}_k = \frac{2}{\phi_k^2}\begin{bmatrix} -\phi_k - 2(\Re(\tilde{X}_k))^2 & -2\Re(\tilde{X}_k)\Im(\tilde{X}_k) \\ -2\Re(\tilde{X}_k)\Im(\tilde{X}_k) & -\phi_k - 2(\Im(\tilde{X}_k))^2 \end{bmatrix}, \tag{3.38}$$

for $k \in \mathcal{K}_f$, and $\mathbb{M}_k = \mathbf{0}_{2\times 2}$, otherwise. Matrix $\mathbb{P}_n$ ($n \in \{0, \cdots, LN-1\}$) is

$$\mathbb{P}_n = \frac{2}{\delta_n^2}\begin{bmatrix} -\delta_n - 2(\Re(\tilde{x}[n]))^2 & -2\Re(\tilde{x}[n])\Im(\tilde{x}[n]) \\ -2\Re(\tilde{x}[n])\Im(\tilde{x}[n]) & -\delta_n - 2(\Im(\tilde{x}[n]))^2 \end{bmatrix}. \tag{3.39}$$

Moreover, if $\mathbf{F}$ is the L-times oversampling IFFT matrix such that $\tilde{\mathbf{x}} = \mathbf{F}^H\tilde{\mathbf{X}}$, $\mathbf{Q}$ consists of the corresponding $d+f$ columns of $\mathbf{F}$ with the column indices in $\mathcal{K}_d \bigcup \mathcal{K}_f$, and $\mathbb{Q}$ is the real-imaginary form of $\mathbf{Q}$.

Two techniques can be applied to improve the computational efficiency. The computation of Eq. (3.33) mainly resides in the matrix multiplication $\mathbb{Q}^T\mathbb{P}\mathbb{Q}$. By using the diagonalization properties of FFT, the complexity of constructing the Hessian matrix $\mathbb{H}$ can be reduced in the similar way as shown in [6]. In addition, the linear

equations in Eq. (3.29) can be solved by Cholesky factorization or conjugate gradient methods.

In the end, in light of the principles of interior-point methods, the step size should be determined so that the new data vector $\tilde{\mathbf{X}}_{\text{new}}$ will not violate the constraints. This requires the step size to be

$$\beta = \xi \min\{\beta_a, \beta_e, \beta_n, \hat{\beta}_k, e\},\ n \in \{0, \cdots, LN-1\},\ k \in \mathcal{K}_f, \tag{3.40}$$

where ξ is selected as a positive number less than 1 to ensure the updated point remain strictly feasible. Here, $\xi = 0.95$ is empirically chosen for fast convergence speed. β_a, β_e, β_n ($n \in \{0, \cdots, LN-1\}$) and $\hat{\beta}_k$ ($k \in \mathcal{K}_f$) are determined by the average power constraint (3.6), EVM minimization (3.3), peak power constraint (3.8) and free subcarrier spectral mask (3.5), respectively. The results are: β_a is

$$b_a = \Re(\mathbf{X}^H \mathbf{S} \mathbf{V}) - e, \tag{3.41}$$

$$\beta_a = \begin{cases} -b_a - \sqrt{b_a^2 - 2\delta_a}, & b_a < 0 \text{ and } b_a^2 - 2\delta_a \geq 0, \quad (3.42) \\ \infty, & \text{otherwise.} \quad (3.43) \end{cases}$$

β_e is

$$a_e = \|\mathbf{V}\|_2^2 - 1, \tag{3.44}$$

$$b_e = e + \Re\left((\tilde{\mathbf{X}} - \mathbf{X})^H \mathbf{S} \mathbf{V}\right), \tag{3.45}$$

$$\beta_e = \begin{cases} \dfrac{-b_e + \sqrt{b_e^2 + a_e \delta_e}}{a_e}, & a_e > 0 \text{ or } (a_e < 0 \text{ and } b_e > 0), \quad (3.46) \\ \dfrac{\delta_e}{2b_e}, & a_e = 0 \text{ and } b_e > 0, \quad (3.47) \\ \infty, & \text{otherwise.} \quad (3.48) \end{cases}$$

β_n ($n \in \{0, \cdots, LN-1\}$) has

$$a_n = |v[n]|^2, \tag{3.49}$$

$$b_n = \Re((\tilde{x}[n])^* v[n]), \tag{3.50}$$

$$\beta_n = \begin{cases} \dfrac{-b_n + \sqrt{b_n^2 + a_n \delta_n}}{a_n}, & a_n \neq 0, \quad (3.51) \\ \dfrac{\delta_n}{2b_n}, & a_n = 0 \text{ and } b_n > 0, \quad (3.52) \\ \infty, & \text{otherwise}, \quad (3.53) \end{cases}$$

where $v[n]$ with $n \in \{0, \cdots, LN-1\}$ is the n-th element of the time-domain updating vector $\mathbf{v} = \mathbf{F}^H \mathbf{V}$. And $\hat{\beta}_k$ ($k \in \mathcal{K}_f$) has

$$\hat{a}_k = |V_k|^2, \quad (3.54)$$

$$\hat{b}_k = \Re(\tilde{X}_k^* V_k), \quad (3.55)$$

$$\hat{\beta}_k = \begin{cases} \dfrac{-\hat{b}_k + \sqrt{\hat{b}_k^2 + \hat{a}_k \phi_k}}{\hat{a}_k}, & \hat{a}_k \neq 0, \quad (3.56) \\ \dfrac{\phi_k}{2\hat{b}_k}, & \hat{a}_k = 0 \text{ and } \hat{b}_k > 0, \quad (3.57) \\ \infty, & \text{otherwise}. \quad (3.58) \end{cases}$$

In summary, the procedure of the iterative customized IPM is

1. Initialize $\tilde{\mathbf{X}}$ so that it satisfies all the constraints. For instance, in the IEEE 802.11a standard, $\tilde{X}_k = 0$ ($k \in \mathcal{K}_f$) satisfies the spectral mask constraint on free subcarriers; $\tilde{X}_{\frac{N}{2}+1} = \sqrt{\sum_{k \in \mathcal{K}_d} |X_k|^2}$ and $\tilde{X}_k = 0$ ($k \in \mathcal{K}_d$ but $k \neq \frac{N}{2} + 1$) maintain the average power on data subcarriers not to be reduced; $\tilde{X}_k = X_k$ ($k \in \mathcal{K}_p$) keeps pilot subcarriers unchanged. The corresponding waveform $\tilde{\mathbf{x}}$ has PAR close to 0dB which satisfies practical deterministic PAR constraints. Also, initialize $e = 1.05\|\mathbf{S}(\mathbf{X} - \tilde{\mathbf{X}})\|_2$, obtained by backing off 5% from the EVM constraint (3.3).

2. Update the variables δ_a, δ_e, δ_n ($n \in \{0, \cdots, LN-1\}$), and ϕ_k ($k \in \mathcal{K}_f$) according to Eqs. (3.20)-(3.23), respectively.

3. Calculate the gradient vector $\mathbb{G}$ and the Hessian matrix $\mathbb{H}$ according to Eqs. (3.32) and (3.33), respectively.

4. Solve Eq. (3.29) for the updating vector $\mathbb{V}$.

5. Determine the step size β according to Eq. (3.40).

6. Update $\tilde{\mathbf{X}}$ and e according to Eqs. (3.27) and (3.28), respectively.

7. Stop if the algorithm converges or the maximum number of iterations has been reached, or return to Step 2 and start a new iteration.

Good convergence can generally be achieved within 10 iterations, for which the difference between the solution EVM and the optimal EVM is less than 0.001.

3.2.3 Performance Analysis

Some properties and numerical results of the proposed EVM optimization algorithm are illustrated in this subsection.

3.2.3.1 Peak Power Limited for the PA Input Signal

According to the constraint (3.8), the PA input signal becomes $\tilde{x}[n]$ whose peak magnitude is limited as

$$\max|\tilde{x}[n]| \leq \sqrt{\frac{\gamma}{\mathrm{IBO}}} \cdot \sigma_x \sqrt{\mathrm{IBO}} = \sqrt{\frac{\gamma}{\mathrm{IBO}}} \cdot \frac{\sqrt{P_{\mathrm{peak}}}}{G}, \tag{3.59}$$

where the second equality of (3.59) is given by Eq. (2.3).

By choosing $\mathrm{IBO} \geq \gamma$ in (3.59), the peak magnitude is always less than or equal to $\frac{\sqrt{P_{\mathrm{peak}}}}{G}$, thus eliminating the possibility of PA saturation as illustrated in Figure 2.3.

3.2.3.2 Average Power

From (3.9), it is straightforward to infer that, on the data subcarriers,

$$E\Big[\sum_{k\in\mathcal{K}_d}|\tilde{X}_k|^2\Big] \geq E\Big[\sum_{k\in\mathcal{K}_d}|X_k|^2\Big] = dP_0. \tag{3.60}$$

Eq. (3.60) indicates that, with the proposed algorithm, the average transmit power on the data subcarriers is not reduced. Also, because the signals on free subcarriers of the original symbol $\mathbf{X}$ are zero, we have,

$$E\Big[\sum_{k\in\mathcal{K}_f}|\tilde{X}_k|^2\Big] \geq E\Big[\sum_{k\in\mathcal{K}_f}|X_k|^2\Big] = 0. \tag{3.61}$$

Recall that the pilot subcarriers are unchanged and $\mathcal{K}_d \cup \mathcal{K}_f \cup \mathcal{K}_p = \{0, \cdots, N-1\}$, we have [c.f. (3.60) and (3.61)],

$$E\Big[\sum_{k=0}^{N-1} |\tilde{X}_k|^2\Big] \geq E\Big[\sum_{k=0}^{N-1} |X_k|^2\Big]. \tag{3.62}$$

By Parseval's theorem, the average power of the time-domain EVM-optimized signal has $\sigma_{\tilde{x}}^2 \geq \sigma_x^2$. Because no clipping occurs at the PA, the average power of the transmitted signal is $G^2\sigma_{\tilde{x}}^2$.

3.2.3.3 Deterministic PAR Constraint

The PAR of the optimized signal $\tilde{\mathbf{x}}$ is upper bounded by the deterministic threshold γ as

$$\text{PAR}(\tilde{\mathbf{x}}) = \max_{n \in \{0, \cdots, LN-1\}} \frac{|\tilde{x}[n]|^2}{\sigma_{\tilde{x}}^2} \leq \gamma. \tag{3.63}$$

To demonstrate the performance of the proposed EVM optimization scheme and the customized IPM algorithm, a few numerical results are illustrated in this section.

If not specifically indicated, the simulation setup follows the IEEE 802.11a standard [2]. $L = 4$, $N = 64$ and the spectral mask as defined in the IEEE 802.11a standard were used [2]. Without loss of generality, the OFDM symbols were drawn from a normalized QPSK constellation ($P_0 = 1$) for which the RMS EVM threshold is $\varepsilon = 0.1$. $p = 4$ subcarriers were used for transmitting the pilot signals at the indices of $\mathcal{K}_p = \{7, 21, 43, 57\}$ with the binary values of $\{1, -1, 1, 1\}$, respectively.

In Figure 3.1, the CCDF curves for the PAR values resulted by the EVM optimization algorithm are plotted for various PAR thresholds, i.e., $\gamma = 3$, 4, 5, 6 and 7dB. The corresponding RMS EVM values of the PAR-reduced symbols are also indicated in the figure. In this example, $f = 12$ free subcarriers were used as allocated in IEEE 802.11a [2]. We observe that these curves do not go beyond the $\eta = \gamma$ lines, thus confirming that the customized IPM does implement the intended deterministic PAR constraint.

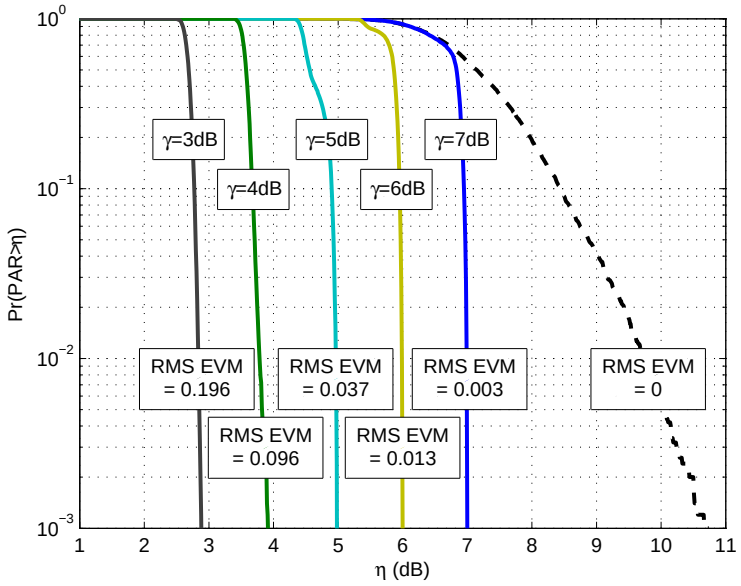

Figure 3.1: CCDF curves of the PAR of the EVM-optimized signal $\tilde{\mathbf{x}}$ for different PAR thresholds γ; the number of free subcarriers is $f = 12$. The PAR CCDF curve of the original OFDM signal is also shown.

3.2.3.4 Spectral Mask Constraint

Because of (3.60), the EVM-optimized signal $\tilde{\mathbf{X}}$ strictly satisfies the relative spectral mask constraint

$$E[|\tilde{X}_k|^2] \leq \mathcal{M}_k P_0 \leq \mathcal{M}_k \tilde{P}_0, \ k \in \mathcal{K}_f, \tag{3.64}$$

where $\tilde{P}_0 = \frac{1}{d} E[\sum_{k \in \mathcal{K}_d} |\tilde{X}_k|^2]$ is the average power on the data subcarriers of $\tilde{\mathbf{X}}$.

The power allocation of the EVM-optimized $\tilde{\mathbf{X}}$ for one random symbol realization is shown in Figure 3.2. The PAR threshold was $\gamma = 3.95$dB in this example. It shows that the signals on free subcarriers of the optimized symbol $\tilde{\mathbf{X}}$ strictly satisfy the spectral mask constraint imposed by standards. In addition, Figure 3.2 demonstrates that the EVM optimization algorithm keeps the pilot subcarriers unchanged. The errors that exhibit on the data subcarriers are the source of EVM.

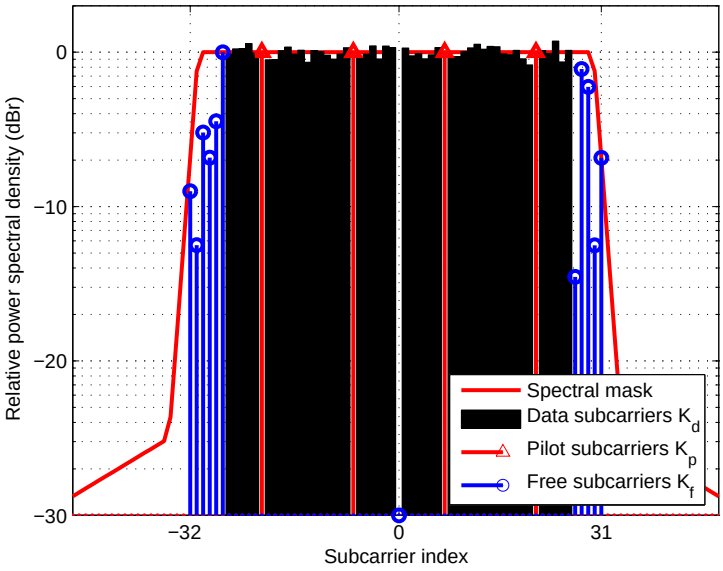

Figure 3.2: One realization of the EVM-optimized power allocation for $\tilde{\mathbf{X}}$; the PAR threshold is $\gamma = 3.95$dB; the number of free subcarriers is $f = 12$.

3.2.3.5 RMS EVM Lower Bounds

The EVM optimization algorithm offers a way to numerically determine the fundamental tradeoff between the in-band distortion and the power efficiency of PPC OFDM transmitters.

On one hand, the lower bound of RMS EVM values, denoted as $\varepsilon_{\min}$, can be determined for the given PAR threshold γ. The EVM optimization algorithm minimizes the symbol-wise EVM of each OFDM symbol. Therefore, the RMS EVM value found by the proposed algorithm is expected to be the minimum for the given deterministic PAR constraint.

Figure 3.3 shows the achievable RMS EVM as a function of the number of free subcarriers f for various PAR thresholds $\gamma = 3$, 4, 5, 6 and 7dB. The tradeoff between RMS EVM and power efficiency can be improved if one is allowed to use more free subcarriers. The cost is the reduced bandwidth efficiency since fewer subcarriers are used for data transmission.

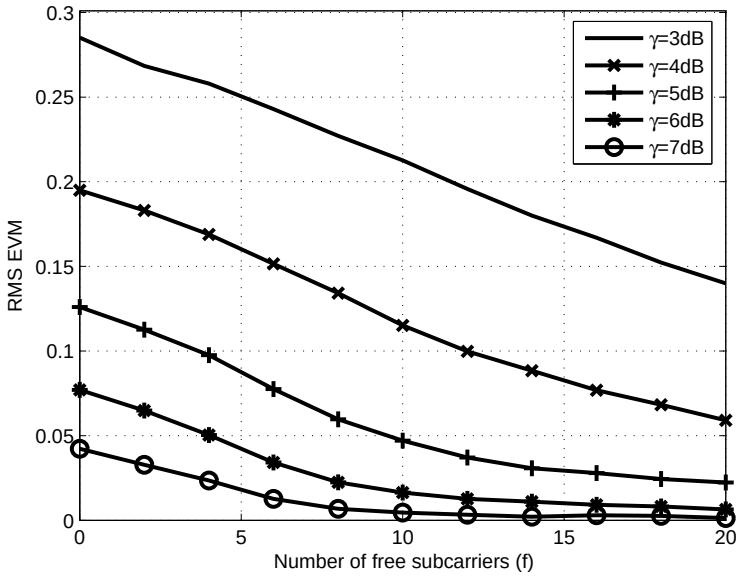

Figure 3.3: RMS EVM of the EVM-optimized signal $\tilde{\mathbf{x}}$ for different numbers of free subcarriers; the PAR threshold is $\gamma = 3$, 4, 5, 6 and 7dB.

In Figure 3.4, the tradeoff curves between the optimized RMS EVM values and the PAR threshold γ are shown for different numbers of free subcarriers ($f = 0$, 4, 8 and 12). The γ versus RMS EVM curves set the boundaries for system parameter designs. The feasibility regions only lie above these curves. For the assumed transmitter with the deterministic PAR constraint and spectral mask requirement, it also gives the lower bound for the achievable RMS EVM threshold $\varepsilon_{\min}$. For instance, Figure 3.4 shows that the minimum RMS EVM threshold is $\varepsilon_{\min} = 0.035$ for $\gamma = 5$dB and $f = 12$. It indicates that if IBO = 5dB is required with respect to the system power efficiency, no distortion-based PAR reduction algorithm can have in-band distortion with RMS EVM less than 0.035.

3.2.3.6 PAR Threshold Lower Bounds

On the other hand, the minimum PAR threshold can be found for the RMS EVM constraint ε as specified in standards.

In general, the higher the PAR threshold γ, the smaller the optimized symbol-wise

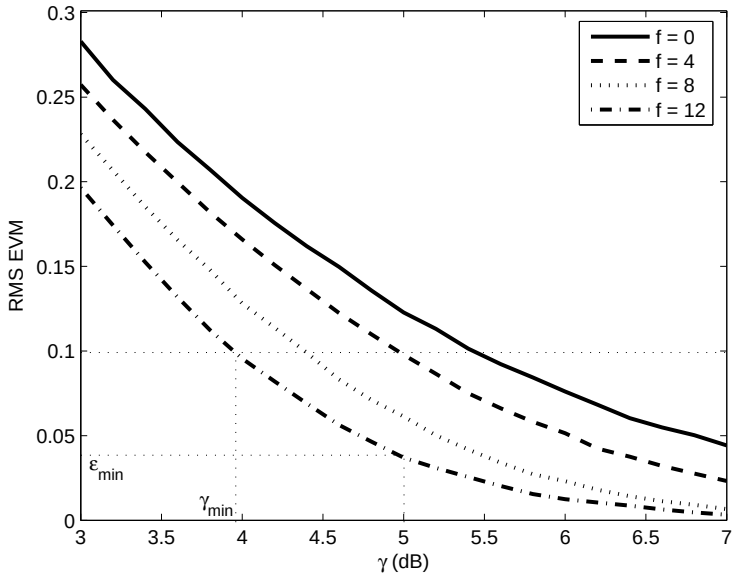

Figure 3.4: RMS EVM of the EVM-optimized signal $\tilde{\mathbf{x}}$ for different PAR threshold γ, when the number of free subcarriers $f = 0$, 4, 8 and 12.

EVM and RMS EVM tend to be. Therefore, we can determine, by off-line Monte Carlo simulations, the lowest possible γ whose corresponding RMS EVM value meets the standard's requirement. The problem can be formulated as follows:

$$\min \quad \gamma \tag{3.65}$$

$$\text{s.t.} \quad \text{RMS EVM} \leq \varepsilon, \tag{3.66}$$

where RMS EVM is a function of γ and has to be numerically calculated. The resulting minimum PAR threshold, denoted as $\gamma_{\min}$, gives the lower bound of the deterministic PAR threshold for the given RMS EVM threshold ε. In other words, no deterministic PAR constraint with $\gamma < \gamma_{\min}$ is feasible for the given RMS EVM and spectral mask constraints in the concerned system.

Figure 3.4 can be again used to determine the minimum PAR threshold $\gamma_{\min}$. For instance, since the RMS EVM threshold is $\varepsilon = 0.1$ for our simulation setup, only the curves below the RMS EVM = 0.1 dotted line are allowed. As a result, the minimum PAR threshold is about $\gamma_{\min} = 3.95$dB when $f = 12$ free subcarriers are to

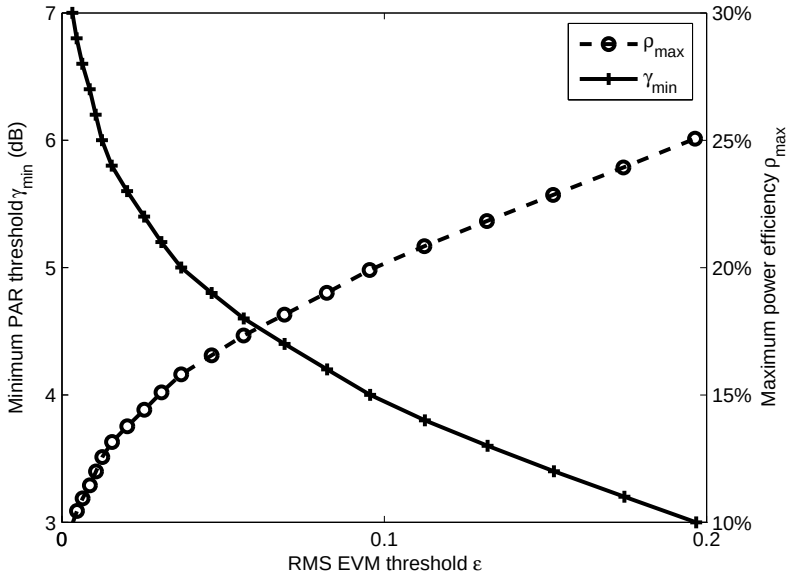

Figure 3.5: The minimum PAR threshold $\gamma_{\min}$ and the maximum power efficiency $\rho_{\max}$ as the functions of RMS EVM threshold ε; the number of free subcarriers is $f = 12$.

be employed. Any requirement for a PAR threshold lower than 3.95dB is unrealistic if the RMS EVM is expected to be ≤ 0.1. When compared with the original OFDM signal, a PAR reduction of 6.6dB is readily achieved at the 10^{-3} CCDF level.

In addition, $\gamma_{\min}$ is shown to be a monotonically decreasing function of the RMS EVM value of the EVM-optimized signals. As shown in Eq. (2.4), the PA power efficiency can be maximized by minimizing the IBO. Also, IBO $\geq \gamma$ is required. Therefore, by setting IBO $= \gamma_{\min}$, the maximum power efficiency is given by

$$\rho_{\max} = \frac{1}{2\gamma_{\min}}. \tag{3.67}$$

For $f = 12$, the upper bound of power efficiency is plotted for different RMS EVM thresholds in Figure 3.5. The greater the target power efficiency is, the more the in-band distortion should be allowed.

3.2.3.7 In the Presence of Predistorted Nonlinear PA

This subsection is dedicated to demonstrate the effectiveness of the EVM optimization algorithm in the presence of practical nonlinear PA.

Instead of the ideal soft-limit model in Eqs. (2.1)-(2.2), practical PAs exhibit other nonlinearities and memory effects besides saturation. Since the EVM and spectral growth should be measured on the output signals of the practical PA, Eq. (3.7) becomes $\tilde{\mathbf{x}} = g(\mathbf{F}^H \tilde{\mathbf{X}})$, where $g(\cdot)$ represents the response of the PA. This change will force the EVM optimization algorithm to adjust the OFDM symbols according to the actual PA response and thus provide the optimal solution. Intuitively, it is equivalent to realizing the EVM optimization and the digital predistortion of the PA response at the same time. However, it also makes the optimization problem too difficult to solve. A closed-form customized IPM method is no longer available for general PAs.

As introduced in Section 2.1, digital predistorters can be adopted to well linearize the practical PAs. Therefore, it is simpler to break the optimal solution into separate blocks, i.e., the concatenation of the EVM optimization algorithm in (3.2)-(3.8) and a digital predistorter as in [26]. Although sub-optimal performance is expected, the numerical results in Figure 3.6 illustrate that the solution is still quite effective.

In the simulation, the deployment of a practical PA, i.e., the PM2105 GaAs power amplifier [78], was assumed[1]. The nonlinearity and memory effects of the adopted PA were compensated by realizing an adaptive DPD with the indirect learning architecture and the memory polynomial as introduced in [26]. Following the notations in [26], the predistorter was assumed to have the memory order of $Q = 3$ and the nonlinearity order of $K = 5$. A block of 20 OFDM symbols was also taken in the training phase for the DPD identification.

In the presence of the linearized PA, Figure 3.6 gives the RMS EVM versus γ

[1]Thanks to Professor J. Stevenson Kenney for the experimental data of PA PM2105.

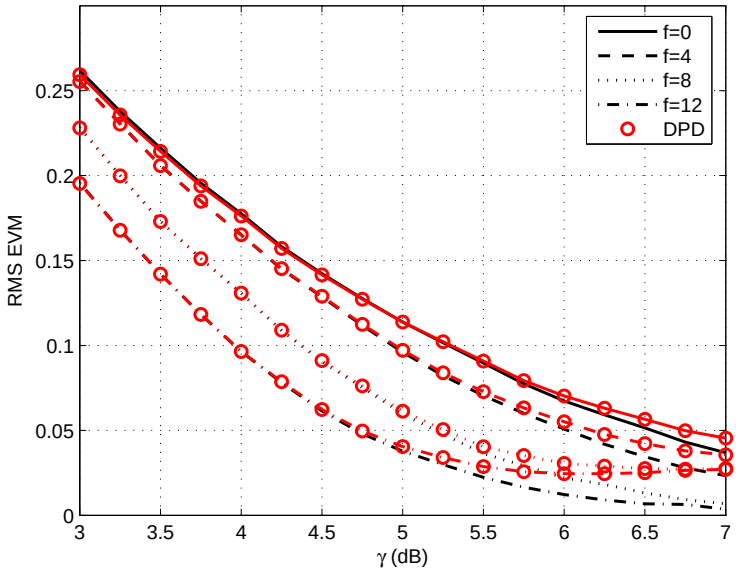

Figure 3.6: The RMS EVM versus PAR threshold γ curves of the EVM-optimized signal $\tilde{\mathbf{x}}$ passed through a linearized PA; the number of free subcarriers $f = 0$, 4, 8 and 12.

curves for different numbers of free subcarriers. Compared with the curves in the SL model, it is shown that the EVM optimization method can still achieve near-optimal RMS EVM values, especially for small PAR thresholds. When the RMS EVM constraint $\varepsilon = 0.1$ is effective, the linearized PA can achieve almost the same PAR threshold (i.e., power efficiency) with the SL case. Therefore, DPD designs further facilitate the applications of the EVM optimization method in practice.

3.2.4 Parameter Optimizations

To reduce the PAR values of OFDM signals is not the ultimate design goal. Rather, the transmission performance, e.g., the error performance and system throughput, should be improved by utilizing the PA power consumption more efficiently. Therefore, the optimal system parameters can be designed within the EVM optimization framework.

3.2.4.1 SNDR Maximization

The signal-to-noise-and-distortion ratio (SNDR) is an effective metric of the ratio between the signal power and the uncorrelated noise plus distortion power [85]. It can substitute SNR in BER or SER expressions to determine the error performance. Since all meaningful BER and SER expressions are monotonic in SNDR, it is important to determine the optimal PAR threshold that maximizes SNDR.

Although the EVM-optimized signal $\tilde{\mathbf{x}}$ (or $\tilde{\mathbf{X}}$) is a highly nonlinear function of the original OFDM signal $\mathbf{x}$ (or $\mathbf{X}$), the data subcarriers of $\tilde{\mathbf{X}}$ can be decomposed according to Bussgang's theorem [88] as

$$\tilde{X}_k = \alpha X_k + \omega_k, \ \forall k \in \mathcal{K}_d, \tag{3.68}$$

where ω_k ($k \in \mathcal{K}_d$) denotes the distortion noise with variance $\sigma_\omega^2 = E[|\tilde{X}_k|^2] - |\alpha|^2 E[|X_k|^2]$. α is a constant chosen so that ω_k is uncorrelated with X_k, i.e., $\alpha = E[X_k^* \tilde{X}_k]/E[|X_k|^2]$ and thus $E[X_k^* \omega_k] = 0$ where the expectations are evaluated over X_k and $\tilde{X}_k$ on $k \in \mathcal{K}_d$ and all OFDM symbols. The SNDR of the kth data subcarrier of the output signal is thus defined as [77]

$$\text{SNDR}_k = \frac{G^2 |h_k|^2 |\alpha|^2 E[|X_k|^2]}{G^2 |h_k|^2 \sigma_\omega^2 + \sigma_k^2}, \ k \in \mathcal{K}_d, \tag{3.69}$$

where h_k is the frequency-domain channel response and σ_k^2 is the channel noise power of the kth subcarrier. It can be further expressed approximately as a function of the RMS EVM and γ as follows [61]

$$\text{SNDR}_k \approx \frac{1 - (\text{RMS EVM})^2}{(\text{RMS EVM})^2 + \frac{2d\sigma_k^2}{rP|h_k|^2} \cdot \gamma}, \ k \in \mathcal{K}_d, \tag{3.70}$$

where $P = 2LNP_{\text{peak}}$ denotes the total power consumed by the PPC class-A PA for transmitting one OFDM symbol, and r is defined as the ratio between the power transmitted on the data subcarriers and the total power, i.e.,

$$r = \frac{E[\sum_{k \in \mathcal{K}_d} |X_k|^2]}{E[\sum_{k=0}^{N-1} |X_k|^2]} = \frac{dP_0}{dP_0 + \sum_{k \in \mathcal{K}_p} |\mathcal{P}_k|^2}, \tag{3.71}$$

which is a constant and can be calculated according to the subcarrier categorization.

In the EVM optimization algorithm, because the optimized RMS EVM is a function of the PAR threshold γ, the SNDR in Eq. (3.70) can be maximized over γ for known channel state information h_k and σ_k^2, i.e.,

$$\gamma^\star = \arg\max_{\gamma} \ \mathrm{SNDR}_k \Big|_{h_k, \sigma_k^2}. \tag{3.72}$$

It is worth noting that, the RMS EVM value that corresponds to the optimal $\gamma^\star$ may be different from (or even greater than) the constraint defined in the standards, but this RMS EVM value and PAR threshold will introduce the optimal SNDR performance for the given transmitters and channel. Intuitively, although in-band distortion may be increased by using a smaller γ, the average transmit power is also boosted such that the channel noise is equivalently suppressed. Using the γ-RMS EVM curves obtained *a priori* by (3.65) and (3.66), the optimal PAR threshold $\gamma^\star$ can be determined by on-line calculation of Eq. (3.72) which is enabled by the SNDR approximation in Eq. (3.70). Then, the optimal tradeoff between in-band distortion and power efficiency can be reached by the EVM optimization algorithm.

Assume flat channels with additive white Gaussian channel noise where $h_k = h$ and $\sigma_k^2 = \sigma^2$ $(\forall k)$ are known at the transmitter. In addition, define the PA-power-to-noise ratio (PNR) for the considered class-A PA and channel as

$$\mathrm{PNR} = \frac{rP|h|^2}{d\sigma^2}, \tag{3.73}$$

which is completely determined by the transmitter setup and channel states. Then the SNDR in Eq. (3.70) can be further simplified as

$$\mathrm{SNDR}_k \approx \frac{1 - (\text{RMS EVM})^2}{(\text{RMS EVM})^2 + \frac{2\gamma}{\mathrm{PNR}}}, \ \forall k \in \mathcal{K}_d. \tag{3.74}$$

For any given PNR, Eq. (3.74) can be numerically evaluated with the help of the γ versus RMS EVM curves shown in Figure 3.4. In Figure 3.7, the γ versus SNDR curves which are obtained from Monte Carlo simulations with Eq. (3.69) and from

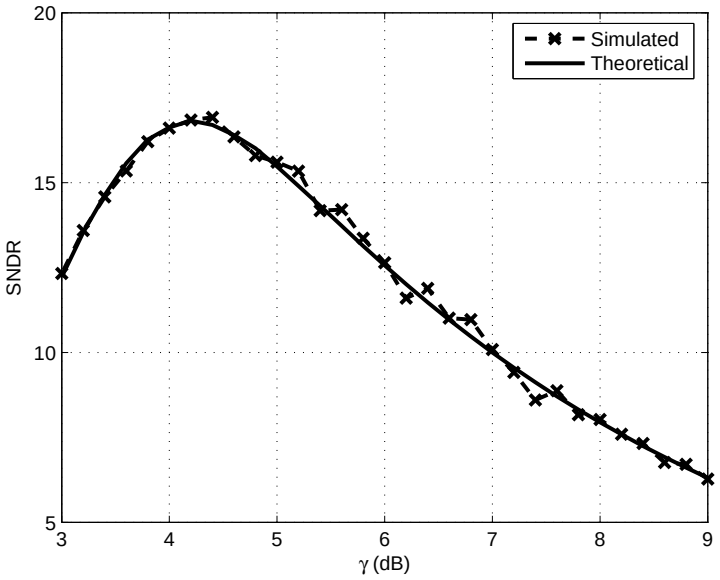

Figure 3.7: The SNDR versus PAR threshold γ curves of the Monte Carlo simulation and the SNDR approximation in Eq. (3.74); PNR = 20dB; the number of free subcarriers is $f = 12$.

the SNDR approximation in Eq. (3.74) are compared. The approximate expression Eq. (3.74) is shown to be fairly accurate. Therefore, the approximation in Eq. (3.74) enables the on-line parameter adjustment to maximum SNDR when channel state information is known. For PNR ranging from 15dB to 30dB, their SNDR curves are plotted in Figure 3.8. As expected, the greater the PNR, the greater the SNDR.

Consequently, the optimal $\gamma^\star$ can be found for the given PNR value. As illustrated in Figure 3.8, the optimal PAR threshold $\gamma^\star$ varies as a function of PNR. Figure 3.9 summarizes the optimal $\gamma^\star$ and the corresponding RMS EVM values for PNR from 15dB to 30dB and $f = 12$. The main observation is, the greater the PNR, the larger the optimal PAR threshold $\gamma^\star$ and the smaller the optimal RMS EVM. Intuitively, when PNR is large, the channel noise has little effect and the distortion noise is dominant. Instead of trying to reduce the PAR threshold and increasing the average transmit power, lower level distortion should be pursued. On the other hand, when the channel noise is not negligible, reducing IBO by introducing nonlinear distortions

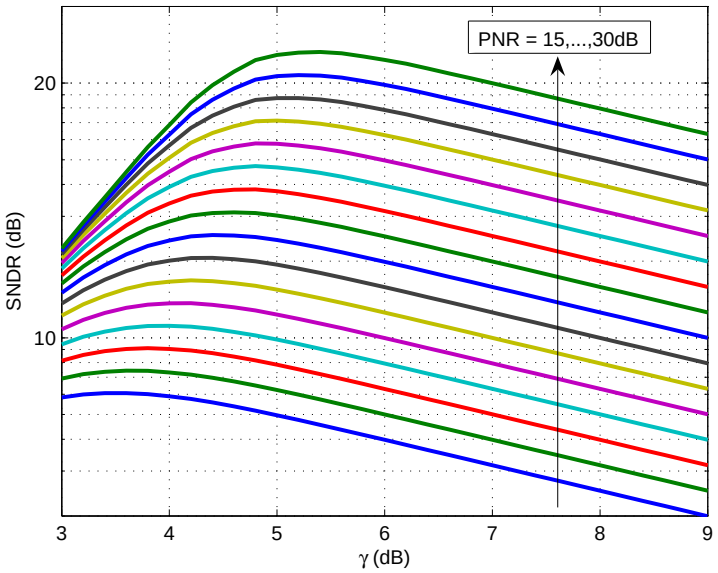

Figure 3.8: SNDR as a function of the PAR threshold γ of EVM-optimized OFDM signal $\tilde{\mathbf{x}}$ with PNR $= 15, 16, \cdots, 30$dB (in step size of 1 dB), and the number of free subcarriers $f = 12$.

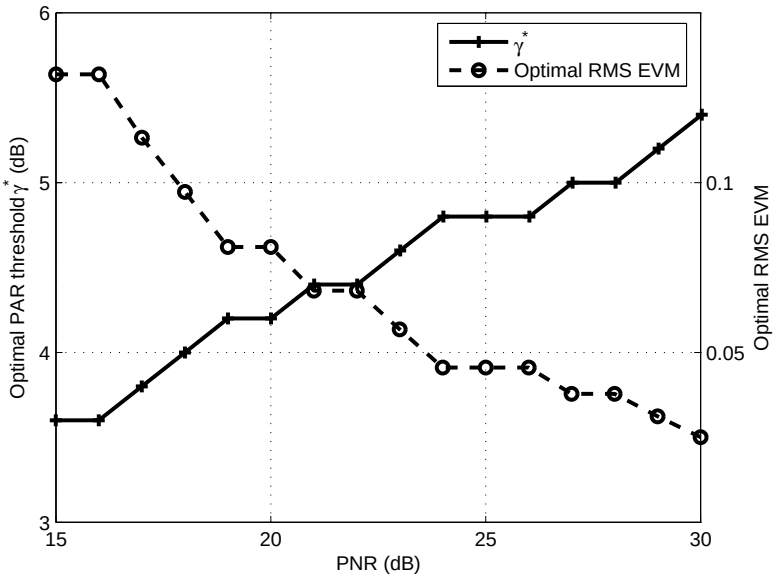

Figure 3.9: The SNDR-maximizing PAR threshold $\gamma^\star$ and RMS EVM values for PNR $= 15, 16, \cdots, 30$dB (in step size of 1dB), and the number of free subcarriers $f = 12$.

can help to suppress the total noise and maximize SNDR. Furthermore, Figure 3.9 demonstrates that the RMS EVM threshold ε given in the standard, which is 0.1 for the simulation setup, is not always optimal. For a small PNR, the optimal RMS EVM can be greater than ε.

3.2.4.2 Throughput Maximization

As was argued in the last subsection, SNDR is analogous to SNR in error rate expressions. Another pertinent performance optimization is system throughput (or mutual information) maximization. The relationship between SNDR and capacity has been derived in [85]. It shows that because the distortion term w_k in Eq. (3.68) is approximately Gaussian distributed, the lower bound of the mutual information on each data subcarrier is $C_k \geq \log_2(1+\text{SNDR}_k)$ bits/symbol ($\forall k \in \mathcal{K}_d$). Accordingly, when a flat channel response is assumed so that $\text{SNDR}_k = \text{SNDR}$, the total system throughput per symbol is lower bounded by

$$\sum_{k\in\mathcal{K}_d} C_k \geq d \cdot \log_2(1+\text{SNDR}) = C \text{ bits/symbol.} \tag{3.75}$$

Unlike SNDR maximization, throughput lower bound maximization involves a trade-off in the number of data subcarriers, d. When more data subcarriers are used, the sum in (3.75) involves more terms and leads to an increase in the throughput. However, these additional terms come at the expense of fewer free subcarriers (smaller f), which means less PAR reduction is possible (see Figure 3.4) and may cause an ultimately lower SNDR.

Therefore, the pair of parameters (γ, f) should be selected so that the throughput is maximized. It can be summarized as the following maximization problem

$$\max_{\gamma,\ f} \quad C, \tag{3.76}$$

where C is defined in Eq. (3.75). This lower bound is implicitly a function of the set of variables (γ, RMS EVM, f). With the help of off-line calculated γ-RMS EVM curves

for different f, the lower bound in Eq. (3.75) can be evaluated and the maximization problem of (3.76) can be solved on-line with known channel state information.

In Figure 3.10, we demonstrate how the throughput lower bound varies with the number of free subcarriers. In this example the PNR value is set to 20dB. The plot shows that the maximum throughput lower bound is achieved at $(\gamma, f) = (5\text{dB}, 0)$ which means all subcarriers should be used for transmitting data and pilot signals, instead of being used to reduce EVM. On the contrary, the corresponding SNDR values will be maximized by using as many free subcarriers as possible. Different objectives yield different optimal system setups.

The optimal thresholds were calculated for different PNR values as shown in Figure 3.11. Surprisingly, for the simulated PNR region, the optimal number of free subcarriers is always 0. Intuitively, the reason is that the symbol-wise EVM has already been minimized by the EVM optimization algorithm. With more free subcarriers, the help on further reducing the symbol-wise EVM is trivial. Instead, subcarriers should be used to transmit data so that the throughput is increased significantly.

This observation further simplifies the throughput maximization problem. The number of free subcarriers can be prescribed to zero so that the throughput maximization problem simplifies to the aforementioned SNDR maximization problem.

3.2.5 PAR Reduction Performance Comparison

The PAR reduction performance of the proposed EVM optimization method is compared with several existing PAR reduction algorithms in this subsection, including the repeated clipping and filtering (RCF) [10], iterative constrained clipping (ICC) [12] and PAR optimization algorithms [6].

In Figure 3.12, the RMS EVM thresholds of these algorithms were all set to 0.1 so that they all satisfied the given RMS EVM constraint in IEEE 802.11a. Specifically, this was achieved by empirically predetermining the clipping threshold at 5.3dB in

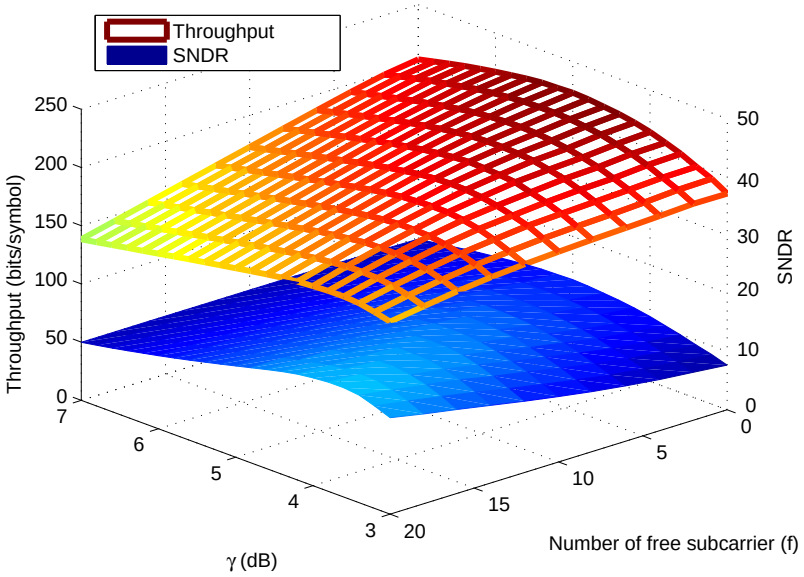

Figure 3.10: Throughput lower bounds and the corresponding SNDR values for the flat channel with PNR = 20dB.

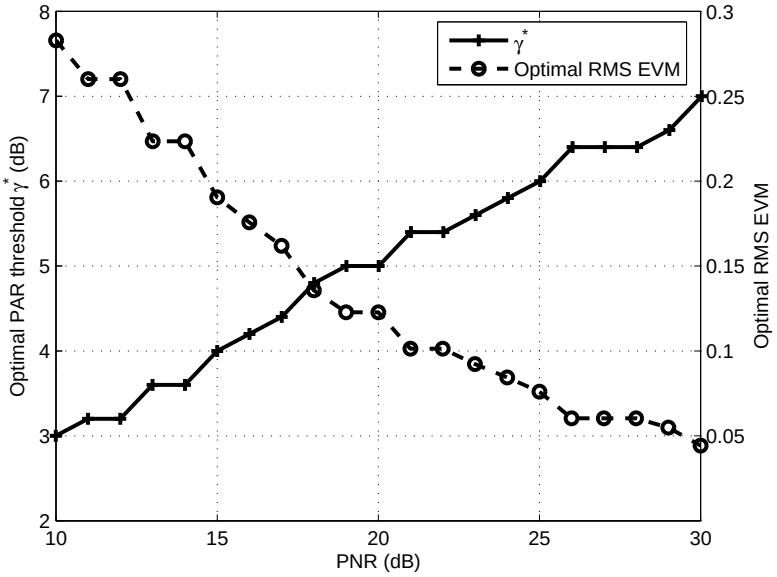

Figure 3.11: The throughput-maximizing PAR threshold $\gamma^\star$ and RMS EVM values for PNR = 10, 11, $\cdots$, 30dB; the optimal number of free subcarriers is always $f = 0$ by calculating the maximization problem in (3.76).

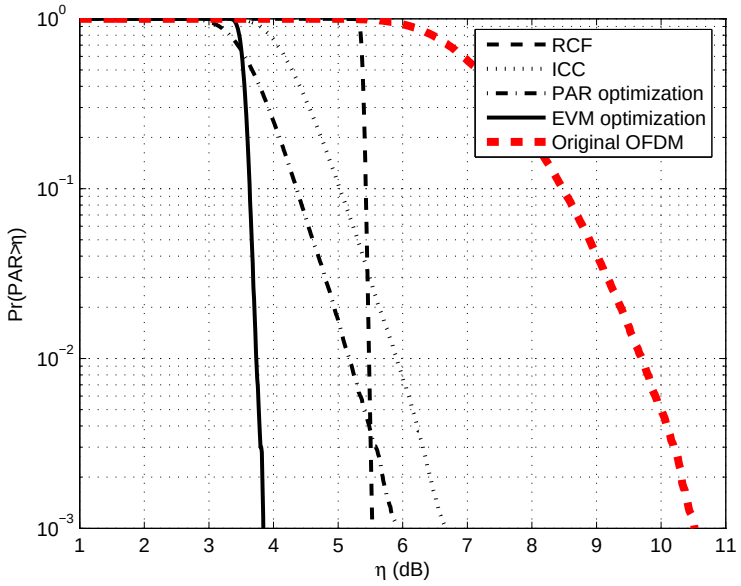

Figure 3.12: CCDF curves of the PAR of the RCF, ICC, PAR optimization, EVM optimization algorithms, and the original OFDM signal; the RMS EVM threshold 0.1 is satisfied by symbol-wise EVM constraints for ICC and PAR optimization, and by RMS EVM constraints for RCF and EVM optimization; $f = 12$.

the RCF algorithm. The ICC and PAR optimization algorithms both enforced a symbol-wise EVM constraint of 0.1. For the ICC algorithm, the clipping threshold of 2.8dB was empirically chosen so that the best PAR reduction performance was obtained at the 10^{-3} CCDF level. 15 iterations were taken for RCF and ICC.

The EVM optimization algorithm is shown to achieve the best PAR reduction performance either with or without the piece-wise linear scaling [76]. Without piece-wise linear scaling, the power efficiency is inversely proportional to the maximum PAR. For the comparisons with RCF and ICC, as well as with the PAR optimization, it is clear from Figure 3.12 that the EVM optimization algorithm has a lower PAR (upper-bounded by the deterministic constraint of 3.95dB) for almost all CCDF levels and thus, will have higher power efficiency. When the piece-wise linear scaling is applied before the PA, on the other hand, the average power efficiency has been shown to be inversely proportional to the harmonic mean of symbol-wise PARs [64, Eq. (18)].

Even though the CCDF curves of the EVM optimization and PAR optimization have a crossing point, it can be shown that the EVM optimization yields the smallest harmonic mean of symbol-wise PAR.

Furthermore, the proposed EVM optimization is the only algorithm that guarantees the deterministic PAR constraint. The CCDF curves of ICC and PAR optimization methods have negative slopes. The clipped signals in the RCF method suffered from peak regrowth due to the filtering, which resulted in the PAR value of 5.55dB at the 10^{-3} CCDF level although 5.3dB clipping ratio was used. In order to compare the γ-RMS EVM curves, the PAR value at the 10^{-3} CCDF level was over-optimistically chosen as the PAR threshold γ for these algorithms in the comparison group. The exact γ-RMS EVM tradeoff should be even worse since 0.1% OFDM symbols are still saturated with IBO $= \gamma$ for these algorithms.

For the same setup, the γ-RMS EVM tradeoff curves of the RCF, ICC, PAR optimization and EVM optimization algorithms are plotted in Figure 3.13. The EVM optimization algorithm achieves the optimal tradeoff between RMS EVM and PAR threshold. It sets the lower bound for other algorithms. The tradeoff curves for the RCF and PAR optimization algorithms were obtained by varying the clipping ratio and the symbol-wise EVM threshold, respectively. For the ICC algorithm, the clipping ratio was also optimized for each symbol-wise EVM threshold off-line so that the resulting PAR was minimized [12]. This provided the best tradeoff that could be achieved by the ICC algorithm. The specific examples shown in Figure 3.12 (i.e., RMS EVM = 0.1) also confirm the tradeoff curves in Figure 3.13.

3.3 MCPTS PAR Reduction Method in OFDM-FDMA Systems

To reduce the PAR of OFDM-based frequency-division multiple access systems, we propose a low-complexity multi-channel partial transmit sequences (MCPTS) method

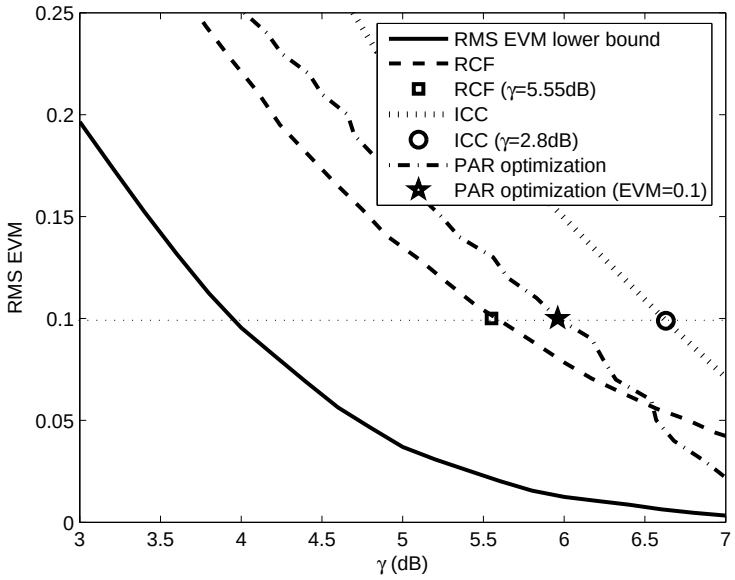

Figure 3.13: The γ-RMS EVM tradeoff curves of the RCF, ICC and PAR optimization methods, compared with the RMS EVM lower bound given by the EVM optimization algorithm; the number of free subcarriers is $f = 12$.

that requires no receiver-side modification and thus is compatible with existing systems.

3.3.1 OFDM-FDMA Systems

OFDM-based frequency-division multiple access (OFDM-FDMA) systems have been defined in several standards to support multiuser communications. In OFDM-FDMA, the frequency spectrum is channelized into adjacent fragments on each of which a (or multiple) separate OFDM user(s) can communicate. For instance, 5-20MHz and 1.25-20MHz channelization schemes were specified in the IEEE 802.11a and the IEEE 802.16 standards, respectively [2, 3]. OFDM-FDMA is also a promising technique for high data rate communications in future cellular systems. It is currently a strong candidate for the downlink multiple access scheme in the Long Term Evolution of cellular systems under consideration by the Third Generation Partnership Project (3GPP) [28].

In practice, however, hardware restrictions present an additional factor for the

base station design, where all downlink (from base station to mobile station) signals are transmitted concurrently. It is possible to configure one PA and one antenna for each channel. However, it will considerably increase the cost of the base station and bring extra difficulty in hardware debugging. Thus, it is much favored to have a single wideband PA transmitting the signals of all channels.

Nevertheless, the downlink signals are summed up in time domain in this case, thus also possessing large PAR values, even if individual PAR reduction method is applied on the OFDM signal of each channel. Therefore, the PAR problem is even more challenging in OFDM-FDMA systems and has to be solved to enable the use of the single-PA base station.

The structure diagram of the base station transmitter in the OFDM-FDMA system is shown in Figure 3.14. Synchronous transmission is assumed in this section, where the start and end times of OFDM symbols among all channels are synchronized [63]. The asynchronous system is addressed and can be found in [65]. Independent OFDM signals are transmitted on M different frequency bands, whose center frequencies are f_m and satisfy a non-overlap condition, $f_{m+1} - f_m \geq \frac{1}{2}(B_{m+1} + B_m)$ $(m = 1, \cdots, M-1)$ where B_m is the frequency bandwidth of the mth channel.

For each of the OFDM signals, data are transmitted on N_m orthogonal subcarriers which make up the OFDM symbol, denoted as $\mathbf{X}_m = [X_{m,0}, \cdots, X_{m,N_m-1}]^T$. For notational simplicity, $B_m = B$ and $N_m = N$ are assumed in this section, but the results can be generalized accordingly. An L-times oversampling IFFT operation is performed to generate the baseband time-domain samples of each channel

$$x_m[n] = \frac{1}{\sqrt{LN}} \sum_{k=0}^{N-1} X_{m,k} e^{\frac{j2\pi kn}{LN}}, \ n = 0, \cdots, LN-1, \tag{3.77}$$

i.e., $\mathbf{x}_m = \mathbf{F}^H \mathbf{X}_m$. Then, the baseband signals is up-converted to passband and combined as the input to the PA, i.e.,

$$x_p[n] = \sum_{m=1}^{M} x_m[n] e^{\frac{j2\pi nTf_m}{LN}}, \tag{3.78}$$

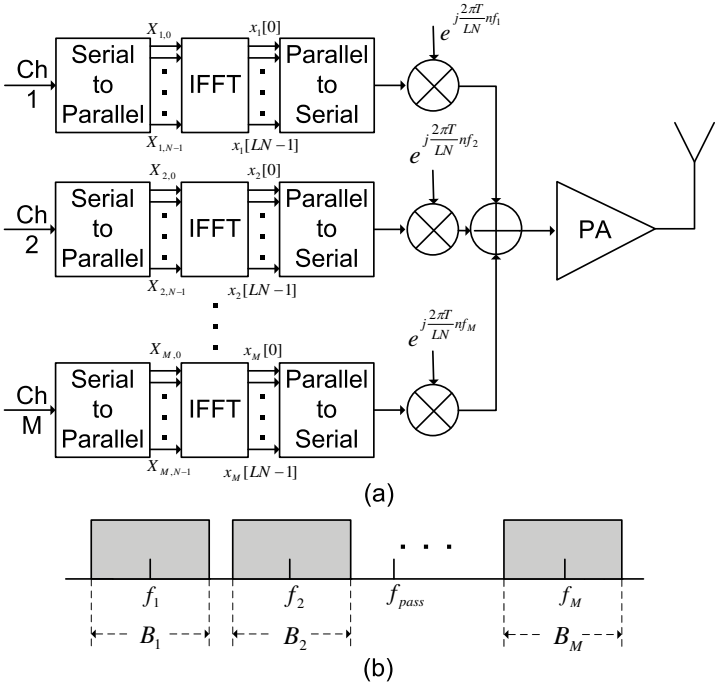

Figure 3.14: The (a) structure and (b) frequency spectrum diagram of the base station in OFDM-FDMA systems.

where $T = N/B$ is the symbol duration. The center frequency of the above passband signal can be found as $f_{\text{pass}} = \frac{1}{2}(f_1 + f_M) + \frac{1}{4}(B_M - B_1)$ and the equivalent baseband signal is $\mathbf{x} = [x[0], \cdots, x[LN-1]]^T$ with $x[n] = x_p[n]e^{-\frac{j2\pi nTf_{\text{pass}}}{LN}}$. Since the baseband PAR can be used to infer the passband dynamic range [100], we consider the symbol-wise PAR defined as

$$\text{PAR}(\mathbf{x}) = \frac{\|\mathbf{x}\|_\infty^2}{\frac{1}{LN}\|\mathbf{x}\|_2^2}. \tag{3.79}$$

For the soft-limit PA, piece-wise linear scaling (PWLS) can be used so that no clipping occurs, in which the OFDM symbol is modified such that $\mathbf{x}_{\text{PWLS}} = P_{\text{peak}}^{1/2}\mathbf{x}/\|\mathbf{x}\|_\infty$. Thus, reduction in the PAR leads to increase in the average transmit power [76].

3.3.2 MCPTS in Synchronous OFDM-FDMA Systems

Partial transmit sequence (PTS) approach has been proposed to reduce the PAR of OFDM signals [73]. The basic idea is to produce U time-domain representations for the same OFDM symbol and transmit the representation with the smallest PAR

value. The set of OFDM subcarrier indices is partitioned into S disjoint sets $\mathbf{S}_s$ ($s = 1, \cdots, S$), having $\bigcup_{s=1,\cdots,S} \mathbf{S}_s = \{0, \cdots, N-1\}$ and $\mathbf{S}_p \bigcap \mathbf{S}_q = \emptyset$ ($p \neq q,\ 1 \leq p, q \leq S$). U independent phase sequences with independent phase shifts on each set $\mathbf{S}_s$, i.e., $\Theta^{(u)} = [e^{j\theta_1^{(u)}}, \cdots, e^{j\theta_S^{(u)}}]^T$ and $\theta_s^{(u)} \in [0, 2\pi)$ ($u \in \{1, \cdots, U\}$), are available to both transmitters and receivers. The superscript is used for the index of the multiple representations and the subscript is used for the index of partitions. In the time domain, U different representations are obtained via

$$\mathbf{x}^{(u)} = \text{IFFT}[\mathbf{X}^{(u)}] = \text{IFFT}[\mathbf{X} \circ \Phi^{(u)}],\ u = 1, \cdots, U, \tag{3.80}$$

where $\circ$ denotes element-wise multiplication, $\Phi^{(u)} = [\phi_0^{(u)}, \cdots, \phi_{N-1}^{(u)}]^T$ and $\phi_k^{(u)} = e^{j\theta_s^{(u)}}$ if $k \in \mathbf{S}_s$. Since phase rotations do not change the average power, we have $\|\mathbf{x}\|_2^2 = \|\mathbf{x}^{(u)}\|_2^2$ ($\forall u \in \{1, \cdots, U\}$). The $\tilde{u}$th sequence will be transmitted whose PAR is the smallest, i.e., $\tilde{u} = \arg \min_{u \in \{1,\cdots,U\}} \text{PAR}(\mathbf{x}^{(u)})$. Inevitably, the index $\tilde{u}$ has to be sent as side information such that the phase shifts can be reversed at the receiver side.

In this section, the PTS method is extended to the OFDM-FDMA system, referred as the MCPTS method. In the synchronous transmitter, the whole frequency-domain symbols $\mathbf{X}_m$ ($m = 1, \cdots, M$) can be regarded as a single data block. The individual symbols to the data block is the same as the subcarrier subsets to the OFDM symbol in the PTS method. Therefore, for the multi-channel system, there is a natural and simple partition scheme determined by the channelization. The number of partitions is $S = M$ and $\mathbf{S}_s$ includes the indices of $\mathbf{X}_m$ ($s = m \in \{1, \cdots, M\}$). The M-by-1 phase sequence $\Theta = [e^{j\theta_1}, \cdots, e^{j\theta_M}]^T$ will then be determined to minimize the PAR value, formulating the MCPTS approach in the following way

$$\min_{\theta_m \in [0, 2\pi)} \quad \text{PAR}(\tilde{\mathbf{x}}) \tag{3.81}$$

$$\text{s.t.} \quad \tilde{\mathbf{x}}_m = e^{j\theta_m} \mathbf{F}^H \mathbf{X}_m = e^{j\theta_m} \mathbf{x}_m \tag{3.82}$$

$$\tilde{x}[n] = \sum_{m=1}^{M} \tilde{x}_m[n] e^{\frac{j2\pi nT}{LN}(f_m - f_{\text{pass}})}. \tag{3.83}$$

In the end, the signal after adaptive linear scaling will be transmitted, i.e., $\mathbf{x}_{\text{PWLS}} = \tilde{\mathbf{x}} P_{\text{peak}}^{1/2} / \|\tilde{\mathbf{x}}\|_\infty$. Each of the partitions in the MCPTS method is just a single channel. With the assumption of ideal channel estimation, this property provides MCPTS a couple of merits that make it favored for this system:

1. Neither side information nor receiver-side modification is needed. The phase rotation is equivalently part of the channel response and can be recovered by the channel estimation capability of each OFDM channel;

2. Since no side information should be transmitted, phase rotation can take on any value (rather than prescribed sequences), leading to better PAR reduction performance. Optimization techniques, such as the particle swarm optimization (PSO) [43], can be used to solve (3.81)-(3.83).

3.3.3 Joint MCPTS and Power Allocation

For the peak power constrained PA, reducing PAR can increase the effective average output power. However, for fading channels, power allocation should also be designed so that the potential average power increase can be effectively utilized. Accordingly, we propose that each subcarrier in each channel be scaled so that the average power of the kth subcarrier in the mth channel is $P_{m,k}$, i.e., $\bar{X}_{m,k} = X_{m,k}(P_{m,k}/E[|X_{m,k}|^2])^{\frac{1}{2}}$. We assume the transmitter has the channel state information (CSI), including the frequency response $h_{m,k}$ and the variance of the Gaussian channel noise $\sigma_{m,k}^2$. The signal-to-noise ratio of a given subcarrier is

$$\text{SNR}_{m,k} = P_{m,k} \frac{|h_{m,k}|^2}{\sigma_{m,k}^2} = \frac{P_{m,k}}{\hat{\sigma}_{m,k}^2}, \tag{3.84}$$

where $\hat{\sigma}_{m,k}^2 = \frac{\sigma_{m,k}^2}{|h_{m,k}|^2}$ is the equivalent channel noise power. The values for $P_{m,k}$ will be determined to minimize the average BER.

Given the peak power constraint, the joint PAR reduction and average BER-minimizing power allocation problem can be formulated as:

$$\min_{P_{m,k},\ \theta_m} \quad \frac{1}{MN}\sum_{m=1}^{M}\sum_{k=0}^{N-1} P_B\left(\mathrm{SNR}_{m,k}\right) \tag{3.85}$$

$$\text{s.t.} \quad \sum_{m=1}^{M}\sum_{k=0}^{N-1} P_{m,k} = \|\tilde{\mathbf{x}}\|_2^2 \le \frac{LNP_{\text{peak}}}{\mathrm{PAR}(\tilde{\mathbf{x}})} \tag{3.86}$$

$$\tilde{x}[n] = \sum_{m=1}^{M} \tilde{x}_m[n] e^{\frac{j2\pi nT}{LN}(f_m - f_{\text{pass}})} \tag{3.87}$$

$$\tilde{\mathbf{x}}_m = e^{j\theta_m}\mathbf{F}^H\bar{\mathbf{X}}_m,\ \forall m \in \{1,\cdots,M\}, \tag{3.88}$$

where $P_B(\mathrm{SNR})$ is the instantaneous BER for the constellation of interest. Eq. (3.86) relates the average power with the peak power constraint and is a very complicated function of both $P_{m,k}$ and θ_m. Because the convexity of this problem is not clear, it is hard to solve.

We propose an iterative algorithm to find a suboptimal solution to this problem. First, for an initial objective average power $P_{\text{av}}^0 \triangleq \frac{LNP_{\text{peak}}}{\mathrm{PAR}^0}$, the BER-minimizing power allocation solves the Lagrangian problem

$$\frac{\partial}{\partial P_{m,k}}\left[-\sum_{m=1}^{M}\sum_{k=0}^{N-1} P_B\left(\frac{P_{m,k}}{\hat{\sigma}_{m,k}^2}\right) - \lambda P_{m,k}\right] = 0 \tag{3.89}$$

$$\sum_{m=1}^{M}\sum_{k=0}^{N-1} P_{m,k} = P_{\text{av}}^0. \tag{3.90}$$

Assuming QPSK modulation with Gray mapping, where $P_B(x) = \mathrm{erfc}(x/\sqrt{2})/2$ [83, P. 271], Eq. (3.89) becomes

$$\frac{1}{\sqrt{\hat{\sigma}_{m,k}^2 P_{m,k}}} e^{-\frac{P_{m,k}}{2\hat{\sigma}_{m,k}^2}} = 2\sqrt{2\pi}\lambda, \tag{3.91}$$

for $m = 1,\cdots,M$ and $k = 0,\cdots,N-1$. $P_{m,k}$ is a function of the Lagrangian parameter λ. By Eq. (3.90), λ can be determined and results in $P_{m,k}$'s. Unfortunately, although $P_{m,k}$ is one-to-one mapping with λ, the functional relationship cannot be described in a closed form.

A closed-form approximate solution to the above problem can be developed by replacing the Q function with the Chernoff upper bound, i.e., $Q(x) < e^{-\frac{x^2}{2}}$. Then, Eq. (3.89) yields

$$P_{m,k} = -2\hat{\sigma}^2_{m,k}[\ln 2\lambda + \ln \hat{\sigma}^2_{m,k}],\ \forall m \in \{1, \cdots, M\},\ k \in \{0, \cdots, N-1\}. \quad (3.92)$$

Combining with Eq. (3.90), the power allocation can be summarized as

$$P_{m,k} = \begin{cases} 2\hat{\sigma}^2_{m,k}\left[\dfrac{P^0_{\text{av}} + 2\sum\limits_{(p,l)\in\mathcal{M}} \hat{\sigma}^2_{p,l} \ln \hat{\sigma}^2_{p,l}}{2\sum\limits_{(p,l)\in\mathcal{M}} \hat{\sigma}^2_{p,l}} - \ln \hat{\sigma}^2_{m,k}\right], & (m,k) \in \mathcal{M}, \quad (3.93) \\ 0, & (m,k) \in \mathcal{O} - \mathcal{M}, \quad (3.94) \end{cases}$$

where $\mathcal{M}$ is the largest possible subset of $\mathcal{O} \triangleq \{(m,k)\}$ ($m \in \{1, \cdots, M\}$, $k \in \{0, \cdots, N-1\}$) so that

$$\mathcal{M} = \left\{(m,k) \middle| \hat{\sigma}^2_{m,k} \leq \hat{\sigma}^2_{p,l}, P_{m,k} > 0, P_{p,l} = 0, \forall (m,k) \in \mathcal{M}, \forall (p,l) \in \mathcal{O} - \mathcal{M}\right\}. \quad (3.95)$$

It can be determined recursively with at most MN iterations.

This upper bound of Q function is not only tight in the log scale but also approximately a constant times of the true value, i.e., $e^{-x^2/2} \approx cQ(x)$, for not too small x. Replacing Q functions by the upper bounds in Eq. (3.85) just multiplies the objective values with a constant scale and does not affect the minimization variables. Therefore, it can provide a near-optimal power allocation scheme which solves Eq. (3.89) in the closed form.

Secondly, because PAR is related to the allocated power, the PAR minimization in MCPTS needs to take the scaling $|\bar{X}_{m,k}|^2 = P_{m,k}$ into consideration. By replacing $\mathbf{x}_m$ and $\mathbf{X}_m$ in Eq. (3.82) with $\bar{\mathbf{x}}_m$ and $\bar{\mathbf{X}}_m$, the minimum PAR can be found as shown in the MCPTS method in (3.81)-(3.83), i.e., $\text{PAR}_{\min} = \arg\min_{\Theta} \text{PAR}(\tilde{\mathbf{x}})$.

Denote $0 < \beta < 1$ as the convergence parameter. If $\text{PAR}_{\min} > \text{PAR}^0$ or $\text{PAR}_{\min} < \beta\text{PAR}^0$, either the objective average power cannot be reached or the MCPTS yields a much greater average power. In both cases, a new iteration begins with $\text{PAR}^0 =$

$\text{PAR}_{\min}$ and $P_{\text{av}}^0 = \frac{LNP_{\text{peak}}}{\text{PAR}_{\min}}$. Otherwise, the algorithm converges. A sub-optimal solution in terms of both the power allocation and the phase sequence is achieved. The iteration stops if this convergence condition is met or the maximum iteration number is reached.

3.3.4 Simulation Results

We present some examples to illustrate the performance improvements. In the simulations, adjacent channels were assumed without guard bands, i.e., $f_{m+1} - f_m = B$. The number of subcarriers was $N = 64$ for every channel.

3.3.4.1 MCPTS

The CCDF curves of the PAR are plotted in Figure 3.15. The constellation was QPSK although our experiments indicated that the PAR reduction performance is insensitive to the constellation choice. When the PSO method is used, the globally minimum PAR can be achieved. However, more than 1,000 iterations were generally necessary for the 10-particle PSO to achieve a good convergence. Instead, similar to PTS, a limited number of phase sequences can be used for searching a small PAR. It provides a tradeoff between PAR reduction performance and complexity.

3.3.4.2 Joint MCPTS and power allocation

In this simulation, the number of channels $M = 8$ and the oversampling rate $L = 8$ were used. For simplicity, we assumed $P_{m,k} = P_m$ and $h_{m,k} = h_m$, but $\{h_m\}$ were independent and identically distributed (i.i.d.) complex Gaussian random variables. The channel noise was white Gaussian with $\sigma_{m,k}^2 = \sigma^2$. In this setup, the PSNR can be defined as

$$\text{PSNR} \triangleq \frac{P_{\text{peak}} \sum_{m=1}^{M} E[|h_m|^2]}{M\sigma^2}. \tag{3.96}$$

Initialization $\text{PAR}^0 = 10\text{dB}$ and convergence parameter $\beta = 0.95$ were used.

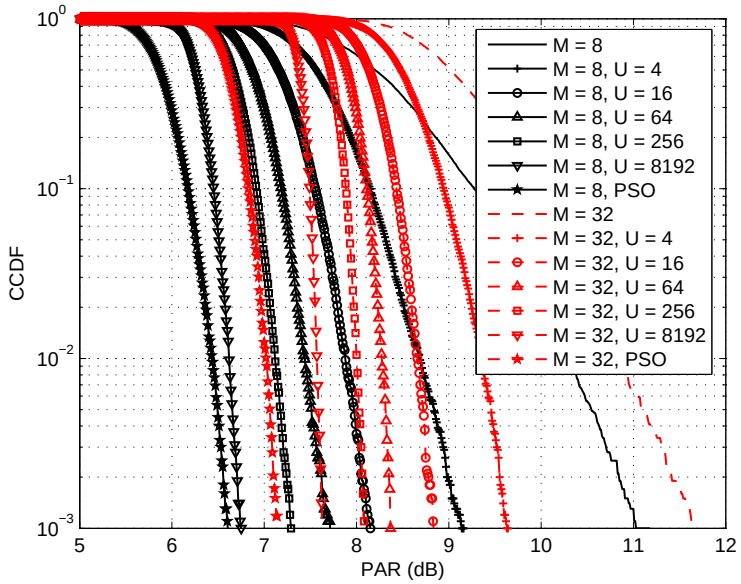

Figure 3.15: CCDF curves of the PAR of the original and MCPTS OFDM-FDMA signals for different numbers of channels ($M = 8$ and 32) and numbers of phase sequences ($U = 4$, 16, 64, 256 and 8192) as well as the PSO method.

Figure 3.16 shows the average BER versus PSNR curves. Two comparative methods are used, where the average power is either equally allocated among channels, i.e., $P_m = P$, or allocated so that every channel has the same SNR and average BER, i.e., $P_m/P_n = \hat{\sigma}_m^2/\hat{\sigma}_n^2$ [32, Chap. 9]. In both methods, we force the condition $P_{\text{av}} = \sum_{m=1}^{M} P_m$. MCPTS can be easily combined with these methods and shown to improve the BER performance. Also, the curve of the proposed joint MCPTS and BER-minimizing power allocation method is plotted in Figure 3.16. It is clear that the proposed joint optimization method leads to much lower BER especially at high PSNR values.

The resulting PAR of the iterative joint method might be, however, greater than using MCPTS for a constant power allocation scheme, e.g., the equal power allocation with MCPTS as shown in Figure 3.17. Intuitively, the joint method optimizes both the magnitude and the phase of each OFDM channel. Although the potential average power increase is less than using only MCPTS, the power is more efficiently allocated

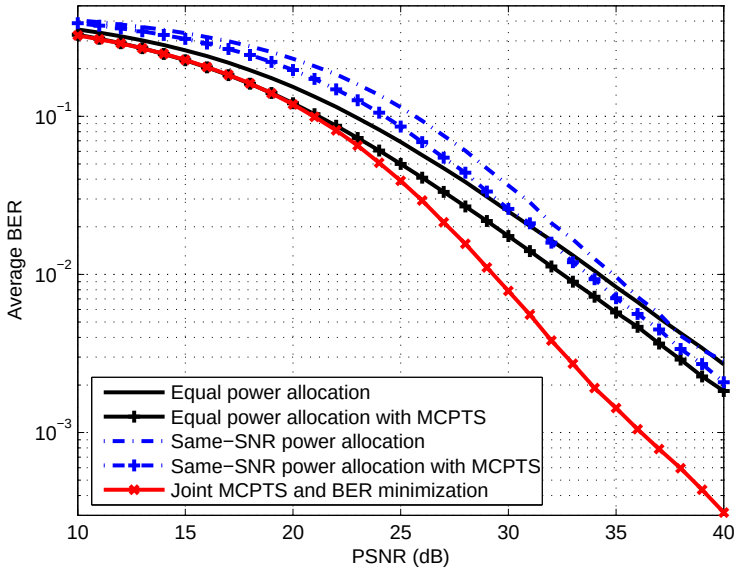

Figure 3.16: Average BER versus PSNR curves for $M = 8$ OFDM-FDMA systems with the equal power allocation, the same-SNR power allocation, and the joint MCPTS and BER minimization power allocation schemes.

among channels.

3.4 Conclusions

To reduce the PAR of OFDM and OFDM-FDMA signals, the EVM optimization algorithm and the multi-channel partial transmit sequences method have been proposed in this chapter. Not only are significant performance improvements achieved, these methods are also compatible with existing systems and standards. As practical solutions to the PAR problem, the proposed research benefits the implementations of OFDM systems.

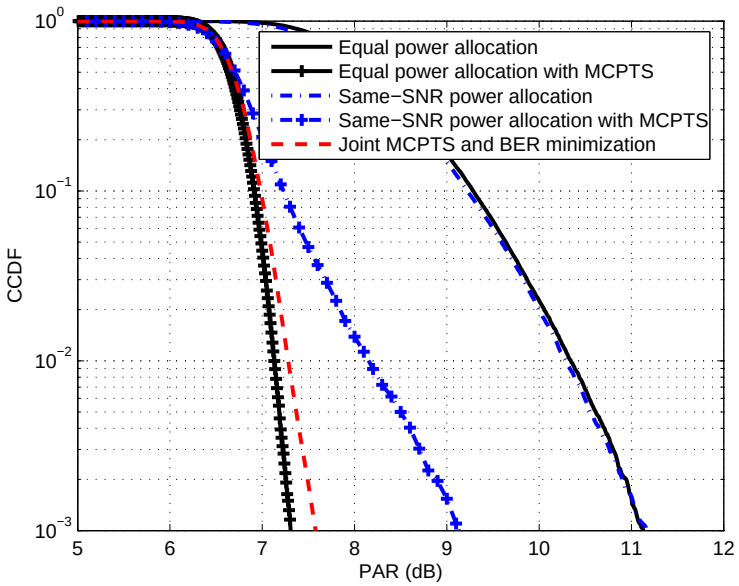

Figure 3.17: CCDF curves of the PAR of $M = 8$ OFDM-FDMA systems with the equal power allocation, the same-SNR power allocation, and the joint MCPTS and BER minimization power allocation schemes.

CHAPTER IV

DIVERSITY-ENABLED PPC SIMO-OFDM TRANSCEIVER DESIGN

By deploying multiple receiving antennas, single-input multiple-output OFDM can further enhance the performance with spatial diversity, i.e., the antenna diversity*. However, due to the large dynamic range of OFDM signals and the nonlinear nature of analog components, it is pragmatic to model the transmitter with a peak power constraint. A natural question to ask is whether PPC SIMO-OFDM transmissions can still enjoy the antenna diversity in this case. In this chapter, the effect of the peak power limit on the error performance of uncoded SIMO-OFDM systems is studied. In the case that the receiver has no information about the transmitter nonlinearity, we show that full antenna diversity can still be collected by carefully designing the transmitters, while the receiver performs a maximum ratio combining (MRC) method which is implemented the same as that in the average power constrained case. On the other hand, when the receiver has perfect knowledge of the transmitter nonlinearity, zero-forcing (ZF) equalizer is able to collect full antenna diversity.*

4.1 Introduction

For single-antenna OFDM systems with clipping at the transmitter, the approximated symbol error rate has been derived for maximum-likelihood sequence detection (MLSD) in [81]. The results show that the clipping nonlinearity leads to a certain (may not be full) multipath diversity order over frequency-selective Rayleigh fading channels. However, MLSD requires near exponential complexity to collect some diversity gain. When the number of subcarriers is large which is usually the case in current

standards, the complexity of MLSD is prohibitive. In such a case, the OFDM system loses its advantage as a simple equalizer which may reduce its practical applicability.

The low-complexity diversity-enabled transceiver design over peak power constrained OFDM channels is of interest. Therefore, instead of the multipath diversity, we focus on the antenna diversity from multiple antennas deployed at the receiver (i.e., SIMO channels). When OFDM signals are linearly transmitted, linear equalizers are sufficient to collect the antenna diversity by optimally combining the multiple faded replicas of the same information bearing signal [30, 96]. However, the question of whether and how the peak power constrained SIMO-OFDM system can still enjoy antenna diversity with linear equalizers has not been addressed in the literature. A few iterative methods to reconstruct the clipped OFDM signals in multi-antenna systems have been proposed in [14, 46, 47]. However, the diversity order has not been quantitatively analyzed.

4.2 SIMO-OFDM System Model

In the uncoded OFDM system with the frequency-domain symbols $\mathbf{X} = [X_0, \cdots, X_{N-1}]^T$ where X_k's are drawn from an ideal constellation Ω, the time-domain waveform can be obtained from $\mathbf{x} = \mathbf{F}^H\mathbf{X}$, whose PAR definition follows in Eq. (2.7).

Without loss of generality, assume the signal is transmitted through the soft-limit PA with the peak power constraint P_{peak} and a unit gain (i.e., $G = 1$ in Eqs. (2.1)-(2.2)). The output signal can be denoted as $y[n] = g(x[n])$ as given in Eqs. (2.1)-(2.2). In this case, the input back-off is defined as $\text{IBO} = \frac{P_{\text{peak}}}{\sigma_x^2}$. Clipping occurs when $\text{PAR}(\mathbf{x}) > \text{IBO}$.

The frequency-domain transmitted in-band subcarriers can thus be obtained from $\mathbf{y} = [y[0], \cdots, y[LN-1]]^T \triangleq g(\mathbf{x})$ as

$$\bar{\mathbf{X}} = \mathbf{F}\mathbf{y}. \tag{4.1}$$

Notice that, by digital clipping and filtering methods, out-of-band spectral growth

can be constrained according to certain spectral mask or totally eliminated [10, 12]. In this case, the following analysis still holds valid and the proposed methods can be modified accordingly by treating the clipping and filtering as a single nonlinear process.

Suppose the receiver is equipped with N_r uncorrelated receiving antennas. After removing the cyclic prefix and performing the FFT, the received signal in frequency-selective Rayleigh fading channels is

$$\mathbf{r} = [\mathbf{r}_1^T, \cdots, \mathbf{r}_{N_r}^T]^T = \mathbf{H}\bar{\mathbf{X}} + \mathbf{w}, \tag{4.2}$$

where $\mathbf{r}_i$ denotes the OFDM symbol received on the ith antenna. $\mathbf{H} = [\mathbf{H}_1, \cdots, \mathbf{H}_{N_r}]^T$, $\mathbf{H}_i = \text{diag}([H_{i,0}, \cdots, H_{i,N-1}])$, and $H_{i,k}$ $(0 \le k \le N-1)$ is the channel frequency response of the kth in-band subcarrier on the ith receiving antenna. In addition, $\mathbf{w} = [\mathbf{w}_1^T, \cdots, \mathbf{w}_{N_r}^T]^T$ and $\mathbf{w}_i = [w_{i,0}, \cdots, w_{i,N-1}]^T$ where $w_{i,k}$ $(0 \le k \le N-1)$ consists of the circularly complex white Gaussian noise with variance N_0.

Unlike linear channels, the average SER is defined in terms of PSNR (see Eq. (2.5)) in peak power constrained channels. Therefore, the definition of diversity order G_d evolves as

$$G_d = \lim_{\text{PSNR}\to\infty} -\frac{\log P_e(\text{PSNR})}{\log \text{PSNR}}. \tag{4.3}$$

For transmitters with a given P_{peak}, the diversity order describes how fast the SER decays with decreasing channel noise power.

4.2.1 Diversity Combining in Linear SIMO Channels

For linear SIMO channels, several diversity combining techniques are available to achieve the antenna diversity [96], e.g., maximal ratio combining (MRC) and selective combining (SC). Before discussing the peak power constrained case, we briefly review the MRC method in the linear SIMO-OFDM channel.

Suppose that the receiver has perfect channel knowledge. Without the peak power limit, the received signal of Eq. (4.2) becomes $\mathbf{r} = \mathbf{HX}+\mathbf{w}$. The MRC method chooses

the $N_r N \times N$ coefficient matrix $\mathbf{C} = [\mathbf{c}_0, \cdots, \mathbf{c}_{N-1}]$ to combine the received signal, where $\mathbf{c}_k$ is the kth column of $\mathbf{C}$. The estimate of $\mathbf{X}$ is thus given as

$$\tilde{\mathbf{X}} = \mathbf{C}^T \mathbf{H}\mathbf{X} + \mathbf{C}^T \mathbf{w}. \tag{4.4}$$

To maximize the post-processing SNR in an uncoded OFDM system, the optimal weights can be shown as [96]

$$\mathbf{c}_k = \frac{\mathbf{h}_k^*}{\mathbf{h}_k^H \mathbf{h}_k}, \tag{4.5}$$

where $\mathbf{h}_k$ is the kth column of $\mathbf{H}$, i.e., $\mathbf{H} = [\mathbf{h}_0, \cdots, \mathbf{h}_{N-1}]$. The corresponding receive SNR is $\mathbf{h}_k^H \mathbf{h}_k$SNR. In the end, the decision $\hat{\mathbf{X}}$ is obtained by hard decoding on $\tilde{\mathbf{X}}$, denoted as $\hat{\mathbf{X}} = \left\langle \tilde{\mathbf{X}} \right\rangle$.

Therefore, for uncoded SIMO-OFDM, MRC is essentially the ZF and also the ML equalizers in the linear SIMO channel with Gaussian noise, i.e., $\mathbf{C}^T = \mathbf{H}^\dagger$ where $\mathbf{H}^\dagger = (\mathbf{H}^H \mathbf{H})^{-1} \mathbf{H}^H$ is the Moore-Penrose pseudo-inverse of $\mathbf{H}$ [71]. When an M-ary QAM is used, the average SER over SIMO Rayleigh fading channels is [68]

$$P_e(\text{SNR}) = \frac{4\sqrt{M} - 4}{\sqrt{M}} \left(\frac{1-\mu}{2} \right)^{N_r} \sum_{i=0}^{N_r - 1} \frac{(N_r - 1 + i)!}{i!(N_r - 1)!} \left(\frac{1+\mu}{2} \right)^i, \tag{4.6}$$

where $\mu = \left(1 + \frac{2(M-1)}{3\text{SNR}}\right)^{-\frac{1}{2}}$. It is ready to show that

$$\lim_{\text{SNR} \to \infty} -\frac{\log P_e(\text{SNR})}{\log \text{SNR}} = N_r. \tag{4.7}$$

In other words, MRC collects full antenna diversity. From the existing literature, however, it is not clear yet whether (and if so, how) full antenna diversity can be achieved in the presence of the peak-power constraint. We address this open question in the following sections.

4.3 Transparent Receivers: A Statistical Model

By "transparent", we mean that the receivers have no information about the transmitter nonlinearities. In this case, no receiver-side cooperation is expected. The

nonlinear distortion noise is dealt with in the same way as the uncorrelated Gaussian channel noise. In this section, a *statistical model* is offered to quantify the clipping distortions. Afterwards, we present an optimal combining receiver and give conditions for the transmitter to enable full antenna diversity in the peak power constrained channel. We will illustrate the concept via several numerical examples.

Definition 4.1 (Statistical model) *According to Bussgang's theorem [88], the clipped waveform $y[n]$ can be decomposed into a linear term $\alpha x[n]$ plus a statistically uncorrelated distortion term $u[n]$, i.e.,*

$$y[n] = \alpha x[n] + u[n], \tag{4.8}$$

where $\alpha = E[x^*[n]y[n]]/E[|x[n]|^2]$ is chosen so that the signal $x[n]$ and the nonlinear distortion noise $u[n]$ are uncorrelated, i.e., $E[x^*[n]u[n]] = 0$. The distortion noise power is $\sigma_u^2 = E[|y[n]|^2] - |\alpha|^2 E[|x[n]|^2]$. The received frequency-domain symbol is thus given as

$$\mathbf{r} = \mathbf{H}'\mathbf{X} + \mathbf{H}\mathbf{v} + \mathbf{w}, \tag{4.9}$$

where $\mathbf{H}' = \alpha\mathbf{H}$ is the equivalent channel frequency response and $\mathbf{v} = \mathbf{F}\mathbf{u}$ is the frequency-domain distortion noise with variance $\sigma_v^2 \triangleq E[\frac{1}{N}\|\mathbf{v}\|_2^2] = E[\frac{1}{LN}\|\mathbf{u}\|_2^2] = \sigma_u^2$.

Clipping causes $|y[n]| \leq |x[n]|$, $|\alpha| \leq 1$ and thus the effective signal power is reduced. In addition, the transparent receiver regards $u[n]$ as uncorrelated channel noise. Thus, instead of SNR, signal-to-noise-and-distortion ratio should be used to incorporate both the signal power attenuation and nonlinear distortions, and characterize the overall SER performance in the given channel [85].

Based on the *statistical model*, the post-processing SNDR of the kth subcarrier is given as

$$\mathrm{SNDR}_k = \frac{|\alpha|^2 \left|\mathbf{c}_k^T \mathbf{h}_k\right|^2 \sigma_x^2}{\left|\mathbf{c}_k^T \mathbf{h}_k\right|^2 \sigma_v^2 + \mathbf{c}_k^H \mathbf{c}_k N_0}, \; k \in \{0, \cdots, N-1\}. \tag{4.10}$$

To maximize the SNDR, the MRC weights are given in the following proposition:

Proposition 4.1 *For transparent receivers that have no information about the transmitter nonlinearity, the optimal MRC weights are given by* $\mathbf{C}$ *whose kth column is* $\mathbf{c}_k = \frac{\mathbf{h}_k'^*}{\mathbf{h}_k'^H \mathbf{h}_k'}$*, where* $\mathbf{h}_k' = \alpha \mathbf{h}_k$ *(*$k \in \{0, \cdots, N-1\}$*).*

Proof: The optimal MRC weights suffice to maximize the SNDR in Eq. (4.10). Taking the first-order derivative of SNDR_k with respect to $\mathbf{c}_k$ and setting it to zero, we obtain

$$\frac{\partial}{\partial \mathbf{c}_k}\mathrm{SNDR}_k = \frac{(\mathbf{c}_k^T \mathbf{h}_k')^* \mathbf{h}_k' \sigma_x^2}{\left|\mathbf{c}_k^T \mathbf{h}_k\right|^2 \sigma_v^2 + \mathbf{c}_k^H \mathbf{c}_k N_0} - \frac{\left|\mathbf{c}_k^T \mathbf{h}_k'\right|^2 \sigma_x^2 ((\mathbf{c}_k^T \mathbf{h}_k)^* \sigma_v^2 \mathbf{h}_k + \mathbf{c}_k^* N_0)}{(\left|\mathbf{c}_k^T \mathbf{h}_k\right|^2 \sigma_v^2 + \mathbf{c}_k^H \mathbf{c}_k N_0)^2} = 0. \quad (4.11)$$

Recall that $\mathbf{h}_k' = \alpha \mathbf{h}_k$. After some basic algebraic manipulations, Eq. (4.11) leads to

$$\mathbf{c}_k^T \mathbf{h}_k' \mathbf{c}_k^* = \mathbf{c}_k^H \mathbf{c}_k \mathbf{h}_k'. \quad (4.12)$$

Obviously, $\mathbf{c}_k = \frac{\mathbf{h}_k'^*}{\mathbf{h}_k'^H \mathbf{h}_k'} = \frac{\mathbf{h}_k^*}{\alpha \mathbf{h}_k^H \mathbf{h}_k}$ satisfies Eq. (4.12). In addition, these weights are channel-normalizing (i.e., $\mathbf{c}_k^T \mathbf{h}_k' = 1$) as well as orthogonal to the channels of other subcarriers (i.e., $\mathbf{c}_k^T \mathbf{h}_l' = 0$, $\forall k \neq l$). Therefore, $\mathbf{C} = [\mathbf{c}_0, \cdots, \mathbf{c}_{N-1}]$ with $\mathbf{c}_k = \frac{\mathbf{h}_k^*}{\alpha \mathbf{h}_k^H \mathbf{h}_k}$ gives the optimal MRC weights and the transparent receiver can decode according to $\hat{\mathbf{X}} = \left\langle \mathbf{C}^T \mathbf{r} \right\rangle$. ■

At first, it appears that the transparent receiver has to know α in order to acquire $\mathbf{C}$, which is inconsistent with the "transparent" definition. In fact, for OFDM systems with embedded pilot subcarriers, since the pilot signals are also attenuated by α, $\mathbf{H}' = \alpha \mathbf{H}$ is the effective channel response which is acquired by channel estimation at the receiver. Therefore, transparent receivers do not need to know α aforehand and the SNDR-maximizing combining weights can be used to achieve the best error performance.

Unlike the linear case, using the optimal MRC weights at the receiver may not guarantee full antenna diversity. The necessary and sufficient condition for achieving the antenna diversity gain is given in the following proposition:

Proposition 4.2 *For OFDM transmitters with a fixed peak power limit* P_{peak}*, the transparent receiver is able to achieve full antenna diversity if and only if the distortion noise vanishes as the PSNR increases.*

Proof: For transparent receivers, the SER performance is a function of the SNDR. Therefore, a necessary condition to achieve the diversity gain is that the post-processing SNDR goes to infinity along with the PSNR. With the optimal MRC weights given in Proposition 4.1, the post-processing SNDR becomes

$$\mathrm{SNDR}_k = \frac{\mathbf{h}_k^H \mathbf{h}_k |\alpha|^2 \sigma_x^2}{\mathbf{h}_k^H \mathbf{h}_k \sigma_v^2 + N_0}. \tag{4.13}$$

For a given peak power limit P_{peak}, increasing PSNR is equivalent to decreasing the noise power N_0. From Eq. (4.13), we have

$$\lim_{N_0 \to 0} \mathrm{SNDR}_k = \lim_{N_0 \to 0} \frac{|\alpha|^2 \sigma_x^2}{\sigma_v^2}. \tag{4.14}$$

Because $|\alpha| \leq 1$ and $\sigma_x^2 \leq P_{\text{peak}}$, $\lim_{N_0 \to 0} \sigma_v^2 = 0$ is the necessary condition for the limit of SNDR in Eq. (4.14) to go to infinity, as well as for the transparent receiver to collect antenna diversity.

On the other hand, when $\lim_{N_0 \to 0} \sigma_v^2 = 0$, the limit of SNDR becomes

$$\lim_{N_0 \to 0} \mathrm{SNDR}_k = \lim_{N_0 \to 0} \mathbf{h}_k^H \mathbf{h}_k \mathrm{SNR}, \tag{4.15}$$

which is the same as the post-processing SNR of the linear channel case in Section 4.2.1. Plugging the SER of $P_e\left(\frac{\mathrm{PSNR}}{\mathrm{IBO}}\right)$ into the diversity gain definition of Eq. (4.3), full antenna diversity can be easily proved. For given P_{peak} and IBO, by referring to Eq. (4.7), we have

$$G_d = \lim_{\mathrm{PSNR} \to \infty} -\frac{\log P_e\left(\frac{\mathrm{PSNR}}{\mathrm{IBO}}\right)}{\log \mathrm{PSNR}} = \lim_{\mathrm{PSNR}' \to \infty} -\frac{\log P_e(\mathrm{PSNR}')}{\log \mathrm{PSNR}' + \log \mathrm{IBO}} = N_r, \tag{4.16}$$

where $\mathrm{PSNR}' = \frac{\mathrm{PSNR}}{\mathrm{IBO}}$.

Therefore, for a fixed P_{peak}, the necessary and sufficient condition for the transparent receiver to collect full antenna diversity is that the distortion noise power vanishes as the PSNR increases. ■

4.3.1 Examples

In the following, we give some examples to illustrate the design for the peak power constrained OFDM transmitter and the model in Eq. (4.8). The performance will be demonstrated in Section 4.5.

4.3.1.1 Constant Clipping

To deal with the large PAR, the simplest transmission scheme is to maintain a constant IBO for all OFDM symbols. When PAR exceeds the IBO, however, clipping occurs which implies that $|\alpha| < 1$ and $\sigma_v^2 > 0$ for the statistical model in Eq. (4.8). Therefore, no antenna diversity can be achieved. As indicated in Proposition 4.2, error floor should be observed.

4.3.1.2 Piece-wise linear scaling

The piece-wise linear scaling (PWLS) method guarantees that no nonlinear distortion happens with the soft-limit PA [76]. It is realized by multiplying a symbol-wise gain on every OFDM symbol before passing it to the PA, namely

$$\bar{\mathbf{x}} = \frac{\sqrt{P_{\text{peak}}}}{\|\mathbf{x}\|_\infty}\mathbf{x}. \tag{4.17}$$

Because clipping never occurs, i.e., $g(\bar{\mathbf{x}}) = \bar{\mathbf{x}}$, thus $\bar{\mathbf{X}} = \frac{\sqrt{P_{\text{peak}}}}{\|\mathbf{x}\|_\infty}\mathbf{X}$. The symbol-wise gain is essentially a part of the channel and can be recovered by receivers with channel estimation. For PWLS, Proposition 4.2 indicates that full antenna diversity can be achieved. In fact, owing to the linear transmission, the post-processing SNDR becomes

$$\begin{aligned} \text{SNDR}_k &= \mathbf{h}_k^H \mathbf{h}_k \frac{E\left[\frac{P_{\text{peak}}}{\|\mathbf{x}\|_\infty^2}|X_k|^2\right]}{N_0} = \mathbf{h}_k^H \mathbf{h}_k \frac{P_{\text{peak}} E\left[\frac{\|\mathbf{x}\|_2^2}{LN\|\mathbf{x}\|_\infty^2}\right]}{N_0} \\ &= \mathbf{h}_k^H \mathbf{h}_k \text{PSNR} \cdot E\left[\text{PAR}(\mathbf{x})^{-1}\right], \end{aligned} \tag{4.18}$$

which is inversely proportional to the harmonic mean of PAR. Still, low power efficiency and coding gain may result due to the large PAR of OFDM signals. Certain

distortionless methods have been proposed to reduce the PAR of OFDM signals, e.g., coding [54], selected mapping [11], tone reservation [100] and optimizations [61]. They can improve the coding gain with respect to tradeoffs among implementation complexity, spectral efficiency and receiver-side cooperation.

4.3.1.3 Optimal clipping

When some channel state information is available at the transmitter, clipping distortion can be methodically introduced to improve the error performance for transparent receivers [84, 85]. Instead of the original OFDM waveform, the following signal is input to the PA

$$\bar{x}[n] = \begin{cases} \frac{\sqrt{P_{\text{peak}}}}{\eta} \cdot \frac{x[n]}{\sigma_x}, & \frac{|x[n]|}{\sigma_x} < \eta, \quad (4.19) \\ \sqrt{P_{\text{peak}}} e^{j\angle x[n]}, & \frac{|x[n]|}{\sigma_x} \geq \eta, \quad (4.20) \end{cases}$$

where $\eta \geq 0$ is called the clipping threshold [84]. Because $|\bar{x}[n]|^2 \leq P_{\text{peak}}$, $\mathbf{y} = \bar{\mathbf{x}}$. α and σ_v^2 in Eq. (4.8) can be numerically determined for different η's. Then, with MRC, the post-processing SNDR for optimal clipping becomes

$$\text{SNDR}_k = \frac{\mathbf{h}_k^H \mathbf{h}_k |\alpha|^2 P_{\text{peak}}}{\eta^2 \mathbf{h}_k^H \mathbf{h}_k \sigma_v^2 + \eta^2 N_0}. \quad (4.21)$$

If the channel noise level N_0 (or PSNR) is known at the transmitter, the optimal clipping threshold can be determined to minimize the average SER, i.e.,

$$\eta^\star = \arg\min_{\eta} \sum_{k=0}^{N-1} E_{\mathbf{h}_k}[P_E(\text{SNDR}_k)], \quad (4.22)$$

where $P_E(\text{SNDR}_k) \approx \frac{4\sqrt{M}-4}{\sqrt{M}} Q\left(\sqrt{\frac{3\text{SNDR}_k}{M-1}}\right)$ is the instantaneous SER for M-ary QAM constellations [83, p. 278]. When the OFDM sample is approximated as a complex Gaussian random variable, a numerical method to solve for $\eta^\star$ is given by [84, Theorem 1].

Unlike PWLS which is trying to avoid any clipping, for a given PSNR, the optimal clipping method is to maximize the SNDR in Eq. (4.21). In the high PSNR region,

a large $\eta^\star$ is yielded in which case $|\alpha| \to 1$ and $\sigma_v^2 \to 0$ [84]. Thus, full antenna diversity is sustained according to Proposition 4.2. On the other hand, in the low PSNR region, some distortion is introduced to achieve a more desired tradeoff for the increase in signal power so that the error performance is optimized. Therefore, the optimal clipping can achieve better coding gain while maintaining the full antenna diversity with a transparent receiver.

4.4 Transmitter Nonlinearity Known at the Receiver: A Deterministic Model

Instead of a random process, the clipping distortion is a deterministic function of the data. When the receiver knows or estimates *a priori* the transmitter nonlinearity, it can exploit the deterministic nature of the clipping process for better performance [79]. We describe a *deterministic model* next to characterize the clipping process.

Definition 4.2 (Deterministic model) *After clipping, the frequency-domain OFDM symbol in Eq. (4.1) can be represented by the following deterministic matrix operation [25, 79]*

$$\bar{\mathbf{X}} = \mathbf{F}\mathbf{\Lambda}\mathbf{F}^H\mathbf{X} = \mathbf{X} + \mathbf{d}, \tag{4.23}$$

where

$$\mathbf{\Lambda} = \text{diag}\left(\left[\min\left(\frac{\sqrt{P_{\text{peak}}}}{|x[0]|}, 1\right), \cdots, \min\left(\frac{\sqrt{P_{\text{peak}}}}{|x[LN-1]|}, 1\right)\right]\right) \tag{4.24}$$

is the function of $\mathbf{X}$ *and* $\mathbf{d} = \mathbf{F}(g(\mathbf{x}) - \mathbf{x})$ *is the frequency-domain representation of the deterministic clipping noise.*

As proven in [80, 81], when IBO $\geq \frac{3\pi(\sqrt{M}-3)^2}{8(M-1)}$ for M-ary QAM ($M \geq 16$) and when the MLSD receiver is used, clipping the Nyquist-rate OFDM signal only causes a constant SNR loss on the SER performance. The effective transmit SNR becomes SNR $\approx \frac{\Delta(\text{IBO})\text{PSNR}}{\text{IBO}}$, where $\Delta(\text{IBO}) \approx 1 - e^{-\text{IBO}} + \frac{1}{2}\text{IBO}\int_{\text{IBO}}^{\infty} e^{-t}/t \; dt \leq 1$. Plugging

this effective SNR into Eq. (4.6), the SER in flat Rayleigh fading SIMO channels is given by

$$P_{\text{MLSD}}(\text{PSNR}, \text{IBO}) \approx P_e \left(\frac{\Delta(\text{IBO}) \cdot \text{PSNR}}{\text{IBO}} \right). \tag{4.25}$$

Although clipping was also shown to enable certain multipath diversity in frequency-selective fading channels [81], we focus on antenna diversity in this section. In addition, the SER performance for clipping and filtering oversampled OFDM signals was shown to be well approximated by that of the Nyquist sampling in fading channels [81]. Therefore, the SER for general SIMO fading channels is approximated by Eq. (4.25), which is referred as the MLSD bound in accordance with [81]. Again, full antenna diversity can be verified similar to Eq. (4.16).

However, MLSD receivers have exponential complexity, which is not practical for implementations especially for a large number of subcarriers. Instead, linear equalizers are usually used as low-complexity solutions, but do not necessarily offer the same diversity orders as MLSD [71]. For the received signal in Eq. (4.2), if $\mathbf{\Lambda}$ is known at the receiver, the ZF equalizer is given as

$$\tilde{\mathbf{X}}_{\text{zf}} = \mathcal{H}^{\dagger}\mathbf{r} = \mathbf{X} + \mathcal{H}^{\dagger}\mathbf{w}, \tag{4.26}$$

where $\mathcal{H} = \mathbf{H}\mathbf{F}\mathbf{\Lambda}\mathbf{F}^{H}$. In the following, we first quantify the diversity order collected by the ZF equalizer when $\mathbf{\Lambda}$ is known. Then, an iterative method will be proposed to jointly estimate both $\mathbf{\Lambda}$ and $\mathbf{s}$ and realize the ZF equalizer in the absence of *a priori* knowledge about $\mathbf{\Lambda}$.

Proposition 4.3 *For clipped OFDM signals through SIMO fading channels with N_r receiving antennas, if the receivers have perfect knowledge of $\mathbf{\Lambda}$ in Eq. (4.24), the diversity order collected by ZF equalizers is N_r.*

Proof: Suppose that the symbol transmitted on the kth subcarrier is X_k, but at the receiver it is erroneously decoded as $X_k' \neq X_k$. The pairwise error probability is given

as [70]

$$\Pr(X_k \to X_k' | \mathcal{H}) = Q\left(\sqrt{\frac{|e_k|^2}{2N_0\Omega_{kk}}}\right), \tag{4.27}$$

where $e_k = X_k - X_k'$ and Ω_{kk} is the (k,k)th element of

$$\mathbf{\Omega} \;=\; (\mathcal{H}^H\mathcal{H})^{-1} = (\mathbf{F}\mathbf{\Lambda}\mathbf{F}^H\mathbf{H}^H\mathbf{H}\mathbf{F}\mathbf{\Lambda}\mathbf{F}^H)^{-1}. \tag{4.28}$$

Because the channel matrix $\mathbf{H}$ has full column rank with probability 1 and $\mathbf{\Lambda}$ is a diagonal matrix with positive real diagonal entries, we have $\mathbf{\Omega} = \mathbf{\Gamma}(\mathbf{H}^H\mathbf{H})^{-1}\mathbf{\Gamma}^H$, where $\mathbf{\Gamma} = (\mathbf{F}\mathbf{\Lambda}\mathbf{F}^H)^{-1}$ is a nonsingular Hermitian and Toeplitz matrix. Since $\mathbf{H}^H\mathbf{H} = \text{diag}\left(\left[\sum_{i=1}^{N_r}|H_{i,0}|^2, \cdots, \sum_{i=1}^{N_r}|H_{i,N-1}|^2\right]\right)$, Ω_{kk} can be expressed as

$$\Omega_{kk} = \sum_{l=0}^{N-1} \frac{|\Gamma_{k,l}|^2}{\sum_{i=1}^{N_r}|H_{i,l}|^2}. \tag{4.29}$$

Since $\mathbf{\Gamma}$ has full rank, $\left\{l \middle| |\Gamma_{k,l}| \neq 0\right\} \neq \emptyset \;\forall k$. Let $p \in \left\{l \middle| |\Gamma_{k,l}| \neq 0\right\}$ and $q = \arg\min_l \sum_{i=1}^{N_r}|H_{i,l}|^2$. We have the following inequalities

$$a\left(\sum_{i=1}^{N_r}|H_{i,p}|^2\right)^{-1} \leq \Omega_{kk} \leq b\left(\sum_{i=1}^{N_r}|H_{i,q}|^2\right)^{-1}, \tag{4.30}$$

where $a \triangleq |\Gamma_{k,p}|^2$ and $b \triangleq \sum_{l=0}^{N-1}|\Gamma_{k,l}|^2$. Therefore, the bounds for the error probability are

$$Q\left(\sqrt{\frac{|e_k|^2\sum_{i=1}^{N_r}|H_{i,p}|^2}{2aN_0}}\right) \leq \Pr(s_k \to s_k' | \mathcal{H}) \leq Q\left(\sqrt{\frac{|e_k|^2\sum_{i=1}^{N_r}|H_{i,q}|^2}{2bN_0}}\right). \tag{4.31}$$

Because the channel responses are complex Gaussian distributed, $\sum_{i=1}^{N_r}|H_{i,p}|^2$ is a chi-squared random variable with $2N_r$ degrees of freedom. Therefore, by averaging over this random variable, the quantity on the left hand side of (4.31) obeys

$$E_{\mathbf{H}}\left[Q\left(\sqrt{\frac{|e_k|^2\sum_{i=1}^{N_r}|H_{i,p}|^2}{2aN_0}}\right)\right] \geq \beta_1\left(\text{SNR}\right)^{-N_r}, \tag{4.32}$$

where SNR $= \frac{\sigma_x^2}{N_0} = \frac{M-1}{6N_0} d_{\min}^2$ for M-ary QAM constellations ($d_{\min}$ is the minimum Euclidean distance of the constellation) and β_1 is a constant that is independent of the SNR. For the right-hand side (RHS) of (4.31), we have [70, Lemma 1]

$$\Pr\left(\sum_{i=1}^{N_r} |H_{i,q}|^2 < \xi\right) \leq N \left(\frac{\xi}{2}\right)^{N_r}, \ \forall \xi \geq 0. \tag{4.33}$$

Integrating the RHS of (4.31) over the channel response gives

$$E_{\mathbf{H}}\left[Q\left(\sqrt{\frac{|e_k|^2 \sum_{i=1}^{N_r} |H_{i,q}|^2}{2bN_0}}\right)\right] = E_{\mathbf{H}}\left[\frac{1}{2}\Pr\left(\sum_{i=1}^{N_r} |H_{i,q}|^2 < \frac{2bN_0\epsilon^2}{|e_k|^2}\right)\right] \tag{4.34}$$

$$\leq E_{\epsilon}\left[\frac{N}{2}\left(\frac{bN_0\epsilon^2}{d_{\min}^2}\right)^{N_r}\right] = \beta_2 (\mathrm{SNR})^{-N_r} \tag{4.35}$$

where ϵ is a Gaussian random variable with zero mean and unit variance and β_2 is a constant independent of the SNR. Therefore, combining (4.31), (4.32) and (4.35), we get

$$\beta_1 (\mathrm{SNR})^{-N_r} \leq P_e = E_{\mathbf{H}}[\Pr(X_k \to X_k' | \mathcal{H})] \leq \beta_2 (\mathrm{SNR})^{-N_r}, \tag{4.36}$$

which means the diversity order collected by the ZF equalizer with known $\mathbf{\Lambda}$ is N_r.

■

Proposition 4.3 states that ZF equalizers can achieve full antenna diversity if the clipping-based matrix $\mathbf{\Lambda}$ is known or can be estimated at the receiver. Moreover, it also indicates that in frequency-selective fading channels, ZF equalizers are *not* able to collect any multipath diversity. It is the compromise that low-complexity solutions have to make. The same fact was previously observed in [81]. It is also worthwhile to mention that, unlike the linear case in Section 4.2.1, MRC is no longer the same as the ZF equalizer in the presence of clipping.

Although $\mathbf{\Lambda}$ is a function of the data $\mathbf{X}$ and can not be known *a priori* at the receiver, the following recursive method can jointly estimate $\mathbf{\Lambda}$ and $\mathbf{X}$. The transmitter peak power limit P_{peak} is assumed available at the receiver. Based on decision

feedback, the proposed iterative method can be summarized in three steps

$$\hat{\mathbf{X}}^{(q)} = \left\langle (\mathbf{H}\mathbf{F}\hat{\mathbf{\Lambda}}^{(q-1)}\mathbf{F}^H)^{\dagger}\mathbf{r} \right\rangle \tag{4.37}$$

$$\hat{\mathbf{x}}^{(q)} = \mathbf{F}^H\hat{\mathbf{X}}^{(q)} \tag{4.38}$$

$$\hat{\mathbf{\Lambda}}^{(q)} = \text{diag}\left(\left[\min\left(\frac{\sqrt{P_{\text{peak}}}}{|\hat{x}^{(q)}[0]|}, 1 \right), \cdots, \min\left(\frac{\sqrt{P_{\text{peak}}}}{|\hat{x}^{(q)}[LN-1]|}, 1 \right) \right] \right), \tag{4.39}$$

where $\hat{}$ denotes the estimation for the corresponding variable and the superscript $^{(q)}$ stands for the iteration index. As the initialization, $\hat{\mathbf{\Lambda}}^{(0)} = \mathbf{I}_{LN\times LN}$.

Calculating the pseudo-inverse in Eq. (4.37) may require high computational complexity, but it can be further simplified as $(\mathbf{H}\mathbf{F}\mathbf{\Lambda}\mathbf{F}^H)^{\dagger} = (\mathbf{F}\mathbf{\Lambda}\mathbf{F}^H)^{-1}\mathbf{H}^{\dagger}$ because of the full column ranks of $\mathbf{F}\mathbf{\Lambda}\mathbf{F}^H$ and $\mathbf{H}$ [34], where $\mathbf{H}^{\dagger} = \mathbf{C}^T$, i.e., the MRC weights. Moreover, the inverse of $\mathbf{F}\mathbf{\Lambda}\mathbf{F}^H$ can be avoided because

$$(\mathbf{F}\mathbf{\Lambda}\mathbf{F}^H)^{-1} = \mathbf{I} - \mathbf{F}(\mathbf{\Lambda} - \mathbf{I})\mathbf{F}^H(\mathbf{F}\mathbf{\Lambda}\mathbf{F}^H)^{-1}. \tag{4.40}$$

In each iteration, the estimate of $\mathbf{X}$ can be recursively updated as

$$\hat{\mathbf{X}}^{(q)} = \left\langle \mathbf{H}^{\dagger}\mathbf{r} - \mathbf{F}(\hat{\mathbf{\Lambda}}^{(q-1)} - \mathbf{I})\mathbf{F}^H\hat{\mathbf{X}}^{(q-1)} \right\rangle. \tag{4.41}$$

Because $\mathbf{F}(\mathbf{\Lambda} - \mathbf{I})\mathbf{F}^H\mathbf{X} = \mathbf{d}$, the clipping noise can be estimated, i.e. $\hat{\mathbf{d}} = \mathbf{F}(g(\hat{\mathbf{x}}) - \hat{\mathbf{x}})$, instead of $\mathbf{\Lambda}$, which avoids the FFT, IFFT and matrix inverse operations for $(\mathbf{F}\mathbf{\Lambda}\mathbf{F}^H)^{-1}$. Therefore, the iterative method in Eqs. (4.42)-(4.44) is equivalent to the following low-complexity method, starting with $q = 1$ and $\hat{\mathbf{d}}^{(0)} = \mathbf{0}_N$,

$$\hat{\mathbf{X}}^{(q)} = \left\langle \mathbf{C}^T\mathbf{r} - \hat{\mathbf{d}}^{(q-1)} \right\rangle \tag{4.42}$$

$$\hat{\mathbf{x}}^{(q)} = \mathbf{F}^H\hat{\mathbf{X}}^{(q)} \tag{4.43}$$

$$\hat{\mathbf{d}}^{(q)} = \mathbf{F}\left(g(\hat{\mathbf{x}}^{(q)}) - \hat{\mathbf{x}}^{(q)}\right). \tag{4.44}$$

We refer to it as the joint MRC and clipping mitigation method [55]. Its complexity is dominated by one pair of FFT/IFFT operations per iteration and on the order of $\mathcal{O}(N \log N)$. Along with the iterations, the mean square error (MSE) of the estimate

$\hat{\mathbf{d}}^{(q)}$ can be defined as

$$\mathrm{MSE}_{\mathbf{d}}^{(q)} \quad = \quad E[\|\mathbf{d} - \hat{\mathbf{d}}^{(q)}\|_2^2]. \tag{4.45}$$

$\mathrm{MSE}_{\mathbf{d}}^{(q)}$ is decreasing quickly, especially in the high PSNR region, which will be shown in Section 4.5. As a result, the joint estimation method can empirically approach the ideal case of ZF equalizers and thus collect full antenna diversity.

Two more remarks about the use of the joint MRC and clipping mitigation method are now in order.

1. The smaller the IBO, the larger the ratio $\frac{\mathrm{PSNR}}{\mathrm{IBO}}$ for a fixed PSNR. At the same time however, $\Delta(\mathrm{IBO})$ in Eq. (4.25) decreases along with the IBO. Therefore, an optimal IBO may exist with respect to the SER performance, which is defined as

$$\mathrm{IBO}^{\star}\Big|_{\mathrm{PSNR}} = \arg\min_{\mathrm{IBO}} P_{\mathrm{sim}}(\mathrm{PSNR}|\mathrm{IBO}, N_r), \tag{4.46}$$

   where $P_{\mathrm{sim}}(\cdot)$ denotes the simulated average SER performance for the joint MRC and clipping mitigation method.

2. The proposed method can be regarded as an extension to the iterative quasi-ML clipping estimation method [101], which was designed for SISO-OFDM systems. However, the quasi-ML clipping estimation method provides poor performance in fading channels. The main reason is that the subcarriers with deep fadings will have low receive SNR and large error probabilities. The clipping estimation propagates the errors and yields degraded estimates for clipping noise and data. In SIMO fading channels, multiple receptions over independently faded channels not only provide the diversity gain for the data error performance, but also achieve better estimation for the clipping noise. The proposed joint MRC and clipping mitigation method thus exploits this benefit for both clipping noise and

data estimation. In Section 4.5, we will show that the SER performance gets close to the MLSD bound within five iterations even for very small IBOs.

In summary, the proposed joint MRC and clipping mitigation method can provide the near-MLSD SER performance. However, it requires the knowledge about the transmitter nonlinearity as well as receiver-side modifications. Otherwise, PWLS or optimal clipping transmitters should be adopted for transparent receivers. In both cases, full antenna diversity can be collected.

4.5 Simulations

For all simulations in this section, the uncoded OFDM system has $N = 512$ subcarriers and uses 16QAM modulation. Unless otherwise specified, frequency-selective Rayleigh fading channel with two taps and $N_r = 2$ receiving antennas are assumed.

In Figure 4.1, the SER versus PSNR curves are plotted for the proposed transceivers in the peak power constrained SIMO-OFDM channel.

First, the ideal case with IBO = 0dB but linear PA (i.e., no clipping, thus $E[|y_n|^2] = P_{\text{peak}}$ and $\Delta(\text{IBO}) = 1$) is plotted as a benchmark in Figure 4.1. Although only constant-envelope modulations (rather than OFDM) may actually achieve this error performance in practice, it gives an SER lower bound for this channel. For OFDM, by setting $\sigma_x^2 = P_{\text{peak}}$ and assuming no clipping happens, Monte Carlo simulation gives the SER curve for this ideal case. The curve agrees well with the theoretical MLSD bound in Eq. (4.25) with IBO = 0dB and $\Delta(\text{IBO}) = 1$.

Using the transparent receivers with the MRC weights given in Proposition 4.1, three transmitter schemes are also compared in Figure 4.1, namely the constant clipping, the PWLS and the optimal clipping approaches. As expected in Section 4.3.1, no antenna diversity can be obtained with the constant clipping method. In fact, the SER reaches an error floor that is determined by the clipping threshold. The PWLS-based transceiver can provide full antenna diversity but poor coding gain. Compared

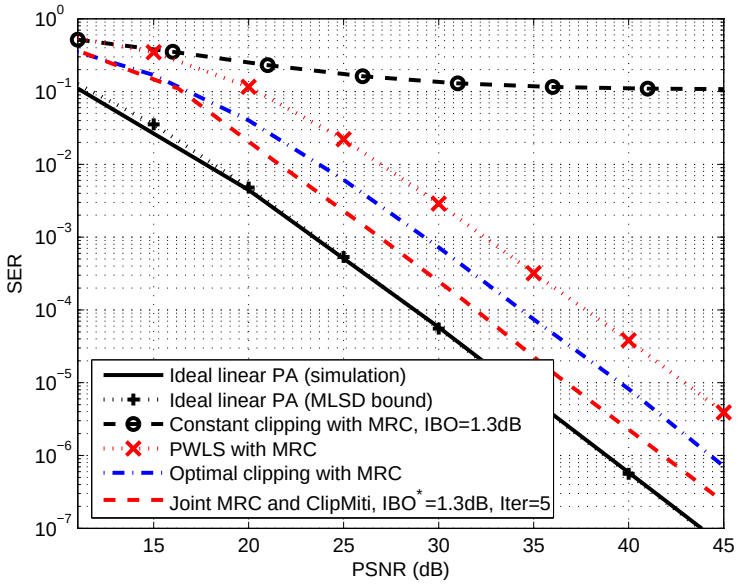

Figure 4.1: The SER versus PSNR curves for the constant clipping (IBO = 1.3dB), PWLS, optimal clipping, joint MRC and clipping mitigation (with the optimal IBO* = 1.3dB and five iterations) schemes, as well as the assumed ideal case with IBO = 0dB but no clipping; $N_r = 2$.

to the case with ideal linear PA, the PSNR degradation $\left(E[\text{PAR}^{-1}]\right)^{-1}$ is more than 9dB in the simulated system, as shown in Figure 4.1. On the other hand, the optimal clipping method achieves about 3dB coding gain better than PWLS.

For the iterative method of Eqs. (4.42)-(4.44), the MSE curves for the estimate of $\mathbf{d}$ (i.e., Eq. (4.45)) are plotted in Figure 4.2. The cases with PSNR = 30dB and 40dB as well as two oversampling ratios ($L = 1$ and 4) are examined. The results illustrate that the MSE decreases quickly along with iterations, especially at high PSNR. For comparison, the corresponding MSE curves are plotted when the SISO iterative clipping mitigation method [101] is adopted on one of the antennas and the combining technique is used subsequently. It demonstrates that the benefit of multiple receiving antennas can be exploited to improve the clipping noise estimation performance. In Figure 4.3, the joint MRC and clipping mitigation method is illustrated to achieve near-MLSD SER performance within five iterations for both the Nyquist-rate and

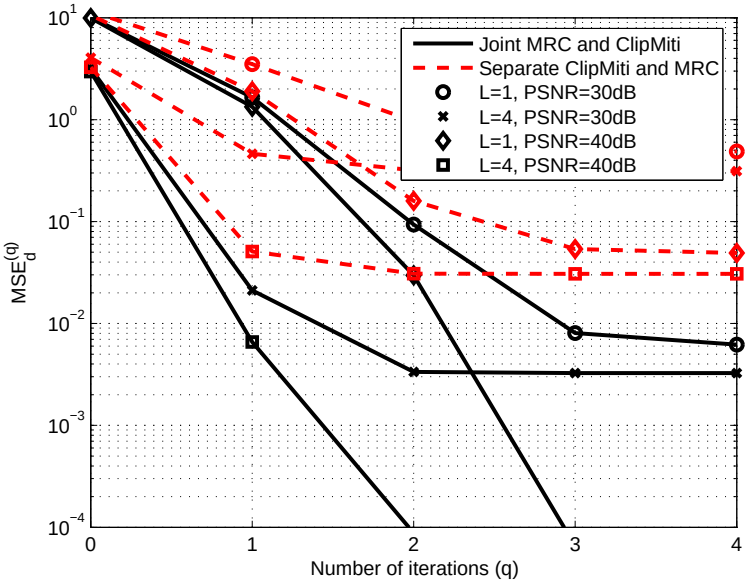

Figure 4.2: $\text{MSE}_{\mathbf{d}}^{(q)}$ versus the number of iterations (q) for the joint MRC and clipping mitigation methods; The corresponding MSE curves of separately using clipping mitigation [101] and MRC methods are also plotted for comparison; IBO = 1dB, $N_r = 2$, the oversampling ratio $L = 1$ or 4, and PSNR = 30dB or 40dB.

oversampled ($L = 4$) OFDM signals. It also works well for more than 2 receiving antennas as shown in Figure 4.4. In contrast, if the SISO iterative clipping mitigation method [101] and MRC are used separately, the antenna diversity cannot be collected even after 100 iterations.

As mentioned in Eq. (4.46), the optimal IBO* can be determined to achieve the best SER for the joint MRC and clipping mitigation method. Some numerical results of the SER versus IBO curves are given for different PSNR values and numbers of antennas in Figure 4.5. The optimal IBO is found to remain about the same for different numbers of antennas. In addition, since diversity gain is achieved, IBO* is generally independent with the PSNR. For example, IBO$^\star \approx 1.3$dB can be found for $N_r = 2$, 3 and 4 receiving antennas. With IBO$^\star = 1.3$dB and five iterations, the SER curve for the joint MRC and clipping mitigation method is plotted back into Figure 4.1 and shown to outperform the other approaches.

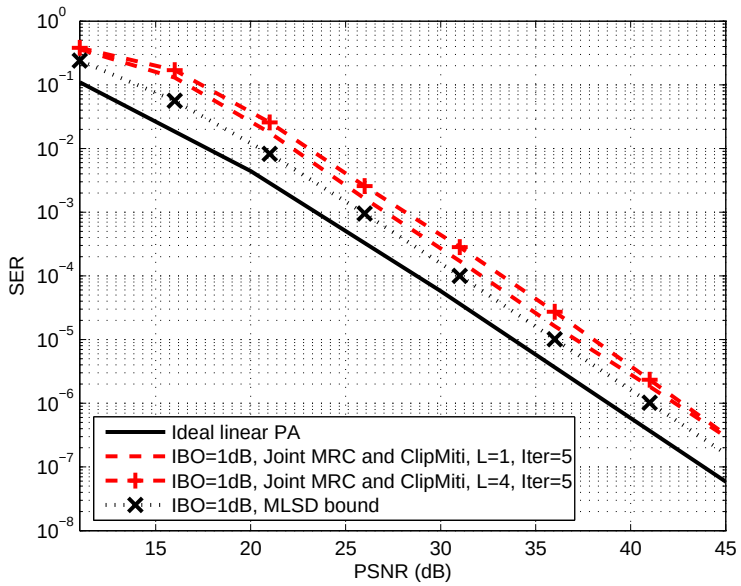

Figure 4.3: SER performance of the joint MRC and clipping mitigation method for both the Nyquist-rate and oversampling OFDM system; The SER curves of the ideal linear PA and the MLSD bound in Eq. (4.25) with IBO = 1dB are also shown for comparison; $N_r = 2$.

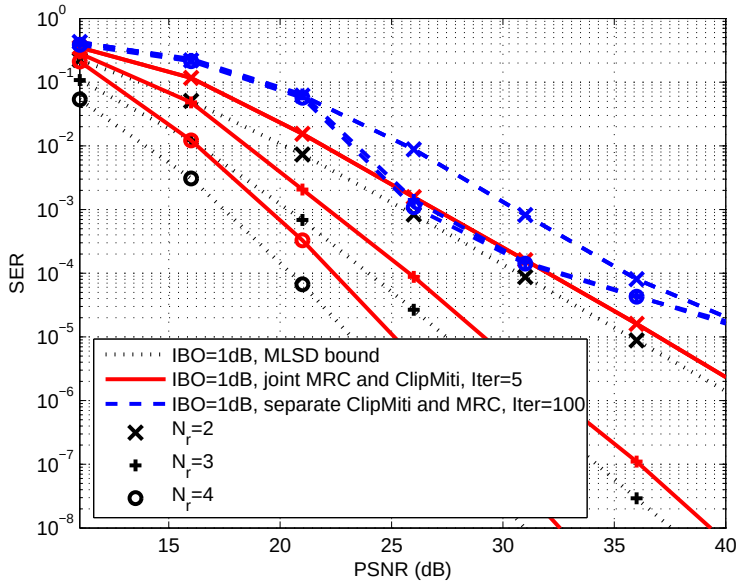

Figure 4.4: SER versus PSNR curves for different numbers of receiving antennas $N_r = 2$, 3 or 4; The proposed joint MRC and clipping mitigation method achieves a near-MLSD SER within five iterations; But separately using clipping mitigation [101] and MRC cannot collect full antenna diversity even after 100 iterations. IBO = 1dB.

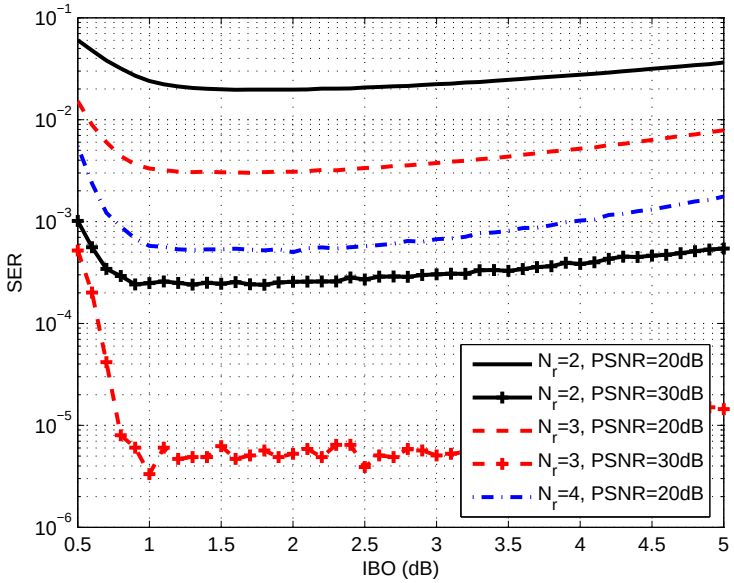

Figure 4.5: For PSNR = 20dB or 30dB, the SER versus IBO curves for the joint MRC and clipping mitigation method with N_r =2, 3 or 4 receiving antennas and 5 iterations.

4.6 Conclusions

In this chapter, we have examined the antenna diversity order in the peak power constrained SIMO-OFDM system. The main conclusion is that full antenna diversity can be achieved for the transparent receiver by intelligently choosing the transmission method. To achieve full antenna diversity, the MRC coefficients are derived for the peak power constrained channel and can be obtained in the same way with those in the linear channel. Additionally, we showed that for systems where the receiver has perfect knowledge of the transmitter nonlinearity, antenna diversity can be achieved with low-complexity linear equalizers. The joint MRC and clipping mitigation method is also proposed to employ the multiple antennas to better estimate both the clipping noise and the data.

CHAPTER V

DIVERSITY-ENABLED PPC COOPERATIVE NETWORKS

Cooperative networks have been receiving a lot of attention recently as a distributed means of improving the reliability of wireless communication links in a fading environment. Without requiring multiple antennas for each terminal, cooperative communication among distributed single-antenna nodes can enhance the reliability of wireless networks by exploiting the available spatial diversity, known as cooperative diversity *[48, 92]. In this chapter, the diversity performance of single- and multi-relay amplify-and-forward cooperative networks is studied. The effects of the peak power constraint and the availabilities of channel state information on the diversity performance are evaluated. Practical relaying strategies are also proposed.*

5.1 Introduction

Owing to the broadcasting nature of wireless communications, the transmission from a source node can be collected by its neighboring nodes, which may act as wireless relays and forward copies of information to the destination via independent fading links, thus enabling the cooperative diversity gain. The two-hop single- and multi-relay networks considered in this chapter are two typical cooperative communication systems [48].

Depending on the functionalities of the relay nodes, the relay strategies can be classified into two main categories, *regenerative* relaying and *non-regenerative* relaying. For regenerative relaying (a.k.a. decode-and-forward (DF) relaying [48]) strategy,

the relay node fully decodes the received signal and transmits the re-encoded symbols to the destination. A well known disadvantage of DF relaying is the loss of the diversity benefits unless sophisticated system designs are employed, e.g., the specified combining method at the destination which accounts for the reliability of the relay links [105], the selective DF strategy relying on cyclic redundancy check (CRC) codes to detect errors at the relay [39], the collaborative hybrid automatic-repeat-request (ARQ) protocols [95], distributed space-time cooperative systems [9], or link-adaptive regeneration (LAR) based DF strategies [18, 106]. The channel estimation, the decoding, and the diversity-enabling modules at the relays and the destination complicate the processing and/or cost extra bandwidth and power.

Non-regenerative relaying strategies such as the amplify-and-forward (AF) protocol in [48, 112], where the relay node simply forwards a scaled version of the received signal to the destination [48], allow simple processing with low operational power consumption at relay nodes. Additionally, the cooperative diversity in Rayleigh fading channels is generally enabled without the need of feedback mechanisms (e.g., ARQ or CRC) [8].

To collect full cooperative diversity, however, the AF protocols encounter two practical issues: (i) The channel state information (CSI) of the source-relay link (i.e., two-hop (2H) channel information) should be accessible to the destination node [49, 87]. Although this may be made feasible via distributed channel estimation and forwarding mechanisms [87, 112], it inevitably increases the system complexity, reduces the spectral efficiency and degrades the system performance. (ii) Another practical concern for AF relaying is that the power scaling factor (PSF) and output signal at the relay may be unbounded. In practice, many RF/analog components in communication devices, e.g., the PA, are peak power constrained [7, 23]. The unboundedness of PSF and/or output signals at the relay may cause peak power saturation and result in an error floor. Therefore, it hinders AF relaying from being

appropriately implemented.

Efforts to improve the performance of non-regenerative relaying networks have been well documented in the literature. For example, to avoid channel estimation at the relay, a fixed-gain protocol has been proposed based on the knowledge of only channel statistics [29, 38]. However, none of them has studied the diversity performance of the fixed-gain protocol, especially when full CSI is not available at the destination. In addition, the unboundedness of the transmit power at the relay remains a problem from the implementation point of view. A PSF that is a piecewise function of the source-relay link CSI has been proposed with the consideration of relay saturation [38]. However, it requires the channel estimation and may still lead to PA saturations at the relay, resulting in the loss of diversity with PPC relay nodes. Based on the AF protocol [48] and the fixed-gain strategy [38], various power distribution schemes have been proposed with respect to different performance metrics and power constraints [31, 37, 69]. For general fading channels, conditions on diversity-enabling fading statistics of the links involving the AF relays are given in [90] so that strategically positioned relay nodes can help to enable cooperative diversity.

Furthermore, how to improve the spectral efficiency of the cooperative network without losing the diversity gain is also an important and practical problem. With regard to spectral efficiency, several schemes have been proposed, including precoders [27], space-time codes [41], two-way relay networks [22, 86], and relay selection schemes [42], etc. However, the aforementioned problems also exist.

Therefore, in this chapter, we first develop diversity-enabled generalized amplify-and-forward (GAF) strategies with practical PSFs at the relay without any ARQ feedback or CSI forwarding at any hop. To address the CSI issue, two maximum ratio combining (MRC) receivers are considered, namely, one-hop (1H) MRC with only 1H CSI and 2H-MRC also having the 2H CSI. The conditions on PSFs for 1H-MRC and 2H-MRC receivers to collect full cooperative diversity are revealed to serve as design

criteria for general diversity-enabled non-regenerative relaying strategies. Based on these guidelines, we analyze the performance of 1H-MRC and 2H-MRC receivers in the peak power constrained relay networks and propose a simple and practical intentional peak power limit AF strategy. The benefits of the proposed method are two-folded: (i) our proposed strategy avoids any saturation at peak power constrained relays; (ii) low-complexity 1H-MRC is able to collect full cooperative diversity order.

Moreover, the asymptotic error performance of the relay selection schemes is analyzed. With respect to the diversity gain function, we investigate the effects of the availabilities of the 1H and 2H CSIs at the destination. A general theorem on diversity gain function is presented as well. It will be shown that fixed-gain AF relaying with the 1H-CSI selection scheme will achieve the same average SER with the 2H-CSI selection, and thus helps simplify the implementation without error performance degradation.

5.2 Signal Model of the Amplify-and-Forward Cooperative Network

We first consider a single-relay network as shown in Figure 5.1, which consists of three nodes: a source (S), a relay (R), and a destination (D).

For half-duplex nodes, two time slots are needed. Source S broadcasts its information symbol x to Relay R and Destination D in the first time slot. In the second time slot, R forwards the received signals to D. We consider the non-regenerative strategy at R, which does not require feedback or repeating mechanism, and thus is simple for practical implementations. Without loss of generality, we assume that every node is equipped with only one antenna and all channels are mutually independent.

With subscripts signifying the corresponding link, e.g., $_{sr}$ denotes the link from S to R, the mathematical model of the baseband input-output relationship can be

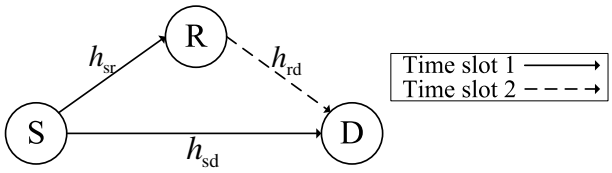

Figure 5.1: Single-relay cooperative network.

formulated as

$$y_{sd} = h_{sd}x + w_{sd}, \tag{5.1}$$

$$y_{sr} = h_{sr}x + w_{sr}, \tag{5.2}$$

$$y_{rd} = \sqrt{\alpha}h_{rd}y_{sr} + w_{rd}, \tag{5.3}$$

where y denotes the received signals, h the fading channel coefficients, and w the additive white Gaussian noise (AWGN). α represents an adaptive PSF at the relay and is assumed to be a function of $|y_{sr}|$ or $|h_{sr}|^2$ that is correctly measured at R. In this chapter, we assume $h_{ij} \sim \mathcal{CN}(0, \sigma_{ij}^2)$, $w_{ij} \sim \mathcal{CN}(0, N_0)$ ($i \in \{s, r\}$ and $j \in \{r, d\}$), and the channels and noises are mutually independent. For notational simplicity, denote $\rho_{ij} \triangleq |h_{ij}|^2$ which is exponentially distributed with mean σ_{ij}^2. The average SNR can be defined as

$$\bar{\gamma} = \frac{P_x}{N_0}, \tag{5.4}$$

where $P_x = E_x[|x|^2]$ is the average transmit power from Source S.

In practice, Relay R is usually subject to an instantaneous peak power constraint P_{peak}, i.e., the output signal of R should satisfy

$$\alpha|y_{sr}|^2 \leq P_{\text{peak}}. \tag{5.5}$$

The peak power constraint is applicable to model many practical scenarios, e.g., in the presence of power amplifiers as discussed in Chapter 2. We further define $P_{\text{peak}} = KP_x$, where $K > 0$ is a finite constant. Therefore, $\bar{\gamma}$ in Eq. (5.4) suffices to characterize the average SNR of the relay network.

In this single-relay network, the destination D performs MRC on the collected signal and estimates the symbol x as

$$\hat{x} = \arg\min_{\tilde{x}\in\Omega} \left| c_1^* y_{sd} + c_2^* y_{rd} - (c_1^* h_{sd} + c_2^* \sqrt{\alpha} h_{sr} h_{rd})\tilde{x} \right|^2, \tag{5.6}$$

where Ω is the constellation of the information symbol x. c_1 and c_2 are the MRC weights for y_{sd} and y_{rd}, respectively. Based on the availability of the 2H CSI at the destination, we define two types of MRC as follows.

Definition 5.1 (1H-MRC and 2H-MRC) *At Destination D, one-hop MRC (1H-MRC) only requires the estimates of one-hop fading coefficients (1H CSI) h_{sd} and $h_r \triangleq \sqrt{\alpha} h_{sr} h_{rd}$. With the assumption of ideal channel estimation at D, the MRC weights of 1H-MRC are given by*

$$c_1 = h_{sd},\ c_2 = h_r, \tag{5.7}$$

and for each channel realization, the instantaneous post-processing SNR is

$$\gamma_{1\mathrm{H}} = \frac{(\rho_{sd} + \alpha\rho_{sr}\rho_{rd})^2}{\rho_{sd} + \alpha\rho_{sr}\rho_{rd} + \alpha^2\rho_{sr}\rho_{rd}^2}\bar{\gamma}. \tag{5.8}$$

When the CSIs of all three links are available at the destination as assumed in most AF papers [48, 87, 112], two-hop MRC (2H-MRC) can be applied, for which the MRC weights become

$$c_1 = h_{sd},\ c_2 = \frac{h_r}{1 + \alpha\rho_{rd}}, \tag{5.9}$$

and the instantaneous SNR is given as

$$\gamma_{2\mathrm{H}} = \left(\rho_{sd} + \frac{\alpha\rho_{sr}\rho_{rd}}{1 + \alpha\rho_{rd}}\right)\bar{\gamma}. \tag{5.10}$$

The difference between 1H-MRC and 2H-MRC is the availability of the 2H CSI h_{sr} at the destination. With the full CSI of each link, 2H-MRC achieves the maximum-likelihood error performance. On the other hand, 1H-MRC is not expected to perform

as well as 2H-MRC. However, its low complexity and ease of deployment, together with the comparable BER performance as we will show later, make 1H-MRC attractive from a practical standpoint.

For notational simplicity, the diversity orders (as defined in Eq. (2.16)) of 1H-MRC and 2H-MRC destinations are denoted as $G_{1\mathrm{H}}$ and $G_{2\mathrm{H}}$, respectively. In addition, in Sections 5.2-5.4, we use $E[\cdot]$ to denote the expectation over all fading channels ρ_{sd}, ρ_{sr} and $\rho_{rd} \in [0, \infty)$. Then, the average BER P_b can be obtained by

$$P_b = E[P_B(\gamma)] = \frac{1}{\sigma_{sd}^2 \sigma_{sr}^2 \sigma_{rd}^2} \int_0^\infty \int_0^\infty \int_0^\infty P_B(\gamma) \exp\left(-\frac{\rho_{sd}}{\sigma_{sd}^2} - \frac{\rho_{sr}}{\sigma_{sr}^2} - \frac{\rho_{rd}}{\sigma_{rd}^2}\right) d\rho_{sd} d\rho_{sr} d\rho_{rd}, \tag{5.11}$$

where the instantaneous SNR γ is a function of $\bar{\gamma}$ and CSI as in Eqs. (5.8) and (5.10), and for M-ary QAM constellations, $P_B(\gamma) \approx \frac{1}{\log_2 M} P_E(\gamma) \approx \frac{\kappa_1}{\log_2 M} Q(\sqrt{\kappa_2 \gamma})$ where $P_E(\gamma)$, κ_1 and κ_2 are given in Section 2.3. For simplicity, 4-ary QAM is assumed in Sections 5.2-5.4 which has $\kappa_1 = 2$ and $\kappa_2 = 1$.

5.3 General Design Criteria for AF Cooperative Networks

The diversity performance of 2H-MRC and 1H-MRC destinations with general AF relaying PSFs is studied in this section. The necessary and sufficient conditions for general PSFs to achieve full diversity are also revealed.

5.3.1 General Amplify-and-Forward Strategy

To study the effect of PSF designs on system performance, we design the generalized amplify-and-forward (GAF) strategy, with the PSF α as a function of ρ_{sr} and subject to certain assumptions given as follows [58]:

A1) $\alpha(\rho_{sr})$ is nonnegative and continuous for $\rho_{sr} \in [0, \infty)$;

A2) $\alpha(\rho_{sr}) = \sum_{i=1}^{\infty} a_{i0} \rho_{sr}^{p_{i0}}$ as $\rho_{sr} \to 0^+$, where $a_{i0} \neq 0$ and $p_{i0} < p_{j0}$ for $i < j$. In other words, there exists $m_0^r > 0$ such that $\alpha(\rho_{sr}) = \sum_{i=1}^{\infty} a_{i0} \rho_{sr}^{p_{i0}}$ for $\rho_{sr} \in [0, m_0^r]$. Note

that if $p_{10} > 0$, $\rho_{sr} = 0$ is an isolated root of $\alpha(\rho_{sr}) = 0$ and p_{10} is defined as the order of smoothness at $\rho_{sr} = 0$ [107]; otherwise, if $p_{10} \leq 0$, $\alpha(0) > 0$;

A3) Define a set $\mathcal{R} = \{r_k | \alpha(r_k) = 0, r_k \in (0, \infty)\} = \bigcup_{k=1,2,\cdots,Z} \left[r_k^l, r_k^r\right]$, where r_k^l and r_k^r are the left and right boundaries of the kth zero interval where $\alpha(\rho_{sr}) = 0$. Z is the number of zero intervals. When $r_k^l = r_k^r$, the kth interval is an isolated zero root. In contrast, due to the continuous assumption of α, there cannot be isolated non-zero points, i.e., it should have $r_k^r < r_{k+1}^l$ rigorously;

A4) If $\mathcal{R} \neq \emptyset$, $\alpha(\rho_{sr}) = \sum_{i=1}^{\infty} a_{ik}^l (r_k^l - \rho_{sr})^{p_{ik}^l}$ as $\rho_{sr} \to r_k^{l-}$ and $\alpha(\rho_{sr}) = \sum_{i=1}^{\infty} a_{ik}^r (\rho_{sr} - r_k^r)^{p_{ik}^r}$ as $\rho_{sr} \to r_k^{r+}$, where $a_{ik}^l, a_{ik}^r > 0$ and $0 < p_{ik}^l < p_{jk}^l$, $0 < p_{ik}^r < p_{jk}^r$ for $i < j$. In other words, denoting $r_0^r = 0$, there exist m_k^l and m_k^r such that $r_{k-1}^r < m_{k-1}^r \leq m_k^l < r_k^l$ for $k = 1, 2, \cdots, Z$ and $m_Z^r > r_Z^r$ if $r_Z^r < \infty$, $\alpha(\rho_{sr}) = \sum_{i=1}^{\infty} a_{ik}^l (r_k^l - \rho_{sr})^{p_{ik}^l}$ $(\forall \rho_{sr} \in [m_k^l, r_k^l])$ and $\alpha(\rho_{sr}) = \sum_{i=1}^{\infty} a_{ik}^r (\rho_{sr} - r_k^r)^{p_{ik}^r}$ $(\forall \rho_{sr} \in [r_k^r, m_k^r])$.

Note that no particular assumptions of average power or peak power constraints are posed on $\alpha(\rho_{sr})$ of GAF strategies yet. The model of $\alpha(\rho_{sr})$ in GAF is general enough to represent the existing PSF designs in literature, e.g., the AF protocol in the high SNR region [48] and the fixed-gain protocol [38]. Moreover, it is also able to incorporate many practical and general constraints, e.g., bounded output signals.

Two more remarks about the use of PSF $\alpha(\rho_{sr})$ are now in order. First, although the PSF α at the relay is assumed as a function of ρ_{sr}, we do not require ρ_{sr} to be available at the destination. Therefore, for the GAF strategy, we can adopt either 1H-MRC or 2H-MRC to detect the transmitted signal based on the availability of the 2H CSI ρ_{sr} at the destination. Secondly, though in this subsection we assume that the relay knows ρ_{sr} as in most AF papers [48, 87, 112], the following results can also be extended to the scenario where the relay does not have ρ_{sr}, e.g., α is designed as a function of $|y_{sr}|$ as discussed in Section 5.4. The GAF design criteria developed here can be applied to guide the design of specific relay networks.

In the following, we analyze the diversity performance of 2H-MRC and 1H-MRC with the GAF strategy, respectively [59].

5.3.2 GAF with 2H-MRC

We first summarize the upper bound for the diversity order achieved by 2H-MRC with GAF strategies in the following proposition.

Proposition 5.1 (Maximum Diversity Order of 2H-MRC) *Consider a non-regenerative relay system with a GAF $\alpha(\rho_{sr})$ at the relay. The diversity order obtained by a 2H-MRC destination is upper bounded by*

$$G_{\text{2H}} \leq 1 + \min_{k \geq 1} \left\{ z_1(p_{10}), z_2(r_k^r - r_k^l), \frac{1}{p_{1k}^r}, \frac{1}{p_{1k}^l} \right\} \tag{5.12}$$

where

$$z_1(t) = \begin{cases} 1, & t \leq 0, \\ \frac{1}{t+1}, & t > 0, \end{cases} \quad \textit{and } z_2(t) = \begin{cases} 0, & t \neq 0, \\ 1, & t = 0. \end{cases} \tag{5.13}$$

Proof: We prove Proposition 5.1 by investigating the effects of the following characteristics of $\alpha(\rho_{sr})$ on the diversity performance: continuous zero interval, a zero point at $\rho_{sr} = 0$, the order of smoothness at r_k^r and r_k^l, respectively.

(i) If $\alpha(\rho_{sr})$ has at least one continuous zero interval, $\exists k \geq 1$ such that $r_k^r \neq r_k^l$ and $\gamma_{\text{2H}} = \rho_{sd}\bar{\gamma}$ $(\forall \rho_{sr} \in [r_k^l, r_k^r])$ [c.f. Eq. (5.10)]. Then, we have [83, p. 818]

$$P_b \geq \int_{r_k^l}^{r_k^r} \int_0^{\infty} \frac{Q(\sqrt{\rho_{sd}\bar{\gamma}})}{\sigma_{sr}^2 \sigma_{sd}^2} \exp\left(-\frac{\rho_{sr}}{\sigma_{sr}^2} - \frac{\rho_{sd}}{\sigma_{sd}^2} \right) d\rho_{sd} d\rho_{sr} \doteq \bar{\gamma}^{-1}. \tag{5.14}$$

Therefore, the diversity order is less than or equal to 1 in this case.

(ii) We show that the diversity is also determined by the order of smoothness around the origin $\rho_{sr} = 0$.

Since the destination has two independently faded receptions and the SNR of 2H-MRC in Eq. (5.10) is the sum of the individual SNRs, the diversity order of 2H-MRC

is the sum of those provided by each independent channel [90]. In the *S-R-D* link, the instantaneous SNR is denoted as

$$\gamma_r = \frac{\alpha(\rho_{sr})\rho_{sr}\rho_{rd}}{1+\alpha(\rho_{sr})\rho_{rd}}\bar{\gamma}. \tag{5.15}$$

Consider the region of $\rho_{sr} \in [0, m_0^r]$, where $\alpha(\rho_{sr}) = \sum_{i=1}^{\infty} a_{i0}\rho_{sr}^{p_{i0}}$ according to (A2). To investigate the diversity order upper bound, here we only consider $p_{10} > 0$ and $a_{10} > 0$, i.e., $\rho_{sr} = 0$ is an isolated zero root. By referring to [18, Lemma 6], $\exists \mu_0 > 0$ that $\alpha(\rho_{sr}) \leq \mu_0 \rho_{sr}^{p_{10}}$ $(\forall \rho_{sr} \in [r_k^r, m_k^r])$. Thus, in this region, the instantaneous SNR on the *S-R-D* link has

$$\gamma_r \leq \alpha(\rho_{sr})\rho_{sr}\rho_{rd}\bar{\gamma} \leq \mu_0 \rho_{sr}^{p_{10}+1}\rho_{rd}\bar{\gamma}. \tag{5.16}$$

Therefore, the average BER of the *S-R-D* link is lower bounded by

$$E[Q(\sqrt{\gamma_r})] \geq \frac{1}{2\sqrt{\pi}\sigma_{sr}^2\sigma_{rd}^2}\int_0^{m_0^r}\int_0^{\infty}\frac{\exp\left(-\frac{1}{2}\mu_0\rho_{sr}^{p_{10}+1}\rho_{rd}\bar{\gamma} - \frac{\rho_{sr}}{\sigma_{sr}^2} - \frac{\rho_{rd}}{\sigma_{rd}^2}\right)}{\sqrt{\frac{1}{2}\mu_0\rho_{sr}^{p_{10}+1}\rho_{rd}\bar{\gamma}+2}}d\rho_{rd}d\rho_{sr}, \tag{5.17}$$

where the inequality is given by (5.16) and [5, 7.1.13]

$$Q(t) \geq \frac{\exp\left(-t^2/2\right)}{\sqrt{\pi}(\frac{t}{\sqrt{2}} + \sqrt{\frac{t^2}{2}+2})} \geq \frac{\exp\left(-t^2/2\right)}{2\sqrt{\pi}\sqrt{\frac{t^2}{2}+2}}. \tag{5.18}$$

Referring to [33, 3.362.2], (5.17) becomes

$$\begin{aligned} E[Q(\sqrt{\gamma_r})] &\geq \frac{1}{2\sigma_{sr}^2\sigma_{rd}^2}\int_0^{m_0^r}\frac{e^{-\frac{\rho_{sr}}{\sigma_{sr}^2}}e^{\theta\epsilon}Q(\sqrt{\theta\epsilon})}{\sqrt{\epsilon}\sqrt{\frac{1}{2}\mu_0\rho_{sr}^{p_{10}+1}\bar{\gamma}}}d\rho_{sr} \\ &\geq \frac{1}{2\sigma_{sr}^2\sigma_{rd}^2}\int_0^{m_0^r}\frac{e^{-\frac{\rho_{sr}}{\sigma_{sr}^2}}e^{\theta\epsilon}Q(\sqrt{\theta\epsilon})}{\epsilon}d\rho_{sr}, \end{aligned} \tag{5.19}$$

where $\theta = 4(\mu_0\rho_{sr}^{p_{10}+1}\bar{\gamma})^{-1}$ and $\epsilon = \frac{1}{2}\mu_0\rho_{sr}^{p_{10}+1}\bar{\gamma} + \frac{1}{\sigma_{rd}^2}$. Because

$$e^{\theta\epsilon}Q(\sqrt{\theta\epsilon}) = \left(\int_{\sqrt{\theta\epsilon}}^{\sqrt{2\theta\epsilon}} + \int_{\sqrt{2\theta\epsilon}}^{\infty}\right)\frac{\exp\left(\theta\epsilon - \frac{u^2}{2}\right)}{\sqrt{2\pi}}du \geq \frac{(\sqrt{2}-1)\sqrt{\theta\epsilon}}{\sqrt{2\pi}}, \tag{5.20}$$

and $\theta\epsilon \geq 2$, (5.19) can be further lower bounded by

$$E[Q(\sqrt{\gamma_r})] \geq C_1 \int_0^{m_0^r} \epsilon^{-1} e^{-\frac{\rho_{sr}}{\sigma_{sr}^2}} d\rho_{sr} \dot{\geq} \int_0^{m_0^r} g(\rho_{sr}) d\rho_{sr}, \tag{5.21}$$

where $C_1 = \frac{\sqrt{2}-1}{2\sqrt{\pi}\sigma_{sr}^2\sigma_{rd}^2}$ and

$$g(\rho_{sr}) = e^{-\frac{\rho_{sr}}{\sigma_{sr}^2}} \left(\rho_{sr} \left(\frac{1}{2}\mu_0\bar{\gamma} \right)^{\frac{1}{1+p_{10}}} + \sigma_{rd}^{-\frac{2}{1+p_{10}}} \right)^{-(1+p_{10})}. \tag{5.22}$$

The inequality $(a+b)^p \geq a^p + b^p$ with $a, b, p > 0$ is also used in reaching (5.21).

If the integrals of $g(\rho_{sr})$ have

$$I_1 \triangleq \lim_{\bar{\gamma}\to\infty} \int_{m_0^r}^{\infty} g(\rho_{sr}) d\rho_{sr} \dot{<} I_2 \triangleq \lim_{\bar{\gamma}\to\infty} \int_0^{\infty} g(\rho_{sr}) d\rho_{sr}, \tag{5.23}$$

The inequality in (5.21) will lead to

$$\lim_{\bar{\gamma}\to\infty} E[Q(\sqrt{\gamma_r})] \dot{\geq} I_2. \tag{5.24}$$

Now denote $\varepsilon = \left(\frac{1}{2}\mu_0\bar{\gamma}\right)^{-\frac{1}{p_{10}+1}} \sigma_{sr}^{-2} \sigma_{rd}^{-\frac{2}{p_{10}+1}}$. By referring to [33, 3.382.4] and [5, 6.5.25], we have

$$I_2 = \lim_{\bar{\gamma}\to\infty} \left(\frac{1}{2}\mu_0\bar{\gamma} \right)^{-1} \sigma_{sr}^{-2p_{10}} e^{\varepsilon} \Gamma\left(-p_{10}, \varepsilon\right) \doteq \bar{\gamma}^{-1} \lim_{\varepsilon\to 0} \Gamma\left(-p_{10}, \varepsilon\right) \doteq \bar{\gamma}^{-(1+p_{10})^{-1}}, \tag{5.25}$$

where $\Gamma(\cdot,\cdot)$ is the incomplete Gamma function. For the left-hand side (LHS) of (5.23), we have

$$I_1 \leq \lim_{\bar{\gamma}\to\infty} \left(\frac{1}{2}\mu_0\bar{\gamma} \right)^{-1} \int_{m_0^r}^{\infty} \frac{e^{-\frac{\rho_{sr}}{\sigma_{sr}^2}}}{\rho_{sr}^{1+p_{10}}} d\rho_{sr} \doteq \bar{\gamma}^{-1}. \tag{5.26}$$

Therefore, for $p_{10} > 0$, the assumption of (5.23) is verified by Eqs. (5.25) and (5.26). As a result, (5.21) leads to

$$\lim_{\bar{\gamma}\to\infty} E[Q(\sqrt{\gamma_r})] \dot{\geq} \bar{\gamma}^{-(1+p_{10})^{-1}}. \tag{5.27}$$

In addition, the diversity order of the direct *S-D* Rayleigh fading channel is 1 [83, p. 818]. Therefore, the diversity order of 2H-MRC is bounded by (c.f. [90])

$$G_{\text{2H}} \leq 1 + (1 + p_{10})^{-1}. \tag{5.28}$$

(iii) According to (A4), $\forall \rho_{sr} \in [r_k^r, m_k^r]$ $(k \geq 1)$, $\alpha(\rho_{sr}) = \sum_{i=1}^{\infty} a_{ik}^r (\rho_{sr} - r_k^r)^{p_{ik}^r}$. Again, p_{1k}^r is the order of smoothness at r_k^r, and $\exists \mu_k^r > 0$ that $\alpha(\rho_{sr}) \leq \mu_k^r (\rho_{sr} - r_k^r)^{p_{1k}^r}$ $(\forall \rho_{sr} \in [r_k^r, m_k^r])$ [18, Lemma 6]. Similar to Eqs. (5.16)-(5.21), we have

$$E[Q(\sqrt{\gamma_r})] \geq C_1 \int_0^{m_k^r - r_k^r} \frac{e^{-\frac{\tilde{\rho}_{sr} + r_k^r}{\sigma_{sr}^2}}}{\frac{1}{2}\mu_k^r m_k^r \tilde{\rho}_{sr}^{p_{1k}^r} \bar{\gamma} + \frac{1}{\sigma_{rd}^2}} d\tilde{\rho}_{sr}, \tag{5.29}$$

where $\tilde{\rho}_{sr} = \rho_{sr} - r_k^r$. For $p_{1k}^r > 1$, following the same process of Eqs. (5.21)-(5.26), (5.29) can be readily shown to have

$$\lim_{\bar{\gamma} \to \infty} E[Q(\sqrt{\gamma_r})] \dot{\geq} \bar{\gamma}^{-1} \lim_{\tilde{\varepsilon} \to 0} \Gamma(1 - p_{1k}^r, \tilde{\varepsilon}) \doteq \bar{\gamma}^{-\frac{1}{p_{1k}^r}}, \tag{5.30}$$

where $\tilde{\varepsilon} = \left(\frac{1}{2}\mu_k^r m_k^r \bar{\gamma}\right)^{-\frac{1}{p_{1k}^r}} \sigma_{sr}^{-2} \sigma_{rd}^{-\frac{2}{p_{1k}^r}}$. Therefore, (5.30) gives

$$G_{\text{2H}} \leq 1 + \min_{k \geq 1} \left\{ 1, \frac{1}{p_{1k}^r} \right\}. \tag{5.31}$$

(iv) For $\rho_{sr} \in [m_k^l, r_k^l]$, the order of smoothness leads to similar bounds on G_{2H}, but the proof is slightly different. In this region, $\exists \mu_k^l > 0$ that $\alpha(\rho_{sr}) \leq \mu_k^l (r_k^l - \rho_{sr})^{p_{1k}^l}$. Accordingly, (5.29) becomes

$$E[Q(\sqrt{\gamma_r})] \geq C_1 \int_0^{r_k^l - m_k^l} \frac{e^{\frac{\tilde{\rho}_{sr} - r_k^l}{\sigma_{sr}^2}}}{\frac{1}{2}\mu_k^l r_k^l \tilde{\rho}_{sr}^{p_{1k}^l} \bar{\gamma} + \sigma_{rd}^{-2}} d\tilde{\rho}_{sr} \tag{5.32}$$

$$\dot{\geq} \int_0^{r_k^l - m_k^l} \left[\tilde{\rho}_{sr} \left(\frac{1}{2}\mu_k^l r_k^l \bar{\gamma} \right)^{\frac{1}{p_{1k}^l}} + \sigma_{rd}^{-\frac{2}{p_{1k}^l}} \right]^{-p_{1k}^l} d\tilde{\rho}_{sr}, \tag{5.33}$$

where $\tilde{\rho}_{sr} = r_k^l - \rho_{sr}$. For $p_{1k}^l > 1$ and $\bar{\gamma} \to \infty$, (5.33) can readily lead to the asymptotic performance that $\lim_{\bar{\gamma} \to \infty} E[Q(\sqrt{\gamma_r})] \dot{\geq} \bar{\gamma}^{-\frac{1}{p_{1k}^l}}$.Therefore, the diversity order is also bounded by

$$G_{\text{2H}} \leq 1 + \min_{k \geq 1} \left\{ 1, \frac{1}{p_{1k}^l} \right\}. \tag{5.34}$$

All in all, by combining the inequalities in (5.14), (5.28), (5.31) and (5.34), the upper bound of diversity order for 2H-MRC is summarized in Proposition 5.1. ■

Unlike the conventional AF protocol [48], Proposition 5.1 shows that for an arbitrary PSF, 2H-MRC may not be able to collect full diversity order even with the 2H CSI. The diversity order is constrained by the order of smoothness of PSF $\alpha(\rho_{sr})$ around the origin ($\rho_{sr} = 0$), as well as the presence of and the orders of smoothness around zero intervals. If $p_{10} > 0$ (i.e., $\alpha(0) = 0$), $\max\{p_{1k}^l, p_{1k}^r\} > 1$ or there are continuous zero intervals ($r_k^l < r_k^r$), Proposition 5.1 shows that 2H-MRC cannot achieve full cooperative diversity order, i.e., $G_{2\mathrm{H}} < 2$. Therefore, it leads to the following necessary conditions on PSF designs for 2H-MRC to obtain full diversity order. Meanwhile, the following theorem shows that these conditions are also sufficient.

Theorem 5.1 (Full Diversity Order of 2H-MRC) *Consider a non-regenerative relay system with a GAF $\alpha(\rho_{sr})$ at the relay. The necessary and sufficient conditions for 2H-MRC in Eq. (5.9) to obtain $G_{2\mathrm{H}} = 2$ are*

C1) $\lim_{\rho_{sr}\to 0} \alpha(\rho_{sr}) > 0$, *i.e.,* $p_{10} \leq 0$;

C2) *If $\mathcal{R} \neq \emptyset$, $r_k^l = r_k^r > 0$ and $p_{1k}^l \leq 1$, $p_{1k}^r \leq 1$ $(\forall k \geq 1)$.*

Proof: Proposition 5.1 gives the necessity of (C1)-(C2). Thus, we focus on showing that (C1) and (C2) are also sufficient for $G_{2\mathrm{H}} = 2$.

The instantaneous SNR of 2H-MRC in Eq. (5.10) is upper bounded by

$$\gamma_{2\mathrm{H}} = \left(\rho_{sd} + \frac{\alpha\rho_{sr}\rho_{rd}}{1 + \alpha\rho_{rd}}\right)\bar{\gamma} \leq (\rho_{sd} + \rho_{sr})\bar{\gamma}, \tag{5.35}$$

which has diversity 2. Thus, $G_{2\mathrm{H}} \leq 2$.

To show that $G_{2\mathrm{H}} \geq 2$ with (C1)-(C2), we consider ρ_{sr} in three contiguous regions, i.e., $\mathcal{U}_1 = [0, B_1)$, $\mathcal{U}_2 = [B_1, B_2)$, and $\mathcal{U}_3 = [B_2, \infty)$ with $0 < B_1 \leq m_1^l \leq m_Z^r \leq B_2$. Both $\mathcal{U}_2$ and $\mathcal{U}_3$ can be empty sets. In these regions, equivalent to (C1)-(C2), $\alpha(\rho_{sr})$ should have:

U1) $\forall \rho_{sr} \in \mathcal{U}_1$, $\exists L_1 > 0$ so that $\alpha(\rho_{sr}) \geq L_1$;

U2) The set of roots is contained in $\mathcal{U}_2$, i.e., $\mathcal{R} \subset \mathcal{U}_2$. In addition, there can be only isolated zero points with the order of smoothness not greater than 1, i.e., $r_k^l = r_k^r \in \mathcal{U}_2$, $p_{1k}^l \leq 1$ and $p_{1k}^r \leq 1$ $(1 \leq k \leq Z)$;

U3) $\forall \rho_{sr} \in \mathcal{U}_3$, the PSF can be represented in a polynomial that $\alpha(\rho_{sr}) = \sum_{i=1}^{\infty} b_i \rho_{sr}^{q_i}$ with $b_i > 0$ and $q_i < q_j$ for $i < j$. It is worth noting that $\alpha(\rho_{sr})$ may approach (but is strictly greater than) zero as $\rho_{sr} \to \infty$ when $q_i < 0$ $(\forall i)$.

With (U1)-(U3), the average BER has

$$P_b = \sigma_{sr}^{-2} E_{\rho_{sd},\rho_{rd}} \left[\left(\int_{\rho_{sr} \in \mathcal{U}_1} + \int_{\rho_{sr} \in \mathcal{U}_2} + \int_{\rho_{sr} \in \mathcal{U}_3} \right) Q\left(\sqrt{\gamma_{2\mathrm{H}}(\alpha)} \right) e^{-\frac{\rho_{sr}}{\sigma_{sr}^2}} d\rho_{sr} \right] \quad (5.36)$$

$$\leq E_1 + E_2 + E_3, \quad (5.37)$$

where $E_i = E[Q(\sqrt{\gamma_{2\mathrm{H}}(\alpha_i)})]$ $(i = 1, 2, 3)$ with $\alpha_i(\rho_{sr}) = \alpha(\rho_{sr})$ for $\rho_{sr} \in \mathcal{U}_i$ and $\alpha_i(\rho_{sr})$ $(\rho_{sr} \notin \mathcal{U}_i)$ adopts constant values to satisfy the continuity assumption, e.g., $\alpha_1(\rho_{sr}) = \alpha(B_1)$ $(\forall \rho_{sr} \notin \mathcal{U}_1)$. The inequality of (5.37) is introduced by extending the integration intervals in Eq. (5.36) to $[0, \infty)$.

In the following, we determine the diversity orders of E_1, E_2 and E_3, respectively.

(i) For $\alpha_1(\rho_{sr})$, we further split $\rho_{sr} \in [0, \infty)$ into two sets: $\mathcal{S} = \{\rho_{sr} | \alpha_1(\rho_{sr}) \leq U_1\}$ and its complement $\bar{\mathcal{S}} = \{\rho_{sr} | \rho_{sr} \geq 0, \rho_{sr} \notin \mathcal{S}\}$, where U_1 is large enough such that $\gamma_{2\mathrm{H}} \approx (\rho_{sd} + \rho_{sr})\bar{\gamma}$, $(\forall \rho_{sr} \in \bar{\mathcal{S}})$. For $\rho_{sr} \in \mathcal{S}$, $\gamma_{2\mathrm{H}}$ has

$$\gamma_{2\mathrm{H}} \geq \left(\rho_{sd} + \frac{L_1 \rho_{sr} \rho_{rd}}{1 + U_1 \rho_{rd}} \right) \bar{\gamma} \triangleq \tilde{\gamma}_{2\mathrm{H}}. \quad (5.38)$$

Thus, by extending the integration intervals again, we have

$$E_1 \leq E\left[Q\left(\sqrt{\tilde{\gamma}_{2\mathrm{H}}} \right) \right] + E\left[Q\left(\sqrt{(\rho_{sd} + \rho_{sr})\,\bar{\gamma}} \right) \right], \quad (5.39)$$

where the second term in the right-hand side (RHS) of (5.39) is exponentially equal to $\bar{\gamma}^{-2}$ in the high SNR region. For the first RHS term of (5.39), we have

$$E\left[Q\left(\sqrt{\tilde{\gamma}_{\mathrm{2H}}}\right)\right] \leq \frac{1}{\left(\frac{1}{2}\sigma_{sd}^2\bar{\gamma}+1\right)\sigma_{rd}^2}\int_0^{\infty}\frac{e^{-\rho_{rd}/\sigma_{rd}^2}}{\frac{L_1\sigma_{sr}^2\bar{\gamma}\rho_{rd}}{2(1+U_1\rho_{rd})}+1}d\rho_{rd} \tag{5.40}$$

$$= \frac{1}{\frac{1}{2}\sigma_{sd}^2\bar{\gamma}+1}\left[\frac{U_1}{\zeta}+\frac{L_1\sigma_{sr}^2\bar{\gamma}}{2\sigma_{rd}^2\zeta^2}\exp\left(\frac{1}{\sigma_{rd}^2\zeta}\right)\Gamma\left(0,\frac{1}{\sigma_{rd}^2\zeta}\right)\right], \tag{5.41}$$

where $\zeta=\frac{1}{2}L_1\sigma_{sr}^2\bar{\gamma}+U_1$. Chernoff bound $Q(t)\leq\exp\left(-\frac{t^2}{2}\right)$ is used in (5.40) and Eq. (5.41) is given by [33, 3.383.5]. Thus, by plugging (5.41) into (5.39), the diversity order of E_1 is lower bounded by

$$\lim_{\bar{\gamma}\to\infty}-\frac{\log E_1}{\log\bar{\gamma}}\geq 1+\min\left\{1,1-\lim_{\bar{\gamma}\to\infty}\frac{\log\Gamma\left(0,\frac{1}{\sigma_{rd}^2\zeta}\right)}{\log\bar{\gamma}}\right\}=2, \tag{5.42}$$

where (5.42) is reached by using l'Hôpital's rule and the derivative of incomplete Gamma function [5, 6.5.25]. Therefore, $G_{\mathrm{2H}}\geq 2$ for $\alpha_1(\rho_{sr})$.

(ii) Without loss of generality, we assume there is only one zero point in $\mathcal{U}_2$, i.e., $Z=1$ and $r_1=r_1^l=r_1^r>0$. Multiple isolated zero roots can be addressed accordingly. For $\rho_{sr}\in[m_1^l,m_1^r]$, $\alpha_2(\rho_{sr})$ is defined as in (A4); $\forall\rho_{sr}\in[B_1,m_1^l)\cup(m_1^r,B_2)$, $\exists L_2$ and U_2 that $0<L_2\leq\alpha_2(\rho_{sr})=\alpha(\rho_{sr})\leq U_2<\infty$. To keep $\alpha_2(\rho_{sr})$ continuous, we assume $\alpha_2(\rho_{sr})=\alpha_2(B_1)$ $(\forall\rho_{sr}\in[0,B_1))$ and $\alpha_2(\rho_{sr})=\alpha_2(B_2)$ $(\forall\rho_{sr}\in[B_2,\infty))$.

As for α_1, α_2 with $\rho_{sr}\in[0,m_1^l)\cup(m_1^r,\infty)$ can be readily proved to yield $G_{\mathrm{2H}}=2$. The diversity order of E_2 is only affected by α_2 around the zero point r_1, i.e.,

$$E_2\dot{\leq}\sigma_{sr}^{-2}E_{\rho_{sd},\rho_{rd}}\left[\left(\int_{r_1}^{m_1^r}+\int_{m_1^l}^{r_1}\right)Q\left(\sqrt{\gamma_{\mathrm{2H}}(\alpha_2)}\right)e^{-\frac{\rho_{sr}}{\sigma_{sr}^2}}d\rho_{sr}\right]. \tag{5.43}$$

For $\rho_{sr}\in[r_1,m_1^r]$, due to the continuity of α_2, $\exists U_3<\infty$ such that $\alpha_2(\rho_{sr})\leq U_3$; meanwhile, $\exists\iota_1^r>0$ so that $\alpha_2(\rho_{sr})\geq\iota_1^r(\rho_{sr}-r_1)^{p_{11}^r}$ [18, Lemma 6]. Therefore, the instantaneous SNR of 2H-MRC has

$$\gamma_{\mathrm{2H}}\geq\left(\rho_{sd}+\frac{\iota_1^r(\rho_{sr}-r_1)^{p_{11}^r}\rho_{sr}\rho_{rd}}{1+U_3\rho_{rd}}\right)\bar{\gamma}\triangleq\tilde{\gamma}_{\mathrm{2H}},\ \forall\rho_{sr}\in[r_1,m_1^r]. \tag{5.44}$$

Similar to the technique used in [87, 107], $G_{2\mathrm{H}} = 2$ can be proved for $\tilde{\gamma}_{2\mathrm{H}}$ in Eq. (5.44). Denote $\tilde{\rho}_{sr} = \rho_{sr} - r_1 \in [0, m_1^r - r_1]$ and $V = v(\tilde{\rho}_{sr}, \rho_{rd}) = \frac{\iota_1^r \tilde{\rho}_{sr}^{p_{11}^r}(\tilde{\rho}_{sr}+r_1)\rho_{rd}}{1+U_3\rho_{rd}}\bar{\gamma}$. Because of (5.44), the first integral of (5.43) is further upper bounded by

$$\sigma_{sr}^{-2} E_{\rho_{sd},\rho_{rd}} \left[\int_{r_1}^{m_1^r} Q\left(\sqrt{\gamma_{2\mathrm{H}}(\alpha_2)}\right) e^{-\frac{\rho_{sr}}{\sigma_{sr}^2}} d\rho_{sr} \right] \leq E\left[Q\left(\sqrt{\rho_{sd}\bar{\gamma} + v(\tilde{\rho}_{sr}, \rho_{rd})}\right)\right], \quad (5.45)$$

where the expectation of the RHS is taken over $\tilde{\rho}_{sr}, \rho_{rd}, \rho_{sd} \in [0, \infty)$.

The first derivative of the PDF of $\tilde{\gamma}_{2\mathrm{H}}$ evaluated at zero is given by [87]

$$\frac{d}{d\tilde{\gamma}} f_{\tilde{\gamma}_{2\mathrm{H}}}(\tilde{\gamma})\Big|_{\tilde{\gamma}=0} = f_{\rho_{sd}}(0) f_V(0). \quad (5.46)$$

$f_V(0)$ can be found as

$$f_V(0) = f_{\tilde{\rho}_{sr}}(0) \int_0^\infty \frac{f_{\rho_{rd}}(t)}{|\nabla v(0,t)|} dt + f_{\rho_{rd}}(0) \int_0^\infty \frac{f_{\tilde{\rho}_{sr}}(t)}{|\nabla v(t,0)|} dt, \quad (5.47)$$

where $|\nabla v(\tilde{\rho}_{sr}, \rho_{rd})|$ is the modulus of the gradient of $v(\rho_{sr}, \rho_{rd})$ [87], i.e.,

$$|\nabla v(\tilde{\rho}_{sr}, \rho_{rd})| = \sqrt{\left|\frac{\partial}{\partial \tilde{\rho}_{sr}} v(\tilde{\rho}_{sr}, \rho_{rd})\right|^2 + \left|\frac{\partial}{\partial \rho_{rd}} v(\tilde{\rho}_{sr}, \rho_{rd})\right|^2}. \quad (5.48)$$

With $0 < p_{11}^r < 1$, we have $|\nabla v(0, \rho_{rd})| = \infty$ and $|\nabla v(\tilde{\rho}_{sr}, 0)| = \iota_1^r \tilde{\rho}_{sr}^{p_{11}^r}(\tilde{\rho}_{sr} + r_1)\bar{\gamma} > \iota_1^r r_1 \tilde{\rho}_{sr}^{p_{11}^r}\bar{\gamma}$. Bringing them into Eq. (5.47), $f_V(0)$ has

$$f_V(0) < \frac{e^{-\frac{r_1}{\sigma_{sr}^2}}}{\iota_1^r r_1 \sigma_{rd}^2 \sigma_{sr}^{2(p_{11}^r-1)}\bar{\gamma}} \Gamma(1 - p_{11}^r) < \infty. \quad (5.49)$$

Therefore, similar to the proof of Proposition 1 in [87], we have $0 < f_V(0) < \infty$, $0 < \frac{d}{d\tilde{\gamma}} f_{\tilde{\gamma}_{2\mathrm{H}}}(\tilde{\gamma})|_{\tilde{\gamma}=0} < \infty$ and $f_{\tilde{\gamma}_{2\mathrm{H}}}(0) = 0$. According to [107], the RHS of (5.45) leads to $G_{2\mathrm{H}} = 2$ for $0 < p_{11}^r < 1$.

The same argument can be made for the second integral in (5.43), the proof of which is similar and thus omitted for simplicity. Therefore, (5.43) shows that $G_{2\mathrm{H}} \geq 2$ for E_2.

(iii) The diversity order of E_3 in (5.37) is determined by $\alpha_3(\rho_{sr})$ in the region of $\rho_{sr} \in [B_2, \infty)$.

Similar to [18, Lemma 6], we can find $\eta > 0$ that $\alpha_3(\rho_{sr}) \geq \eta \rho_{sr}^{q_1}$ $(\forall \rho_{sr} \in [B_2, \infty))$. Denote

$$\gamma_{2\mathrm{H}} \geq \left(\rho_{sd} + \frac{\rho_{sr}\rho_{rd}}{\eta^{-1}\rho_{sr}^{-q_1} + \rho_{rd}} \right) \bar{\gamma} \triangleq \tilde{\gamma}_{2\mathrm{H}}. \tag{5.50}$$

When $q_1 \geq -1$, $\gamma_{2\mathrm{H}}$ is further lower bounded by

$$\gamma_{2\mathrm{H}} \geq \left(\rho_{sd} + \frac{\rho_{sr}\rho_{rd}}{\eta^{-1}\rho_{sr} + \rho_{rd}} \right) \bar{\gamma}, \tag{5.51}$$

the RHS of which has been shown to achieve the diversity order 2 [87]. If $q_1 < -1$, otherwise, denote $V = v(\rho_{sr}, \rho_{rd}) = \frac{\rho_{sr}\rho_{rd}}{\eta^{-1}\rho_{sr}^{-q_1} + \rho_{rd}} \bar{\gamma}$. $G_{2\mathrm{H}} = 2$ can be also proved for $\tilde{\gamma}_{2\mathrm{H}}$ in Eq. (5.50) with the same technique used in [87, 107] and Eqs. (5.44)-(5.49) above. Thus, we have that E_3 also yields $G_{2\mathrm{H}} \geq 2$.

Combining Eq. (5.35) and the diversity order lower bounds for the terms of E_1, E_2 and E_3, we see that (C1) and (C2) are also sufficient for 2H-MRC to achieve $G_{2\mathrm{H}} = 2$. It suffices to complete the proof for Theorem 5.1. ■

In contrast to the general link-adaptive regenerative relay networks for which $\alpha(0) = 0$ is a necessary condition to enable full cooperative diversity [18], the PSF in GAF that enables 2H-MRC to achieve full cooperative diversity order should **not** start with $\alpha(0) = 0$. Thus, the intuitive linear PSF $\alpha(\rho_{sr}) = \rho_{sr}$, which scales down the symbols with poor source-relay link qualities, does not provide full cooperative diversity order. Theorem 5.1 also requires that $\alpha(\rho_{sr}) = 0$ can only have isolated roots and $\alpha(\rho_{sr})$ approaches these roots linearly or concavely. According to Theorem 5.1, infinite $\alpha(\rho_{sr})$ is not necessary for $G_{2\mathrm{H}} = 2$. Therefore, bounded PSFs are not only practical, but can also lead to full cooperative diversity order at the destination with 2H-MRC.

As a special example, the fixed-gain protocol [38] satisfies both the conditions (C1) and (C2). Thus, with Theorem 5.1, full cooperative diversity can be readily shown for it, which is summarized in the following corollary.

Corollary 5.1 *Consider a non-regenerative relay system with a fixed-gain PSF* $\alpha(\rho_{sr}) = C > 0$ *at the relay. The diversity order achieved by 2H-MRC in Eq. (5.9) is* $G_{\mathrm{2H}} = 2$.

The major disadvantage of 2H-MRC is the requirement of the 2H CSI at the destination, which increases the transmission overhead. Besides the estimates of h_{sd} and h_r which are accessible by traditional point-to-point channel estimation methods (e.g., via pilot subcarriers in OFDM systems [74]), 2H-MRC also needs to know ρ_{sr} at the destination, which is impractical in certain communication environments.

5.3.3 GAF with 1H-MRC

Compared with 2H-MRC, 1H-MRC given in Eq. (5.7) only needs h_{sd} and h_r. Without the transmission of h_{sr}, the spectral efficiency is greatly improved and the processing at both relay and destination is also simplified. Now, a natural question is whether 1H-MRC can still collect full cooperative diversity order? The answer is positive, however, more conditions on PSF designs are required compared with those for 2H-MRC. In the following theorem, we reveal the necessary conditions.

Theorem 5.2 (Full Diversity Order of 1H-MRC) *Consider a non-regenerative relay system with a GAF* $\alpha(\rho_{sr})$ *at the relay. In addition to (C1) and (C2), another necessary condition for the 1H-MRC in Eq. (5.7) to achieve* $G_{\mathrm{1H}} = 2$ *is*

$$p_{10} \geq -\frac{1}{2}. \tag{5.52}$$

Proof: The difference between the instantaneous SNRs of 2H-MRC and 1H-MRC can be shown as

$$\Delta_\gamma \triangleq \gamma_{\mathrm{2H}} - \gamma_{\mathrm{1H}} = (1+\lambda)^{-1}\rho_{sd}\bar{\gamma} \geq 0, \tag{5.53}$$

where $\lambda = 2\alpha^{-1}\rho_{rd}^{-1} + \alpha^{-2}\rho_{rd}^{-2} + \alpha^{-2}\rho_{sr}^{-1}\rho_{rd}^{-2}\rho_{sd} + \alpha^{-3}\rho_{sr}^{-1}\rho_{rd}^{-3}\rho_{sd}$. Thus, the diversity orders achieved by 2H-MRC and 1H-MRC destinations have $G_{\mathrm{2H}} \geq G_{\mathrm{1H}}$. It indicates that (C1)-(C2) are also necessary for 1H-MRC to achieve full diversity order.

In addition, $\forall \kappa > 0$ and $\forall \delta > 0$, if $\alpha \geq \kappa \rho_{sr}^{-\frac{1}{2}-\delta}$ for the region of $\rho_{sr} \in [0, \epsilon]$, λ has

$$\lambda \leq \frac{1}{\kappa \rho_{rd}} \left(2\epsilon^{\frac{1}{2}+\delta} + \frac{\epsilon^{1+2\delta}}{\kappa \rho_{rd}} + \frac{\epsilon^{2\delta} \rho_{sd}}{\kappa \rho_{rd}} + \frac{\epsilon^{\frac{1}{2}+3\delta} \rho_{sd}}{\kappa^2 \rho_{rd}^2} \right). \tag{5.54}$$

By choosing a small enough ϵ, (5.54) can lead to $\lambda \ll 1$. As a result, $\Delta_\gamma \approx \rho_{sd} \bar{\gamma}$ and $\gamma_{1\mathrm{H}} \approx \gamma_{2\mathrm{H}} - \rho_{sd} \bar{\gamma} = \frac{\alpha \rho_{sr} \rho_{rd}}{1+\alpha \rho_{rd}} \bar{\gamma} \leq \rho_{sr} \bar{\gamma}$ with the non-zero probability $\Pr(\rho_{sr} \leq \epsilon)$. In this case, the diversity order is upper bounded by $G_{1\mathrm{H}} \leq 1$.

Therefore, besides (C1) and (C2), another necessary condition for 1H-MRC to achieve full cooperative diversity is $\alpha \leq \kappa \rho_{sr}^{-\frac{1}{2}}$ as $\rho_{sr} \to 0$, i.e., $p_{10} \geq -\frac{1}{2}$. ■

As revealed by Theorem 5.1, for 2H-MRC to obtain full diversity order, $\alpha(\rho_{sr}) > 0$ for $\rho_{sr} \to 0^+$ is sufficient. When 1H-MRC is adopted at the destination, we further require that $\alpha(\rho_{sr})$ does not go to infinity faster than $\rho_{sr}^{-\frac{1}{2}}$. In Section 5.3.4, we will verify this result by showing that 1H-MRC cannot achieve diversity order 2 with the conventional AF protocol [48, Eq. (9)], which has $\alpha(\rho_{sr}) \doteq \rho_{sr}^{-1}$ in the high SNR region. Nevertheless, the condition (5.52) is not difficult to satisfy, e.g., the fixed-gain protocol.

5.3.4 Simulation Results

Numerical examples are presented in this subsection to verify the GAF design criteria for two-hop single-relay networks. The average BER P_b versus average SNR $\bar{\gamma}$ curves are plotted for Rayleigh fading channels with unit variance, i.e., $\sigma_{ij}^2 = 1$ ($i \in \{s, r\}$ and $j \in \{r, d\}$). Unless otherwise specified, QPSK modulation are adopted. In addition, ideal CSI is assumed available at the destination node: h_{sr}, h_{sd} and h_r are known for 2H-MRC, while 1H-MRC only requires h_{sd} and h_r.

First, we validate our claims for 2H-MRC and 1H-MRC in Theorems 5.1 and 5.2 by applying some existing or generic PSFs, including $\alpha = 1$ [38], the AF protocol [48, Eq. (9)], $\alpha_{Aa} = \rho_{sr}^{-1}$ which is used in [36], $\alpha_{Ab} = \rho_{sr}^{-\frac{1}{4}}$, $\alpha_{Ac} = \rho_{sr} + 1$ which is an affine PSF, and α_{Ad} which is the bounded PSF of α_{Aa} in Figure 5.2(a).

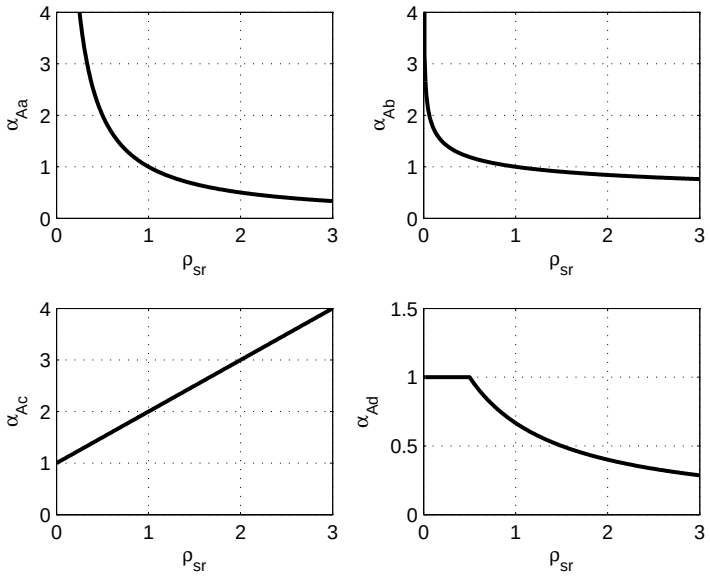

(a) Examples of power scaling factors.

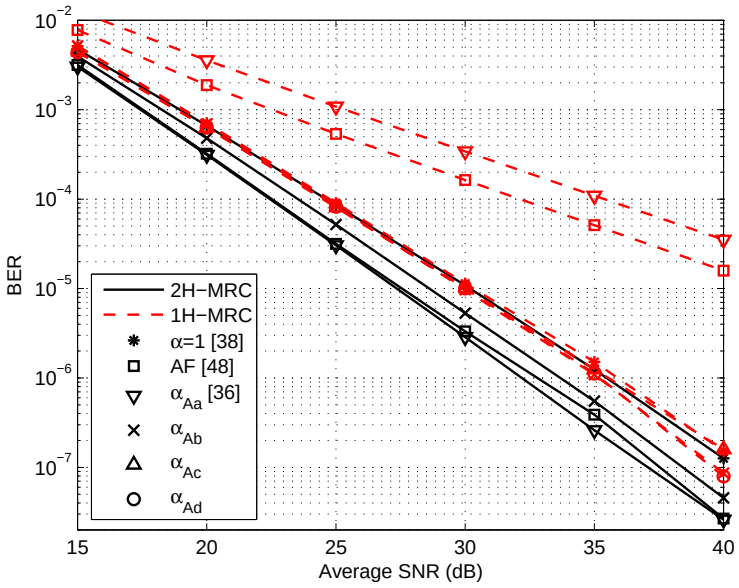

(b) Comparisons with some existing PSFs.

Figure 5.2: Comparisons of PSFs for 1H-MRC and 2H-MRC.

As shown in Figure 5.2(b), full cooperative diversity order cannot be achieved by 1H-MRC with $\alpha_{Aa} = \rho_{sr}^{-1}$ and the AF protocol in [48], because the necessary condition provided by Theorem 5.2 is violated in the high SNR region. In other words, although these protocols are widely adopted, 2H-MRC is necessary in achieving the cooperative diversity. In contrast to α_{Aa}, α_{Ab} satisfies Eq. (5.52). In Figure 5.2(b), it is shown that α_{Ab} enables full diversity order for both 1H-MRC and 2H-MRC, verifying Theorem 5.2 again. The fixed-gain protocol [38] $\alpha = 1$ satisfies the conditions in Theorems 5.1 and 5.2. With $\alpha = 1$, both 1H-MRC and 2H-MRC achieve full diversity order 2 and similar BER performance, as shown in Figure 5.2(b). However, a fixed gain $\alpha = 1$ may generate unbounded output signals at the relay when $\rho_{sr} \to \infty$ and may not be used in peak power constrained relay networks.

The BER curves for 2H-MRC with α_{Ac} and α_{Ad} are close to the corresponding curves of 1H-MRC, and are thus omitted in order not to overcrowd Figure 5.2(b). Both 1H-MRC and 2H-MRC achieve full diversity order with α_{Ac} and α_{Ad}, which indicates that the "tail" of α does not affect the diversity order as long as $\alpha(\rho_{sr}) > 0$ for $\rho_{sr} \to \infty$.

Besides the diversity performance and the need of 2H CSI, the choice of PSF should also take coding gains and other practical requirements into consideration. As indicated by Figure 5.2(b), with the same diversity order, the greater the average relay output power, the better the coding gain. Nevertheless, the average relay output power cannot be arbitrarily large. It is confined by practical concerns, such as the boundedness of PSF and the peak power constraint, which will be discussed in Section 5.4.

The examples of PSFs α_{Ba} to α_{Bd} shown in Figure 5.3(a) are employed to illustrate the effects on diversity order of bounded $\alpha(\rho_{sr})$ with zero intervals. The BER curves are plotted in Figure 5.3(b) for α_{Ba}-α_{Bd} as well as the fixed gain $\alpha = 1$. With these PSF examples, 1H-MRC is shown to achieve almost the same BER performance to

2H-MRC.

When α has continuous zero intervals (e.g., α_{Ba}), Proposition 5.1 indicates that no cooperative diversity can be obtained, i.e., $G_{\text{2H}} = 1$. For α_{Bb} where $\alpha(0) = 0$ is an isolated zero root with $p_{10} = 2$, the diversity order is upper bounded by $\frac{4}{3}$ according to Proposition 5.1. In addition, Proposition 5.1 shows that G_{2H} is also bounded by $1 + (p_{1k}^l)^{-1}$ and $1 + (p_{1k}^r)^{-1}$ if $\mathcal{R} \neq \emptyset$. α_{Bc} approaches the root concavely and should provide $G_{\text{2H}} = 2$ according to Theorem 5.1. For α_{Bd}, however, the orders of smoothness around $r_1^l = r_1^r = 0.5$ are $p_{11}^l = 3$ and $p_{11}^r = 1$. In accordance with Proposition 5.1, $G_{\text{2H}} \leq \frac{4}{3} < 2$ for α_{Bd}. All the above claims for the diversity orders of α_{Ba} to α_{Bd} are verified in Figure 5.3(b).

These two tests show that Theorems 5.1 and 5.2 provide general guidelines on designing PSFs for GAF strategies which guarantee full cooperative diversity orders. Following these guidelines, practical PSFs can be designed to simplify the cooperative network implementation without sacrificing the performance. Within this scope, the next section is dedicated to design practical AF relaying strategies for the peak power constrained relay network with only 1H CSI available at both the relay and the destination.

5.4 Intentional Peak Power Limit AF Relaying

The peak power constraint at the relay node imposes additional requirements on α. Surprisingly, the extra constraints may lead to implementation and performance advantages. In this section, we will show that by designing PSFs to meet the peak power constraint at the relay, the relay processing can be actually simplified. In addition, a practical peak power constrained AF strategy is designed to enable the low-complexity 1H-MRC to achieve full diversity order.

To meet the peak power constraint in (5.5), the PSF α should satisfy

$$\alpha \leq \frac{P_{\text{peak}}}{|y_{sr}|^2}. \tag{5.55}$$

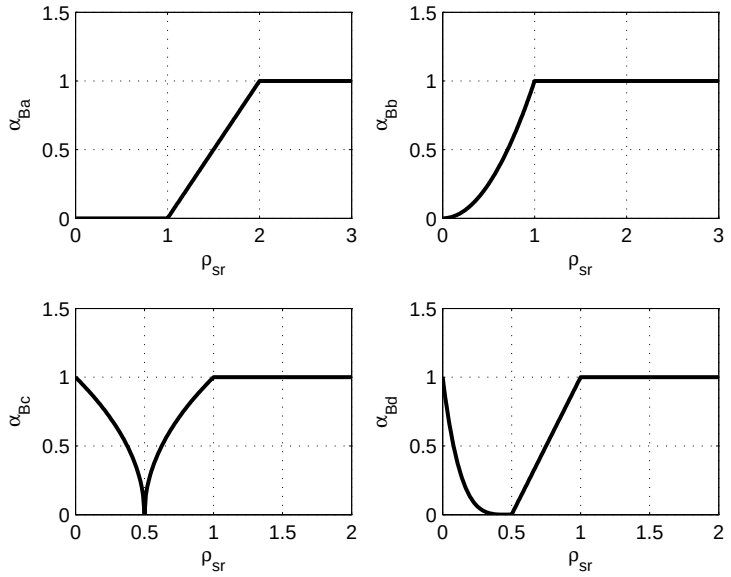

(a) Examples of power scaling factors.

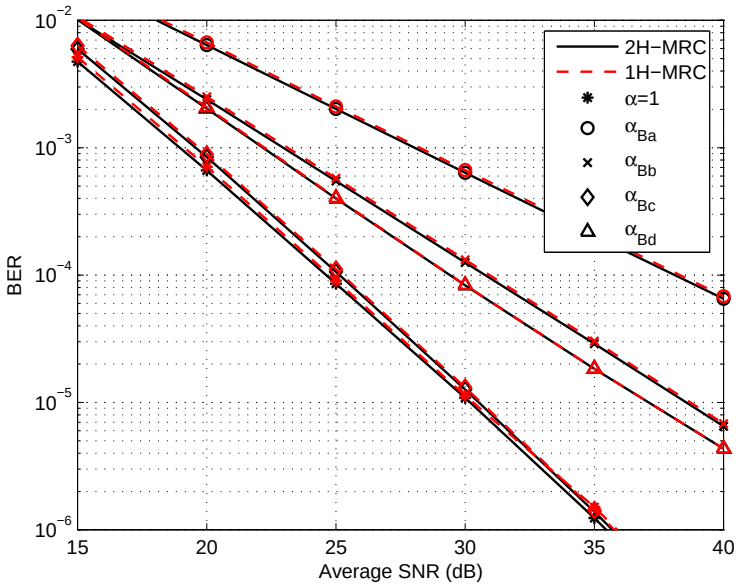

(b) Comparisons with different PSFs.

Figure 5.3: Effect of zero roots in PSFs.

Thus, α should be designed as a function of the received signal y_{sr}, instead of ρ_{sr}. In this case, the channel estimation of ρ_{sr} can be avoided which greatly simplifies processing at the relay node. In fact, ρ_{sr} will also be shown to be unnecessary at the destination, i.e., 1H-MRC suffices to obtain full diversity order, while the 1H CSI h_r and h_{sd} can be estimated by traditional channel estimation methods with embedded pilot symbols [74]. We start the analysis with $\alpha(y_{sr}) = \frac{P_{\text{peak}}}{|y_{sr}|^2}$, by which the relay node completely avoids saturation and achieves the maximum PA power efficiency at the relay.

Although $\alpha(y_{sr}) = \frac{P_{\text{peak}}}{|y_{sr}|^2}$ is used, the following proposition indicates that $\alpha(y_{sr})$ can be analyzed equivalently with the corresponding $\alpha(\rho_{sr})$ when the diversity order is concerned.

Proposition 5.2 *Consider a non-regenerative relay network with the 1H-MRC or 2H-MRC at the destination. The PSF* $\alpha(y_{sr}) = \frac{P_{\text{peak}}}{|y_{sr}|^2}$ *leads to the same diversity order with* $\alpha(\rho_{sr}) = \frac{\eta}{\rho_{sr}}$*, where* $\eta > 0$ *is a finite constant.*

Proof: The instantaneous SNR of 2H-MRC can be found as

$$\tilde{\gamma}_{\text{2H}} \triangleq \rho_{sd}\bar{\gamma} + \frac{\rho_{sr}\rho_{rd}E_x[\alpha|x|^2]}{(1+\rho_{rd}E_x[\alpha])N_0}. \tag{5.56}$$

In addition, in the high average SNR region, $|y_{sr}|^2 \approx \rho_{sr}|x|^2$. Therefore, we have

$$\alpha(y_{sr}) \approx \frac{P_{\text{peak}}}{\rho_{sr}|x|^2}. \tag{5.57}$$

When $\bar{\gamma} \to \infty$, by plugging Eq. (5.57) and $P_{\text{peak}} = KP_x$ into Eq. (5.56), we have

$$\tilde{\gamma}_{\text{2H}} \approx \left(\rho_{sd} + \frac{K\rho_{rd}}{1+\eta_1 K\frac{\rho_{rd}}{\rho_{sr}}}\right)\bar{\gamma}, \tag{5.58}$$

where $\eta_1 \triangleq E_x\left[\frac{P_x}{|x|^2}\right]$ is a modulation-dependent constant. By replacing $\frac{\eta_1 K}{\rho_{sr}}$ with $\alpha(\rho_{sr})$, Eq. (5.58) gives

$$\tilde{\gamma}_{\text{2H}} \approx \left(\rho_{sd} + \eta_1^{-1}\frac{\alpha(\rho_{sr})\rho_{sr}\rho_{rd}}{1+\alpha(\rho_{sr})\rho_{rd}}\right)\bar{\gamma}, \tag{5.59}$$

which is equivalent with $\gamma_{2\mathrm{H}}$ in Eq. (5.10) and thus provides the same diversity performance.

Similarly, for 1H-MRC, the instantaneous SNR in the high average SNR region is given by

$$\tilde{\gamma}_{1\mathrm{H}} \triangleq \frac{\rho_{sd}^2 P_x + 2\rho_{sd}\rho_{sr}\rho_{rd}E_x[\alpha|x|^2] + \rho_{sr}^2\rho_{rd}^2 E_x[\alpha^2|x|^2]}{(\rho_{sd} + \rho_{sr}\rho_{rd}E_x[\alpha] + \rho_{sr}\rho_{rd}^2 E_x[\alpha^2])N_0} \tag{5.60}$$

$$\approx \frac{\rho_{sd}^2 + 2K\rho_{sd}\rho_{rd} + \eta_1 K^2\rho_{rd}^2}{\rho_{sd} + \eta_1 K\rho_{rd} + \eta_2 K^2\frac{\rho_{rd}^2}{\rho_{sr}}}\bar{\gamma}, \tag{5.61}$$

where $\eta_2 \triangleq E_x\left[\frac{P_x^2}{|x|^4}\right]$ is also a modulation-dependent constant and has $1 \leq \eta_1 \leq \eta_2$. Therefore, with $\alpha(\rho_{sr}) = \frac{K}{\rho_{sr}}$ in Eq. (5.8), Eq. (5.61) has $\eta_2^{-1}\gamma_{1\mathrm{H}} \leq \tilde{\gamma}_{1\mathrm{H}} \leq \eta_1\gamma_{1\mathrm{H}}$. The constants in front of $\gamma_{1\mathrm{H}}$ do not affect the diversity order, neither does the constant linear coefficients in $\alpha(\rho_{sr})$. Therefore, $\alpha(y_{sr})$ is equivalent with $\alpha(\rho_{sr}) \propto \rho_{sr}^{-1}$ in terms of the diversity performance. ■

Proposition 5.2 enables us to extend the results in Section 5.3 to analyze the diversity performance for $\alpha(y_{sr})$. Because $\alpha(\rho_{sr}) \propto \rho_{sr}^{-1}$ satisfies Theorem 5.1, we arrive the following corollary immediately.

Corollary 5.2 *Consider a non-regenerative relay network with the PSF* $\alpha(y_{sr}) = \frac{P_{\mathrm{peak}}}{|y_{sr}|^2}$ *at the relay. 2H-MRC can collect full cooperative diversity order, i.e.,* $G_{2\mathrm{H}} = 2$.

For 1H-MRC, however, $\alpha(\rho_{sr}) \propto \rho_{sr}^{-1}$ does not satisfy the necessary condition (5.52) in Theorem 5.2. Therefore, $G_{1\mathrm{H}} < 2$ follows. The following corollary shows that actually $G_{1\mathrm{H}} = 1$.

Corollary 5.3 *Consider a non-regenerative relay network with the PSF* $\alpha(y_{sr}) = \frac{P_{\mathrm{peak}}}{|y_{sr}|^2}$ *at the relay. The diversity order achieved by 1H-MRC is* $G_{1\mathrm{H}} = 1$.

Proof: With Proposition 5.2, it is equivalent to prove that $\alpha(\rho_{sr}) = \rho_{sr}^{-1}$ leads to $G_{1\mathrm{H}} = 1$ for 1H-MRC.

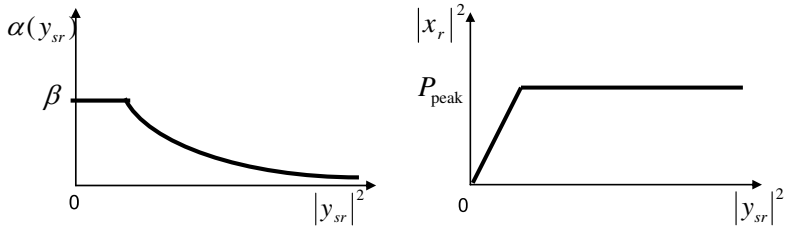

(a) The IPPL PSF as a function of the received signal power.

(b) The input-output relationship of the signal power at the IPPL relay node.

Figure 5.4: The intentional peak power limit AF relaying strategy.

In this case, the instantaneous SNR of 1H-MRC in Eq. (5.8) is bounded by

$$\frac{\rho_{sr}\rho_{rd}}{\rho_{sr}+\rho_{rd}}\bar{\gamma} \leq \rho_{sr}\frac{\rho_{sd}+\rho_{rd}}{\rho_{sr}+\rho_{rd}}\bar{\gamma} \leq \gamma_{1\text{H}} \leq \frac{(\rho_{sd}+\rho_{rd})^2}{\rho_{rd}^2}\rho_{sr}\bar{\gamma} \leq 4\rho_{sr}\bar{\gamma}, \tag{5.62}$$

where $\rho_{sd} \leq \rho_{rd}$ is assumed for the last inequality. Thus, the first and the last terms of (5.62) give lower and upper bounds for $\gamma_{1\text{H}}$ with the non-zero probabilities of 1 and $\Pr(\rho_{sd} \leq \rho_{rd})$, respectively. Because both these bounds have diversity order 1 [87], we have $G_{1\text{H}} = 1$ for $\alpha(y_{sr}) = \frac{P_{\text{peak}}}{|y_{sr}|^2}$. ■

Corollary 5.3 illustrates that full cooperative diversity order cannot be collected by the low-complexity 1H-MRC destination when $\alpha(y_{sr}) = \frac{P_{\text{peak}}}{|y_{sr}|^2}$ is used to satisfy the peak power constraint. Moreover, this PSF is still not practical in the sense that α is not bounded, i.e., the "refilling" gain may go infinite. Interestingly, by introducing a "clipped" PSF

$$\alpha(y_{sr}) = \min\left\{\frac{P_{\text{peak}}}{|y_{sr}|^2}, \beta\right\}, \tag{5.63}$$

where $\beta > 0$ is a finite constant, both of these problems are solved. We refer to this PSF as an intentional peak power limit (IPPL) strategy [60]. The PSF and the input-output relationship of the signal power in the IPPL relaying strategy are illustrated in Figure 5.4(a) and 5.4(b), respectively.

Similar to Proposition 5.2, the following proposition facilitates us to analyze the diversity performance of the IPPL strategy.

Proposition 5.3 *Consider a non-regenerative relay network with the 1H-MRC at the destination. The diversity order of the IPPL strategy is no less than that of the PSF* $\alpha_0(\rho_{sr}) \triangleq \min\left\{\frac{K}{\rho_{sr}}, \beta\right\}$ *at the relay, where* $K = \frac{P_{\text{peak}}}{P_x}$.

Proof: To prove that $G_{1\text{H}}$ of $\alpha(y_{sr})$ in Eq. (5.63) is no less than $G_{1\text{H}}$ of $\alpha_0(\rho_{sr})$, we only need to show that there exists a constant $P > 0$ such that the instantaneous SNR $\tilde{\gamma}_{1\text{H}}(\alpha(y_{sr}))$ is not smaller than $P \cdot \tilde{\gamma}_{1\text{H}}(\alpha_0(\rho_{sr}))$, where $\tilde{\gamma}_{1\text{H}}(\alpha)$ is given in Eq. (5.60). We split $\rho_{sr} \in [0, \infty)$ into two regions and analyze the instantaneous SNR in these regions separately.

For $\rho_{sr} > \frac{K}{\beta}$, in the high average SNR region, the instantaneous SNR with the IPPL PSF can be lower bounded by

$$\begin{aligned}
&\tilde{\gamma}_{1\text{H}}\left(\alpha(y_{sr})\middle|\rho_{sr} > \frac{K}{\beta}\right) \\
&\geq \frac{\rho_{sd}^2 + 2K\rho_{sd}\rho_{rd}\Pr(|x|^2 > P_x) + K^2\rho_{rd}^2 E_x\left[\frac{P_x}{|x|^2}\middle||x|^2 > P_x\right]}{\rho_{sd} + K\rho_{rd}\eta_1 + K^2\eta_2\frac{\rho_{rd}^2}{\rho_{sr}}}\bar{\gamma} && (5.64)\\
&\geq A_1\frac{\rho_{sd}^2 + 2K\rho_{sd}\rho_{rd} + K^2\rho_{rd}^2}{\rho_{sd} + K\rho_{rd} + K^2\frac{\rho_{rd}^2}{\rho_{sr}}}\bar{\gamma} && (5.65)\\
&= A_1\tilde{\gamma}_{1\text{H}}\left(\alpha_0(\rho_{sr})\middle|\rho_{sr} > \frac{K}{\beta}\right), && (5.66)
\end{aligned}$$

where $\eta_1 = E_x\left[\frac{P_x}{|x|^2}\right]$, $\eta_2 = E_x\left[\frac{P_x^2}{|x|^4}\right]$, $A_1 = \eta_2^{-1}\min\left\{\Pr(|x|^2 > P_x), E_x\left[\frac{P_x}{|x|^2}\middle||x|^2 > P_x\right]\right\}$, and the inequality (5.64) is given by plugging the following inequalities into Eq. (5.60):

$$\begin{aligned}
E_x[\alpha(y_{sr})] &\leq \frac{P_{\text{peak}}}{\rho_{sr}}E_x[|x|^{-2}], && (5.67)\\
E_x[\alpha^2(y_{sr})] &\leq \frac{P_{\text{peak}}^2}{\rho_{sr}^2}E_x[|x|^{-4}], && (5.68)
\end{aligned}$$

$$\begin{aligned}
E_x[\alpha(y_{sr})|x|^2] &= \beta E_x\left[|x|^2\middle||x|^2 \leq \frac{P_{\text{peak}}}{\beta\rho_{sr}}\right] + \frac{P_{\text{peak}}}{\rho_{sr}}\Pr\left(|x|^2 > \frac{P_{\text{peak}}}{\beta\rho_{sr}}\right) && (5.69)\\
&\geq \frac{P_{\text{peak}}}{\rho_{sr}}\Pr(|x|^2 > P_x), \text{ for } \rho_{sr} > \frac{K}{\beta}, && (5.70)
\end{aligned}$$

$$E_x[\alpha^2(y_{sr})|x|^2] = \beta^2 E_x\left[|x|^2\Big||x|^2 \le \frac{P_{\text{peak}}}{\beta\rho_{sr}}\right] + \frac{P_{\text{peak}}^2}{\rho_{sr}^2}E_x\left[|x|^{-2}\Big||x|^2 > \frac{P_{\text{peak}}}{\beta\rho_{sr}}\right] \tag{5.71}$$

$$\ge \frac{P_{\text{peak}}^2}{\rho_{sr}^2}E_x\left[|x|^{-2}\Big||x|^2 > P_x\right], \text{ for } \rho_{sr} > \frac{K}{\beta}. \tag{5.72}$$

For $\rho_{sr} \le \frac{K}{\beta}$, instead of (5.67) and (5.68), we have $E_x[\alpha(y_{sr})] \le \beta$ and $E_x[\alpha^2(y_{sr})] \le \beta^2$. In addition, Eqs. (5.69) and (5.71) lead to $E_x[\alpha(y_{sr})|x|^2] \ge \beta A_2$ and $E_x[\alpha^2(y_{sr})|x|^2] \ge \beta^2 A_2$, where $A_2 = E_x\left[|x|^2\big||x|^2 \le P_x\right]$. Accordingly, when $\rho_{sr} \le \frac{K}{\beta}$, the instantaneous SNR with the IPPL PSF has

$$\tilde{\gamma}_{1\text{H}}\left(\alpha(y_{sr})\Big|\rho_{sr} \le \frac{K}{\beta}\right) \ge \frac{A_2}{P_x}\tilde{\gamma}_{1\text{H}}\left(\alpha_0(\rho_{sr})\Big|\rho_{sr} \le \frac{K}{\beta}\right). \tag{5.73}$$

By combining (5.66), (5.73) and letting $P = \min\left\{A_1, \frac{A_2}{P_x}\right\}$, we have

$$\tilde{\gamma}_{1\text{H}}(\alpha(y_{sr})) \ge P\tilde{\gamma}_{1\text{H}}(\alpha_0(\rho_{sr})). \tag{5.74}$$

Therefore, the diversity order $G_{1\text{H}}$ for the IPPL strategy is no less than $G_{1\text{H}}$ of $\alpha_0(\rho_{sr}) = \min\left\{\frac{K}{\rho_{sr}}, \beta\right\}$. ■

Consequently, we have the following theorem to illustrate that 1H-MRC can be used to achieve full diversity order with the IPPL strategy in Eq. (5.63).

Proposition 5.4 (Full Diversity Order of 1H-MRC with the IPPL Strategy) *Consider a non-regenerative relay network with $\alpha(y_{sr})$ in Eq. (5.63) at the relay. 1H-MRC at the destination collects full cooperative diversity order, i.e., $G_{1\text{H}} = 2$.*

Proof: The upper bound of the instantaneous SNR can be given as

$$\gamma_{1\text{H}} \le (\rho_{sd} + \alpha(\rho_{sr})\rho_{sr}\rho_{rd})\bar{\gamma} \le (\rho_{sd} + \beta\rho_{sr}\rho_{rd})\bar{\gamma}. \tag{5.75}$$

The RHS of (5.75) can be proved to have the diversity order 2 as $\bar{\gamma} \to \infty$, which gives $G_{1\text{H}} \le 2$ for 1H-MRC.

For the lower bound of $G_{1\text{H}}$, due to Proposition 5.3, we only need to show that $G_{1\text{H}} = 2$ with the PSF $\alpha_0(\rho_{sr}) = \min\left\{\frac{K}{\rho_{sr}}, \beta\right\}$. $\alpha_0(\rho_{sr})$ satisfies the necessary conditions in Theorem 5.2. In the following, we show that it is also sufficient for $G_{1\text{H}} = 2$.

With $\alpha_0(\rho_{sr})$, $\gamma_{1\mathrm{H}}$ can be lower bounded by

$$\gamma_{1\mathrm{H}} \geq \frac{\rho_{sd}+\alpha_0(\rho_{sr})\rho_{sr}\rho_{rd}}{1+\alpha_0(\rho_{sr})\rho_{rd}}\bar{\gamma} \geq \begin{cases} \gamma_1 \triangleq \dfrac{\rho_{sd}+\beta\rho_{sr}\rho_{rd}}{1+\beta\rho_{rd}}\bar{\gamma}, & \rho_{sr} \leq \frac{K}{\beta}, \quad (5.76) \\ \gamma_2 \triangleq \dfrac{\rho_{sd}+K\rho_{rd}}{1+\beta\rho_{rd}}\bar{\gamma}, & \rho_{sr} > \frac{K}{\beta}. \quad (5.77) \end{cases}$$

Similar to (5.39), by extending the integration intervals, the average BER of 1H-MRC has

$$P_b \leq E[Q(\sqrt{\gamma_1})] + E[Q(\sqrt{\gamma_2})], \tag{5.78}$$

and the diversity order is determined by the lowest one of γ_1 and γ_2.

For γ_1, we need to further split it into two cases, i.e.,

$$\gamma_1 = \begin{cases} \gamma_{1a} \triangleq \left(\rho_{sr} + \dfrac{\rho_{D1}}{1+\beta\rho_{rd}}\right)\bar{\gamma}, & \rho_{sd} \geq \rho_{sr}, \quad (5.79) \\ \gamma_{1b} \triangleq \left(\rho_{sd} + \dfrac{\beta\rho_{rd}\rho_{D2}}{1+\beta\rho_{rd}}\right)\bar{\gamma}, & \rho_{sd} < \rho_{sr}, \quad (5.80) \end{cases}$$

where $\rho_{D1} = \rho_{sd} - \rho_{sr}$ when $\rho_{sd} \geq \rho_{sr}$ and $\rho_{D2} = \rho_{sr} - \rho_{sd}$, otherwise. Due to the strong memoryless property of exponential distribution, ρ_{D1} and ρ_{D2} are still exponentially distributed. ρ_{D1} is independent with ρ_{sr} and ρ_{rd}, and ρ_{D2} is independent with ρ_{sd} and ρ_{rd}, respectively [93]. Again, $E[Q(\sqrt{\gamma_1})] \leq E[Q(\sqrt{\gamma_{1a}})] + E[Q(\sqrt{\gamma_{1b}})]$. With the same technique used in [87] and Eqs. (5.44)-(5.49) in Section 5.3, it is ready to prove that $E[Q(\sqrt{\gamma_{1a}})] \doteq \bar{\gamma}^{-2}$. Additionally, Corollary 5.1 gives that $E[Q(\sqrt{\gamma_{1b}})] \doteq \bar{\gamma}^{-2}$. Therefore, $E[Q(\sqrt{\gamma_1})] \dot{\leq} \bar{\gamma}^{-2}$.

For the second term in (5.78), we have

$$E[Q(\sqrt{\gamma_2})] \leq \frac{1}{\sigma_{sd}^2\sigma_{rd}^2}\int_0^\infty \frac{\exp\left(-\left(\frac{K\bar{\gamma}}{2(1+\beta\rho_{rd})}+\frac{1}{\sigma_{rd}^2}\right)\rho_{rd}\right)}{\frac{\bar{\gamma}}{2(1+\beta\rho_{rd})}+\frac{1}{\sigma_{sd}^2}}d\rho_{rd}, \tag{5.81}$$

where the Chernoff bound for Q-function is used. By substituting $\theta = \frac{\bar{\gamma}}{2(1+\beta\rho_{rd})}$, the

above inequality leads to

$$E[Q(\sqrt{\gamma_2})] \leq \bar{\gamma}\frac{\exp(\beta^{-1}\sigma_{rd}^{-2})}{2\beta\sigma_{sd}^2\sigma_{rd}^2}\int_0^{\frac{\bar{\gamma}}{2}}\frac{\exp\left(-\frac{\bar{\gamma}}{2\beta\sigma_{rd}^2\theta}\right)}{\theta^2(\theta+\sigma_{sd}^{-2})}\exp\left(\frac{K}{\beta}\left(\theta-\frac{\bar{\gamma}}{2}\right)\right)d\theta \quad (5.82)$$

$$\dot{\leq} \bar{\gamma}\left[\int_0^{\frac{\bar{\gamma}}{2}}\frac{\exp\left(-\frac{m\bar{\gamma}}{2\beta\sigma_{rd}^2\theta}\right)}{\theta^{3m}}d\theta\right]^{\frac{1}{m}}\left[\int_0^{\frac{\bar{\gamma}}{2}}\exp\left(n\frac{K}{\beta}\left(\theta-\frac{\bar{\gamma}}{2}\right)\right)d\theta\right]^{\frac{1}{n}} \quad (5.83)$$

where Hölder's inequality is used ($\forall m, n > 1$ and $\frac{1}{m}+\frac{1}{n}=1$) [33, 11.313]. The second integral of (5.83) approaches a constant as $\bar{\gamma}$ goes to infinity and does not affect the diversity performance. The first integral to the power of $\frac{1}{m}$ is exponentially equal to $\bar{\gamma}^{-3+\frac{1}{m}}$ as $\bar{\gamma}\to\infty$ [33, 3.471.1]. Because m can arbitrarily approach 1, (5.83) leads to $E[Q(\sqrt{\gamma_2})]\dot{\leq}\bar{\gamma}^{-2}$.

Therefore, $P_b\dot{\leq}\bar{\gamma}^{-2}$ in (5.78) and thus $G_d \geq 2$. Combined with (5.75) and Proposition 5.3, the IPPL strategy has $G_{1\mathrm{H}} = 2$. ■

The physical meaning of Eq. (5.63) is when the received signal is weak ($|y_{sr}|$ is small), the IPPL strategy will not assign a too large gain (not greater than β) because the forwarded symbol is likely to cause an error at the destination. As a result, in contrast to $\alpha(y_{sr}) = \frac{P_{\mathrm{peak}}}{|y_{sr}|^2}$, the noise on the source-relay link will not be arbitrarily amplified and cause the 1H-MRC destination which has no noise normalization to lose diversity. In addition, intentionally capping on α is also necessary, because an unbounded coefficient is not possible to implement in hardware. Thus, α in Eq. (5.63) models a practical and diversity-enabled power scaling scheme for the peak power constrained relay. It is worth noting that the finite value of β does not affect the diversity performance.

The aforementioned designs and analysis can be easily generalized to block-wise communication systems, e.g., OFDM systems. In the block-wise transmission, a block of symbols, i.e., $\mathbf{x} = [x_0, \cdots, x_{N-1}]^T$ where N is the block size, is transmitted from Source S in the first time slot. Each of the received blocks for Relay R and Destination D also consists of N symbols, i.e., $N \times 1$ vectors $\mathbf{y}_{ij}$. Without loss of

generality, we assume block fading channels, where h_{ij} remains constant during each time slot. Therefore, the system model can still be represented as Eqs. (5.1)-(5.3) with x, y and w replaced by $\mathbf{x}$, $\mathbf{y}$ and $\mathbf{w}$, respectively. In this case, by substituting $|y_{sr}|^2$ with $\|\mathbf{y}_{sr}\|_\infty^2$, the IPPL strategy is ready to be extended to block-wise systems.

Overall, the proposed IPPL strategy is one of the practical solutions that achieve full diversity with 1H-MRC and a good coding gain, while addressing the aforementioned practical concerns.

Following the simulation setup in Section 5.3, a few numerical results are shown as follows to illustrate the performance of the IPPL relaying strategy. In Figure 5.5, the BER performance of the schemes discussed in Corollaries 5.2-5.3 and Proposition 5.4 is demonstrated for different QAM constellations. Specifically, with $\alpha(y_{sr}) = \frac{P_{\text{peak}}}{|y_{sr}|^2}$, 2H-MRC can collect full cooperative diversity order, i.e., $G_{\text{2H}} = 2$, as indicated by Corollary 5.2. With this PSF, however, Figure 5.5 shows that 1H-MRC can only achieve $G_{\text{1H}} = 1$ as mentioned in Corollary 5.3. With the proposed IPPL strategy $\alpha(y_{sr})$ in Eq. (5.63), Proposition 5.4 proves that 1H-MRC can also collect full cooperative diversity order, which is illustrated in Figure 5.5.

In Figure 5.6, the IPPL α in Eq. (5.63) is further applied to the relay nodes with different peak power resources. Although the coding gains may degrade along with the decrease of the peak power constraint, 1H-MRC can still collect full cooperative diversity order. Figure 5.6 also shows that $\alpha = \frac{P_{\text{peak}}}{|y_{sr}|^2}$ can only enable 1H-MRC to achieve $G_{\text{1H}} = 1$. In this case, however, 1H-MRC performs better with a smaller peak power constraint. It is mainly because a smaller P_{peak} (thus a smaller α) diminishes the effect of the channel noise of the source-relay link on the post-processing SNR. Therefore, the lack of noise normalization is less detrimental to the error performance of 1H-MRC with a small P_{peak}.

In Eq. (5.63), β is a parameter subject to design. As indicated by Proposition 5.4, the choice of β should not affect the diversity performance. Figure 5.7 corroborates

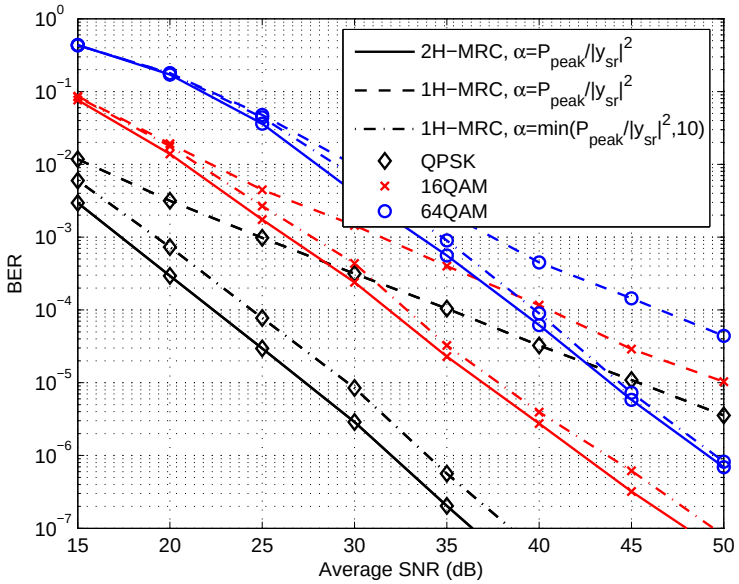

Figure 5.5: Average BER versus average SNR curves for 1H-MRC and 2H-MRC with $\alpha = \frac{P_{\text{peak}}}{|y_{sr}|^2}$ and $\alpha = \min\left\{\frac{P_{\text{peak}}}{|y_{sr}|^2}, \beta = 10\right\}$; $P_{\text{peak}} = P_x$; different QAM modulations are compared.

this point. However, a too small β will otherwise lead to a low power efficiency at the relay node and thus a small coding gain.

The proposed IPPL strategy can be extended to block-wise communication systems with ease. In Figure 5.8, the transmitted block of symbols is assumed as $\mathbf{x} = [x_0, \cdots, x_{N-1}]^T$, where x_k $(k \in [0, N-1])$ are independent QPSK-modulated signals. Figure 5.8 illustrates that the BER performance of the 1H-MRC method with the IPPL strategy is close to that achieved by 2H-MRC.

It is worth noting that the proposed method is also applicable to multi-carrier systems, e.g., OFDM. In this case, the block of symbols in OFDM systems becomes $\mathbf{x} = \mathbf{F}^H\mathbf{X}$ as introduced in Section 2.2. The BER performance for the OFDM systems with different numbers of subcarriers N is shown in Figure 5.9. Because the dynamic range of OFDM symbols increases as the block size N, a larger N may lead to a smaller power efficiency at the relay node, thus a smaller coding gain.

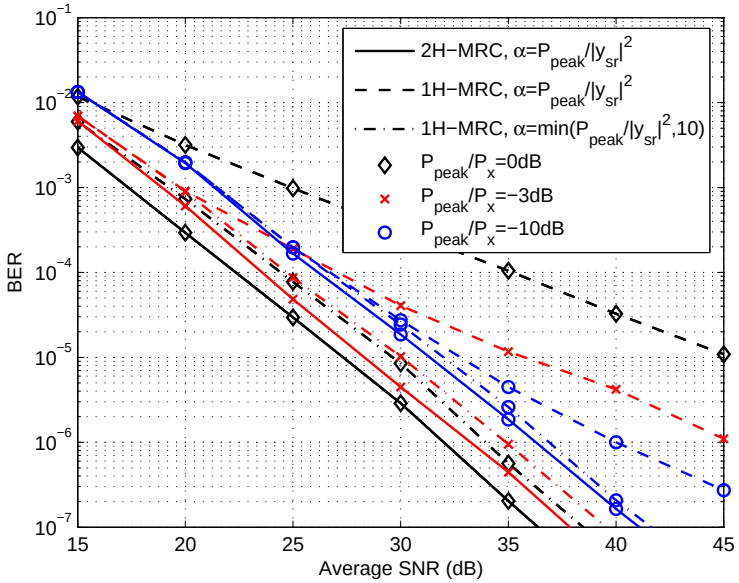

Figure 5.6: Average BER versus average SNR curves for 2H-MRC and 1H-MRC with $\alpha = \frac{P_{\text{peak}}}{|y_{sr}|^2}$ and $\alpha = \min\left\{\frac{P_{\text{peak}}}{|y_{sr}|^2}, \beta = 10\right\}$; different relay peak power constraints are compared, i.e., $K = \frac{P_{\text{peak}}}{P_x} = 0$, -3 and -10dB.

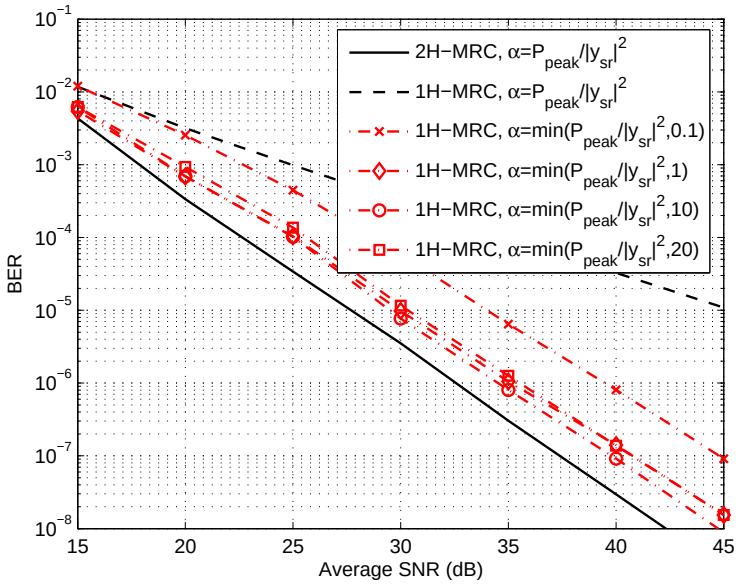

Figure 5.7: Average BER versus average SNR curves for 2H-MRC and 1H-MRC with $\alpha = \frac{P_{\text{peak}}}{|y_{sr}|^2}$ and $\alpha = \min\left\{\frac{P_{\text{peak}}}{|y_{sr}|^2}, \beta\right\}$ where $\beta = 0.1$, 1, 10 and 20 are used; $P_{\text{peak}} = P_x$.

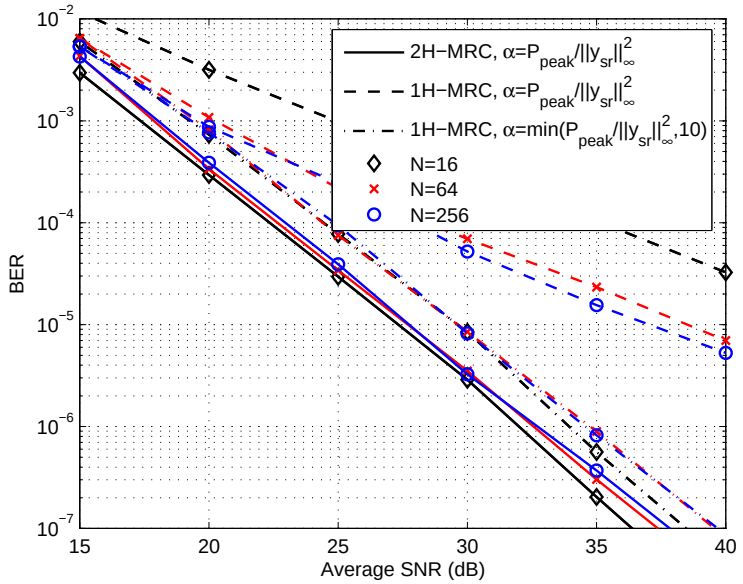

Figure 5.8: Average BER versus average SNR curves for 1H-MRC and 2H-MRC with $\alpha = \frac{P_{\text{peak}}}{||\mathbf{y}_{sr}||^2_\infty}$ and $\alpha = \min\left\{\frac{P_{\text{peak}}}{||\mathbf{y}_{sr}||^2_\infty}, \beta = 10\right\}$; $P_{\text{peak}} = P_x$; block sizes $N = 16$, 64 and 256 are used.

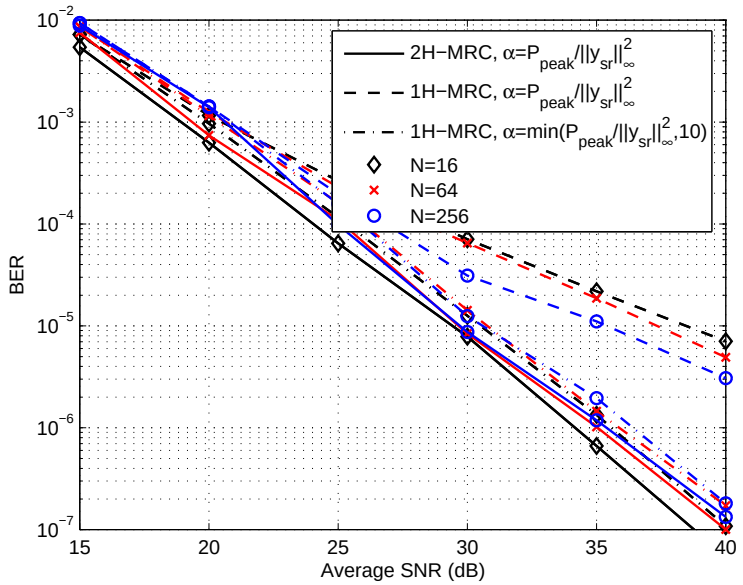

Figure 5.9: Average BER versus average SNR curves for 1H-MRC and 2H-MRC with $\alpha = \frac{P_{\text{peak}}}{||\mathbf{y}_{sr}||^2_\infty}$ and $\alpha = \min\left\{\frac{P_{\text{peak}}}{||\mathbf{y}_{sr}||^2_\infty}, \beta = 10\right\}$; $P_{\text{peak}} = P_x$; OFDM modulations with block sizes $N = 16$, 64 and 256 are used.

5.5 Multi-Relay Cooperative Networks

Utilizing more than one relay node can further improve the error performance by providing higher diversity orders or better diversity gain functions [42, 87, 106]. In this section, the diversity performance as well as the spectral efficiency issue of the multi-relay cooperative network will be studied.

5.5.1 Half-Duplex Multi-Relay AF Relaying Strategy

Suppose that the network enables the source and destination nodes to use N_r relay nodes for cooperation. The network diagram is shown in Figure 5.10. Assume also that the channels among all nodes (i.e., the source, N_r relay and destination nodes) are i.i.d. Rayleigh faded and corrupted by additive white Gaussian channel noise with the power of N_0.

Denote the channel gains from the source to the ith relay and from the ith relay to the destination as h_{si} and h_{id} ($i \in \{1, \cdots, N_r\}$), respectively. The received signals at each relay node can be thus expressed as

$$y_{si} = h_{si}x + w_{si},\ i \in \{1, \cdots, N_r\}. \tag{5.84}$$

In the AF relay network, each relay node forwards an amplified version of the received signal in its assigned time slot as it does in the single-relay case. So the transmitted signal of the ith relay is

$$x_{ri} = \sqrt{\alpha_i} y_{si}, \tag{5.85}$$

where α_i is the PSF. At the destination, 1H-MRC and 2H-MRC [c.f. Eqs. (5.6), (5.7), and (5.9)] can be readily extended for the multi-relay networks by combining the $N_r + 1$ received signal copies with corresponding weights.

The proposed IPPL strategy can be used at the multiple relays and achieve the same conclusions on diversity orders as in Section 5.4. Figure 5.11 shows that with $\alpha(y_{sr}) = \frac{P_{\text{peak}}}{|y_{sr}|^2}$, $G_{\text{2H}} = N_r + 1$ and $G_{\text{1H}} = 1$. Meanwhile, the IPPL strategy is still

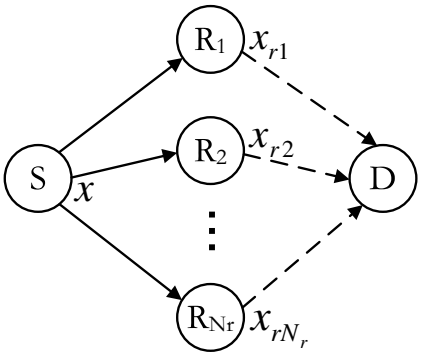

Figure 5.10: Multi-relay network with N_r relay nodes.

applicable with multiple peak power constrained relay nodes. The proposed α in Eq. (5.63) guarantees full cooperative diversity with the 1H-MRC destination, i.e., $G_{1\mathrm{H}} = N_r + 1$ for an N_r-relay network. It is worth mentioning that 2H-MRC in multi-relay networks would require the 2H CSIs of all links between the source and the relay nodes, which is particularly impractical to implement.

However, simply extending the single-relay AF strategy to multi-relay networks results in poor spectral efficiency. Since all relays should transmit over mutually orthogonal channels, similar to the single-relay case discussed in Sections 5.2-5.4, time-division multiplexing (TDM) can be adopted. In this case, $N_r + 1$ time slots will be needed to transmit each symbol. In the first time slot, the source node broadcasts the symbol x to the destination and the N_r relay nodes. Then, one time slot will be needed for every relay node to forward the signal, thus requiring N_r extra time slots in total. The time-slot assignment is summarized in Table 5.1. Therefore, the TDM scheme is highly spectral inefficient.

5.5.2 Relay Selection Schemes

In multi-relay networks, relay selection schemes can be used to exploit the cooperative diversity gain without further losing spectral efficiency [15, 42]. Rather than $N_r + 1$, when certain relay nodes have been selected to assist the transmission, two time slots are enough to achieve the cooperative diversity in the multi-relay network.

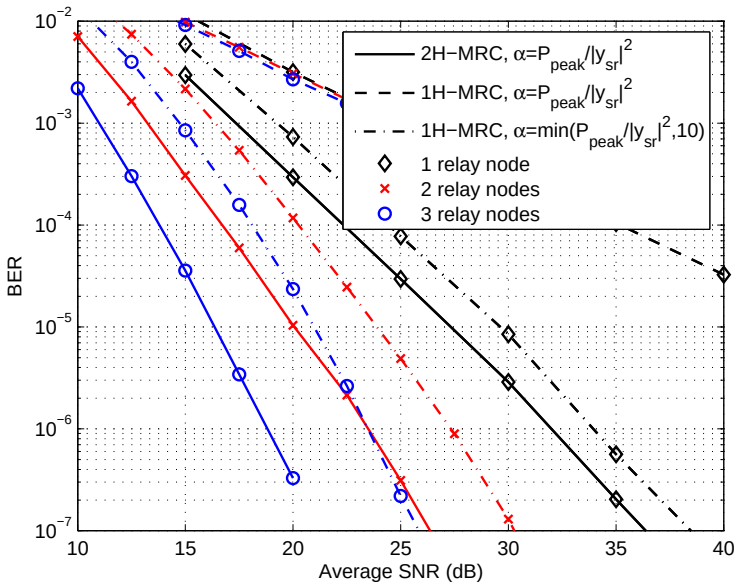

Figure 5.11: Average BER versus average SNR curves for 1H-MRC and 2H-MRC with $\alpha = \frac{P_{\text{peak}}}{|y_{sr}|^2}$ and $\alpha = \min\left\{\frac{P_{\text{peak}}}{|y_{sr}|^2}, \beta = 10\right\}$; $P_{\text{peak}} = P_x$; $N_r = 1$, 2 and 3 relay nodes are used.

Table 5.1: The time-slot assignment in the TDM multi-relay AF strategies.

Time slot	Tx\Rx	Relay 1	Relay 2	$\cdots$	Relay N_r	Destination
1	Source	x	x	$\cdots$	x	x
2	Relay 1					x_{r1}
3	Relay 2					x_{r2}
$\vdots$	$\vdots$					$\vdots$
$N_r + 1$	Relay N_r					x_{rN_r}

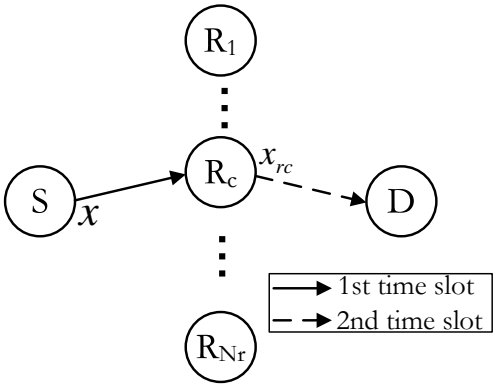

Figure 5.12: The transmission period of single-relay selection schemes in an N_r-relay network.

In this section, we mainly focus on the single-relay selection schemes where only one of the N_r relay nodes is chosen to cooperate for any symbol. Following the assumptions in literature [15, 42], for each given channel realization, a training step is assumed in which the destination gathers the necessary CSIs, selects the cooperating relay and delivers the selection decision to relay nodes via feedback mechanisms.

In the transmission period, the diagram of the network is shown in Figure 5.12. Two time slots are needed for the transmission in the half-duplex AF relay network. In the first time slot, the source node broadcasts its information symbol x to the relay nodes. Notice that, for simplicity, it is assumed that there is no direct link between the source and the destination in this subsection. The following results can be easily generalized in the presence of the direct link though. Assume the cth relay is selected for cooperation. Then, in the second time slot, the cth relay node amplifies its received signal by a power scaling factor α_c and forwards it to the destination.

In this case, the instantaneous SNR at the destination can be given as

$$\gamma = \gamma_c = \frac{\alpha_c \rho_{sc} \rho_{cd} P_x}{(\alpha_c \rho_{cd} + 1) N_0} = \frac{\alpha_c \rho_{sc} \rho_{cd}}{\alpha_c \rho_{cd} + 1} \bar{\gamma}, \ c \in \{1, \cdots, N_r\}, \tag{5.86}$$

where $P_x = E_x[|x|^2]$, $\rho_{si} = |h_{si}|^2$ and $\rho_{id} = |h_{id}|^2$ ($i \in \{1, \cdots, N_r\}$) for notational simplicity. γ_i is used to denote the instantaneous SNR if the ith relay is selected.

Based on the availability of CSIs at the destination, we consider two different

selection schemes:

Definition 5.2 (1H-CSI and 2H-CSI selection schemes) *In the 1H-CSI selection scheme, the relay is selected only based on the 1H CSI, i.e.,* $h_i \triangleq \sqrt{\alpha_i} h_{si} h_{id}$ *(*$i \in \{1, \cdots, N_r\}$*). Specifically, for each channel realization, the cth relay node is selected to cooperate if*

$$c = \arg \max_{i \in \{1, \cdots, N_r\}} |h_i|^2. \tag{5.87}$$

In addition to the 1H CSI, if the destination also possesses the 2H CSI (i.e., ρ_{si} *or* $\alpha_i \rho_{id}$*) of all relay paths, the instantaneous SNR* γ_i *of each relay will be known at the destination. Therefore, the 2H-CSI selection picks the cth relay as*

$$c = \arg \max_{i \in \{1, \cdots, N_r\}} \gamma_i. \tag{5.88}$$

The 2H-CSI selection has the optimal error performance among single-relay selection schemes because it maximizes the receive SNR. However, unlike the 1H CSI which incorporates the AF relay node as a transparent part of the channel and can be estimated at the destination, the 2H CSI could only be estimated at the relay and made accessible to the destination via forwarding mechanisms [49, 112]. It inevitably increases the system complexity, reduces the spectral efficiency and exposes the system performance to further degradations. The needlessness of the 2H CSI for decoding at the destination further makes the 2H-CSI selection costly and redundant. Therefore, if the 1H-CSI selection can provide comparable error performance, its low complexity and ease of deployment make it attractive from a practical standpoint.

The diversity performance also depends on the design of the PSF α_i. In this subsection, the relay nodes are assumed subject to an average power constraint P_i. In this case, two kinds of α_i are usually used, i.e., an instantaneous gain

$$\alpha_{0,i} = \frac{P_i}{\rho_{si} P_x + N_0}, \tag{5.89}$$

and a fixed gain

$$\alpha_{1,i} = \frac{P_i}{\sigma_{si}^2 P_x + N_0}, \tag{5.90}$$

where σ_{si}^2 denotes the variance of ρ_{si} [38, 48].

In this subsection, the diversity performance of the concerned PSFs with both 1H-CSI and 2H-CSI selection schemes in Rayleigh fading channels is studied.

We will show that the instantaneous gain can provide full diversity order ($G_d = N_r$) for the 2H-CSI selection (a.k.a, the best relay selection in [42]), but only $G_d = 1$ for the 1H-CSI selection (a.k.a, the nearest neighbor selection in [42]).

In contrast to the instantaneous gain, the fixed gain is independent with the instantaneous channel gain ρ_{si} and thus simplifies the relay processing. In addition, we will show that the fixed-gain AF relaying ($\alpha_{1,i} = C_i > 0$) enables both the 2H-CSI and the 1H-CSI selection schemes to achieve the diversity gain function $G_f(\bar{\gamma}) = \bar{\gamma}^{-N_r}(\ln \bar{\gamma})^{N_r}$ and thus the full diversity order $G_d = N_r$.

5.5.3 Theorem on Diversity Gain Function

When diversity gain function is needed to characterize the asymptotic error performance (see Section 2.3), e.g., in the relay selection schemes we will show later, the existing theories about diversity order in [107] are no longer sufficient. The major contribution of this subsection is thus to unveil the dependency of the diversity gain function on the PDF of the instantaneous SNR, which can be approximated by the products of polynomials and logarithm functions at the origin. The proposed theorem provides a simple and general way to evaluate the asymptotic error performance that involves the diversity gain function and coding gain by only investigating the PDF of the instantaneous SNR around the origin.

The single-user uncoded communication system is of concern, which satisfies the following general assumptions:

A1) The instantaneous SNR at the receiver is $\gamma = \beta\bar{\gamma}$, where β is a non-negative random variable depending on the channel realization;

A2) For $\beta \to 0^+$, the PDF of β can be approximated by

$$f_\beta(\beta) = a\beta^m(\ln \beta^{-1})^n + o(\beta^m(\ln \beta^{-1})^n), \tag{5.91}$$

where $a > 0$, $m > -1$ and $n \geq 0$ are channel-dependent constants;

A3) Additive white Gaussian channel noise is assumed so that the average SER is given by $P_e = E_\beta[\kappa_1 Q(\sqrt{\kappa_2 \beta\bar{\gamma}})]$, where κ_1 and κ_2 are constellation-specific constants, e.g., $\kappa_1 = 4(1 - M^{-\frac{1}{2}})$ and $\kappa_2 = \frac{3}{M-1}$ for M-ary QAM modulations [83, p. 278].

As a special case, when $n = 0$, Proposition 1 in [107] has revealed that the diversity order of the concerned system is $G_d = m + 1$. However, the existing results are no longer sufficient to characterize the diversity gain function (i.e., $n > 0$). In addition, because $(\ln \beta^{-1})^n = o(\beta^{-t})$ $(\forall t > 0)$, the results in [107] fail to accurately evaluate the diversity performance. For instance, with the PDF of β following Eq. (5.91) for $\beta \to 0^+$, later we will prove that the diversity gain function $G_f(\bar{\gamma}) = \bar{\gamma}^{-(m+1)}(\ln \bar{\gamma})^n$ is achieved, leading to the diversity order of $G_d = m + 1$. Proposition 1 in [107], however, only indicates that the diversity order may be any value between m and $m + 1$.

For the considered general assumptions, the following theorem explicitly gives the closed-form bounds on the asymptotic error performance [57].

Theorem 5.3 (Asymptotic SER bounds) *For a system that satisfies the assumptions (A1)-(A3), at high average SNR ($\bar{\gamma} \to \infty$), the average SER P_e only depends on the PDF of β at $\beta \to 0^+$, and can be lower and upper bounded as*

$$G_l\bar{\gamma}^{-(m+1)}(\ln \bar{\gamma})^n + o(\bar{\gamma}^{-(m+1)}(\ln \bar{\gamma})^n) \leq P_e \leq G_u\bar{\gamma}^{-(m+1)}(\ln \bar{\gamma})^n + o(\bar{\gamma}^{-(m+1)}(\ln \bar{\gamma})^n). \tag{5.92}$$

The coefficients are given as

$$A = \frac{a\kappa_1 2^{\tilde{m}-\frac{1}{2}}}{\kappa_2^{\tilde{m}+\frac{1}{2}}(m+1)\sqrt{\pi}} \prod_{k=0}^{\tilde{m}} (m+\frac{1}{2}-k) \tag{5.93}$$

$$G_l = A\left(I(n)\left(\frac{2}{\kappa_2}\right)^{m-\tilde{m}+\frac{1}{2}} \Gamma\left[m-\tilde{m}+\frac{1}{2},\frac{1}{2}\right] + e^{-\frac{1}{2}}\left(m-\tilde{m}+\frac{1}{2}\right)^{-1}\right) \tag{5.94}$$

$$G_u = A\left(\left(\frac{2}{\kappa_2}\right)^{m-\tilde{m}+\frac{1}{2}} \Gamma\left[m-\tilde{m}+\frac{1}{2},\frac{1}{2}\right] + \left(m-\tilde{m}+\frac{1}{2}\right)^{-1}\right), \tag{5.95}$$

where $\tilde{m} = \lfloor m \rfloor$ *is the largest integer that is not greater than* m*, the product in Eq. (5.93) is 1 if* $\tilde{m} = -1$*, and* $\Gamma[\cdot,\cdot]$ *is the incomplete Gamma function [5, 6.5.3].* $I(x)$ *is an indicator function that*

$$I(x) = \begin{cases} 1, & x = 0, \end{cases} \tag{5.96}$$

$$\begin{cases} 0, & x > 0. \end{cases} \tag{5.97}$$

Proof: Let $\delta > 0$ be a small constant so that Eq. (5.91) holds true for $\beta < \delta$. We can split the integral intervals in evaluating P_e as

$$P_e = E_\beta\left[\kappa_1 Q\left(\sqrt{\kappa_2\beta\bar{\gamma}}\right)\right] = \kappa_1(I_1+I_2+I_3) + o(I_1+I_2+I_3), \tag{5.98}$$

where

$$I_1 = \frac{a}{\sqrt{2\pi}} \int_0^{\sqrt{\kappa_2\delta\bar{\gamma}}} e^{-\frac{x^2}{2}} \int_0^{\frac{x^2}{\kappa_2\bar{\gamma}}} \beta^m (\ln\beta^{-1})^n d\beta dx \tag{5.99}$$

$$I_2 = \frac{a}{\sqrt{2\pi}} \int_{\sqrt{\kappa_2\delta\bar{\gamma}}}^{\infty} e^{-\frac{x^2}{2}} dx \int_0^{\delta} \beta^m (\ln\beta^{-1})^n d\beta \tag{5.100}$$

$$I_3 = \int_\delta^\infty Q(\sqrt{\kappa_2\beta\bar{\gamma}}) f_\beta(\beta) d\beta. \tag{5.101}$$

We start by analyzing the easy ones, I_2 and I_3. With I_3, it is readily bounded as

$$I_3 < Q(\sqrt{\kappa_2\delta\bar{\gamma}}) < e^{-\frac{\kappa_2\delta}{2}\bar{\gamma}} = o(\bar{\gamma}^{-(m+1)}(\ln\bar{\gamma})^n), \text{ for } \bar{\gamma}\to\infty. \tag{5.102}$$

For I_2, because the two integrals in Eq. (5.100) are separable, we have

$$I_2 = aBQ(\sqrt{\kappa_2\delta\bar{\gamma}}) = o(\bar{\gamma}^{-(m+1)}(\ln\bar{\gamma})^n), \text{ for } \bar{\gamma}\to\infty, \tag{5.103}$$

where $B = \int_0^{\delta} \beta^m (\ln \beta^{-1})^n d\beta$ is a finite and positive constant for $m > -1$ and $n \geq 0$ [33, 4.272.6].

Therefore, both I_2 and I_3 are not the dominant term in the asymptotic P_e. For I_1, however, it is more complicated. First, for $\bar{\gamma} \to \infty$, via integration by parts, the second integral in I_1 has

$$\int_0^{\frac{x^2}{\kappa_2 \bar{\gamma}}} \beta^m (\ln \beta^{-1})^n d\beta = \frac{1}{m+1} \left(\ln \frac{\kappa_2 \bar{\gamma}}{x^2} \right)^n \left(\frac{x^2}{\kappa_2 \bar{\gamma}} \right)^{m+1} + o(\bar{\gamma}^{-(m+1)} (\ln \bar{\gamma})^n). \quad (5.104)$$

Plugging Eq. (5.104) into Eq. (5.99), I_1 reads

$$I_1 \doteq \frac{a\sqrt{\kappa_2 \bar{\gamma}}}{2(m+1)\sqrt{2\pi}} \int_0^1 e^{-\frac{\kappa_2 \delta \bar{\gamma}}{2} v} \left(\ln \frac{1}{\delta v} \right)^n \delta^{m+\frac{3}{2}} v^{m+\frac{1}{2}} dv, \quad (5.105)$$

where $v = \frac{x^2}{\kappa_2 \delta \bar{\gamma}}$ is used to substitute x. For $m \geq 0$, via integration by parts again, the RHS of Eq. (5.105) further leads to

$$\begin{aligned} I_1 &\doteq \frac{a\delta^{m+\frac{3}{2}} \kappa_2^{\frac{1}{2}} \bar{\gamma}^{\frac{1}{2}}}{2(m+1)\sqrt{2\pi}} \Bigg[-\frac{2}{\kappa_2 \delta \bar{\gamma}} \left(\ln \delta^{-1} \right)^n e^{-\frac{\kappa_2 \delta}{2} \bar{\gamma}} + \frac{2}{\kappa_2 \delta \bar{\gamma}} \\ &\quad \int_0^1 e^{-\frac{\kappa_2 \delta \bar{\gamma}}{2} v} v^{m-\frac{1}{2}} \left[\left(m + \frac{1}{2} \right) \left(\ln \frac{1}{\delta v} \right)^n - n \left(\ln \frac{1}{\delta v} \right)^{n-1} \right] dv \Bigg] \quad (5.106) \\ &\doteq \frac{a\delta^{m+\frac{1}{2}} \left(m + \frac{1}{2} \right)}{(m+1)\sqrt{2\pi}} (\kappa_2 \bar{\gamma})^{-\frac{1}{2}} \int_0^1 e^{-\frac{\kappa_2 \delta \bar{\gamma}}{2} v} \left(\ln \frac{1}{\delta v} \right)^n v^{m-\frac{1}{2}} dv. \quad (5.107) \end{aligned}$$

Due to the exponential equality, terms with lower orders are omitted in Eq. (5.107). Carrying on the integration by parts repeatedly, Eqs. (5.106)-(5.107) will eventually lead to

$$I_1 \doteq \frac{a 2^{\tilde{m}} \prod_{k=0}^{\tilde{m}} (m + \frac{1}{2} - k)}{(m+1)\sqrt{2\pi}} (\kappa_2 \bar{\gamma})^{-(\tilde{m}+\frac{1}{2})} \int_0^1 \delta e^{-\frac{\kappa_2 \delta \bar{\gamma}}{2} v} \left(\ln \frac{1}{\delta v} \right)^n (\delta v)^{m-\tilde{m}-\frac{1}{2}} dv. \quad (5.108)$$

Notice that, if the product term equals 1 when $-1 < m < 0$, Eq. (5.108) is the same as Eq. (5.105). Therefore, Eq. (5.108) is valid for all $m > -1$.

Now the question becomes to evaluate the integral in the RHS of Eq. (5.108). By splitting the integration interval, it can be expressed as

$$\left(\int_0^{1/(\delta\bar{\gamma})} + \int_{1/(\delta\bar{\gamma})}^{1} \right) \delta e^{-\frac{\kappa_2 \delta\bar{\gamma}}{2} v} \left(\ln \frac{1}{\delta v} \right)^n (\delta v)^{m-\tilde{m}-\frac{1}{2}} dv \triangleq I_{11} + I_{12}. \tag{5.109}$$

When $(\delta\bar{\gamma})^{-1} \leq v \leq 1$, we have $\ln \delta^{-1} \leq \ln(\delta v)^{-1} \leq \ln \bar{\gamma}$. For $\bar{\gamma} \to \infty$, due to the definition of incomplete Gamma function and its asymptotic value [5, 6.5.3, 6.5.32], the second integral of Eq. (5.109) can be bounded as

$$\begin{aligned} I_{12} &\leq (\ln \bar{\gamma})^n \int_{1/(\delta\bar{\gamma})}^{1} \delta e^{-\frac{\kappa_2 \delta\bar{\gamma}}{2} v} (\delta v)^{m-\tilde{m}-\frac{1}{2}} dv & (5.110) \\ &= \left(\frac{2}{\kappa_2} \right)^{m-\tilde{m}+\frac{1}{2}} \Gamma\left[m - \tilde{m} + \frac{1}{2}, \frac{\kappa_2}{2} \right] \bar{\gamma}^{-(m-\tilde{m}+\frac{1}{2})} (\ln \bar{\gamma})^n, & (5.111) \end{aligned}$$

and

$$\begin{aligned} I_{12} &\geq (\ln \delta^{-1})^n \left(\frac{2}{\kappa_2} \right)^{m-\tilde{m}+\frac{1}{2}} \Gamma\left[m - \tilde{m} + \frac{1}{2}, \frac{\kappa_2}{2} \right] \bar{\gamma}^{-(m-\tilde{m}+\frac{1}{2})} & (5.112) \\ &= o\left(\bar{\gamma}^{-(m-\tilde{m}+\frac{1}{2})} (\ln \bar{\gamma})^n \right), \text{ for } n > 0. & (5.113) \end{aligned}$$

On the other hand, $e^{-\frac{\kappa_2}{2}} \leq e^{-\frac{\kappa_2 \delta\bar{\gamma}}{2} v} \leq 1$ for $0 \leq v \leq (\delta\bar{\gamma})^{-1}$. Thus, for $\bar{\gamma} \to \infty$, I_{11} in Eq. (5.109) has

$$\begin{aligned} I_{11} &\leq \int_0^{1/(\delta\bar{\gamma})} \delta \left(\ln \frac{1}{\delta v} \right)^n (\delta v)^{m-\tilde{m}-\frac{1}{2}} dv & (5.114) \\ &= \left(m - \tilde{m} + \frac{1}{2} \right)^{-n-1} \Gamma\left[n+1, \left(m - \tilde{m} + \frac{1}{2} \right) \ln \bar{\gamma} \right] & (5.115) \\ &\doteq \left(m - \tilde{m} + \frac{1}{2} \right)^{-1} \bar{\gamma}^{-(m-\tilde{m}+\frac{1}{2})} (\ln \bar{\gamma})^n, & (5.116) \end{aligned}$$

where Eq. (5.115) is given by [5, 5.1.4] and [5, 5.1.45], and Eq. (5.116) is based on the derivative of the incomplete Gamma function [5, 6.5.25]. Additionally, we have the lower bound on I_{11} as

$$I_{11} \geq e^{-\frac{\kappa_2}{2}} \left(m - \tilde{m} + \frac{1}{2} \right)^{-1} \bar{\gamma}^{-(m-\tilde{m}+\frac{1}{2})} (\ln \bar{\gamma})^n. \tag{5.117}$$

In summary, by combining Eqs. (5.98), (5.108), (5.111), (5.113), (5.116) and (5.117), the bounds for the asymptotic SER are proved and summarized in the theorem. ■

With regard to diversity performance, Theorem 5.3 indicates that the concerned system achieves the diversity gain function $G_f(\bar{\gamma}) = \bar{\gamma}^{-(m+1)}(\ln \bar{\gamma})^n$ and the diversity order $G_d = m + 1$ at high SNR.

5.5.4 Diversity Performance of Relay Selection Schemes

For simplicity, independent flat Rayleigh fading channels with unit variance are considered, i.e., h_{si} and h_{id} ($i \in \{1, \cdots, N_r\}$) are i.i.d. complex Gaussian random variables with zero mean and variance $\sigma_{si}^2 = \sigma_{id}^2 = 1$. In addition, the relays are assumed to have the same average power constraints with the source, i.e., $P_i = P_x$. Thus, the instantaneous gain becomes $\alpha_{0,i} = (\rho_{si} + \bar{\gamma}^{-1})^{-1}$ and the fixed PSF becomes $\alpha_{1,i} = (1 + \bar{\gamma}^{-1})^{-1}$.

5.5.4.1 Instantaneous-Gain Relays with the 2H-CSI Selection Scheme

In the high SNR region,

$$\alpha_{0,i} = \rho_{si}^{-1}, \text{ for } \bar{\gamma} \to \infty. \tag{5.118}$$

Accordingly, the instantaneous SNR for each relay path becomes

$$\gamma_i = \frac{\rho_{si}\rho_{id}\bar{\gamma}^2}{1 + \rho_{si}\bar{\gamma} + \rho_{id}\bar{\gamma}}, \ i \in \{1, \cdots, N_r\}. \tag{5.119}$$

In the 2H-CSI selection, the relay selection c is determined by

$$c = \arg \max_{i \in \{1, \cdots, N_r\}} \gamma_i. \tag{5.120}$$

The SNR is thus

$$\gamma = \gamma_c. \tag{5.121}$$

Therefore, the SER can be given by

$$P_e = E_\gamma \left[\kappa_1 Q\left(\sqrt{\kappa_2 \gamma}\right)\right] = \kappa_1 E_n \left[F_\gamma\left(\frac{n^2}{\kappa_2}\right)\right], \tag{5.122}$$

where $n \sim \mathcal{N}(0,1)$ and $F_\gamma(t)$ is the CDF of γ evaluated at t. Because of Eqs. (5.120)-(5.121) and the relay paths are i.i.d., $F_\gamma(t)$ can be evaluated as

$$F_\gamma(t) = (F_{\gamma_i}(t))^{N_r}, \tag{5.123}$$

where $F_{\gamma_i}(t) = \frac{2t}{\bar{\gamma}}$. So, we have

$$P_e = E_n \left[2^{N_r}\left(\frac{n^2}{k\bar{\gamma}}\right)^{N_r}\right] \doteq \bar{\gamma}^{-N_r}, \text{ for } \bar{\gamma} \to \infty. \tag{5.124}$$

5.5.4.2 Instantaneous-Gain Relays with the 1H-CSI Selection Scheme

In the 1H-CSI selection, the relay selection becomes

$$c = \arg \max_{i \in \{1,\cdots,N_r\}} |h_i|^2 = \arg \max_{i \in \{1,\cdots,N_r\}} \alpha_{0,i}\rho_{si}\rho_{id}. \tag{5.125}$$

Because of Eq. (5.118) in the high SNR region, the relay selection Eq. (5.125) is equivalently

$$c = \arg \max_{i \in \{1,\cdots,N_r\}} \rho_{id}, \tag{5.126}$$

which is the 'nearest neighbor' relay selection scheme mentioned in [42]. Since the proof in [42] is not correct, a simple proof for the same conclusion is provided as follows.

Here, the receive SNR has

$$\gamma = \frac{\rho_{sc}\rho_{cd}}{\rho_{sc} + \rho_{cd}}\bar{\gamma} = \beta(\rho_{sc}, \rho_{cd})\bar{\gamma}. \tag{5.127}$$

According to Proposition 1 in [107], we just need to show the PDF of

$$\beta(\rho_{sc}, \rho_{cd}) = \frac{\rho_{sc}\rho_{cd}}{\rho_{sc} + \rho_{cd}} \tag{5.128}$$

has the zero-th order of smoothness around $\beta \to 0^+$, i.e., $0 < f_\beta(0) < \infty$.

Because of Eq. (5.126), the PDF of ρ_{cd} (the maximum of N_r exponential distributed random variables) has

$$f_{\rho_{cd}}(t) = N_r(1 - e^{-t})^{N_r - 1} e^{-t}. \tag{5.129}$$

Meanwhile, because

$$f_{\rho_{sc}}(t) = e^{-t}, \tag{5.130}$$

we have

$$\begin{aligned} f_\beta(0) &= f_{\rho_{sc}}(0) \int \frac{f_{\rho_{cd}}(b)}{|\nabla \beta(0,b)|} db + f_{\rho_{cd}}(0) \int \frac{f_{\rho_{sc}}(a)}{|\nabla \beta(a,0)|} da & (5.131)\\ &= f_{\rho_{sc}}(0) + f_{\rho_{cd}}(0) & (5.132)\\ &= 1. & (5.133) \end{aligned}$$

Therefore, the order of smoothness for $f_\beta(\beta)$ around $\beta = 0$ is 0. The diversity order of the SNR $\gamma = \beta\bar{\gamma}$ is $G_d = 1$.

5.5.4.3 Fixed-Gain Relays with the 2H-CSI Selection Scheme

The fixed PSF has $\alpha_{1,i} = C \triangleq (1 + \bar{\gamma}^{-1})^{-1}$ $(\forall i \in \{1, \cdots, N_r\})$. Consequently, the 2H-CSI selection scheme yields the instantaneous receive SNR that

$$\gamma = \beta\bar{\gamma} = \max_{i \in \{1, \cdots, N_r\}} \beta_i \bar{\gamma}, \tag{5.134}$$

where $\beta = \beta_c$ and $\beta_i = \frac{\rho_{si}\rho_{id}}{\rho_{id} + C^{-1}}$. According to Theorem 5.3, the asymptotic error performance is determined by the PDF of β around $\beta \to 0^+$, which thus becomes our focus in this subsection.

Since ρ_{si} and ρ_{id} are i.i.d., β_i $(i \in \{1, \cdots, N_r\})$ are also i.i.d. random variables so that β_1 suffices to represent them in the sense of distribution. Because of Eq. (5.134), the CDF of β can be found as $F_\beta(\beta) = (F_{\beta_1}(\beta))^{N_r}$. Thus, the PDF of β is

$$f_\beta(\beta) = \frac{d}{d\beta} F_\beta(\beta) = N_r (F_{\beta_1}(\beta))^{N_r - 1} f_{\beta_1}(\beta). \tag{5.135}$$

In [38], the CDF and PDF of β_1 have been unveiled as

$$F_{\beta_1}(t) = 1 - 2e^{-t}\sqrt{\frac{t}{C}}K_1\left(2\sqrt{\frac{t}{C}}\right) \tag{5.136}$$

$$f_{\beta_1}(t) = 2e^{-t}\left[\sqrt{\frac{t}{C}}K_1\left(2\sqrt{\frac{t}{C}}\right) + \frac{1}{C}K_0\left(2\sqrt{\frac{t}{C}}\right)\right],\ t > 0, \tag{5.137}$$

where $K_0(\cdot)$ and $K_1(\cdot)$ are the zero and first-order modified Bessel functions of the second kind [5, 9.6.2]. Because of [5, 9.6.8, 9.6.9],

$$\lim_{x\to 0+} K_0(x) = -\lim_{x\to 0+} \ln\frac{x}{2} \tag{5.138}$$

$$\lim_{x\to 0+} K_1(x) = \lim_{x\to 0+} \frac{1}{x}. \tag{5.139}$$

Thus, for $t \to 0^+$, we can find

$$f_{\beta_1}(t) \doteq \frac{2}{C}\ln\frac{1}{\sqrt{t}} = \frac{1}{C}\ln\frac{1}{t}. \tag{5.140}$$

In addition, using l'Hôpital's rule and [5, 9.6.28], it is ready to show that

$$\lim_{t\to 0^+} \frac{1 - 2\sqrt{t}K_1(2\sqrt{t})}{t - t\ln t} = \lim_{t\to 0^+} \frac{2K_0(2\sqrt{t})}{-\ln t} = 1, \tag{5.141}$$

and the asymptotic CDF in Eq. (5.136) has

$$\lim_{t\to 0^+} F_{\beta_1}(t) = \lim_{t\to 0^+} \frac{t}{C}\ln\frac{C}{t}. \tag{5.142}$$

Therefore, bringing Eqs. (5.140) and (5.142) into Eq. (5.135), the PDF of β has

$$f_\beta(\beta) = \frac{N_r}{C^{N_r}}\beta^{N_r-1}(\ln\beta^{-1})^{N_r} + o(\beta^{N_r-1}(\ln\beta^{-1})^{N_r}),\ \text{for } \beta \to 0^+. \tag{5.143}$$

Following the notations used in (A2), we have

$$a = \frac{N_r}{C^{N_r}},\ m = N_r - 1,\ n = N_r. \tag{5.144}$$

The asymptotic error performance can be bounded according to Theorem 5.3, and it achieves the diversity gain function of $G_f = \bar{\gamma}^{-N_r}(\ln\bar{\gamma})^{N_r}$.

5.5.4.4 Fixed-Gain Relays with the 1H-CSI Selection Scheme

Let $\rho_i = \rho_{si}\rho_{id}$ ($i \in \{1, \cdots, N_r\}$). Requiring only $|h_i|^2 = C\rho_i$, the 1H-CSI selection determines the index c of the selected relay node according to Eq. (5.87). In this case, the instantaneous receive SNR becomes

$$\gamma = \frac{\rho_c}{\rho_{cd} + C^{-1}}\bar{\gamma} \triangleq \beta(\rho_c, \rho_{cd})\bar{\gamma}. \tag{5.145}$$

The PDF of $\beta(\rho_c, \rho_{cd}) \triangleq \rho_c/(\rho_{cd} + C^{-1})$ can be determined by [83, p. 31]

$$f_\beta(\beta) = \int\int_{\{a,b|\frac{a}{b+C^{-1}}=\beta\}} \frac{f_{\rho_c,\rho_{cd}}(a,b)}{|\nabla\beta(a,b)|} dadb, \tag{5.146}$$

where $|\nabla\beta(\rho_c = a, \rho_{cd} = b)|$ is the modulus of the gradient of $\beta(\rho_c, \rho_{cd})$

$$|\nabla\beta(a,b)| = \frac{\sqrt{a^2 + (b + C^{-1})^2}}{(b + C^{-1})^2}. \tag{5.147}$$

To evaluate Eq. (5.146), the missing piece is the joint PDF of ρ_c and ρ_{cd}, which can be further decomposed into $f_{\rho_c,\rho_{cd}}(a,b) = \sum_{i=1}^{N_r} p_c(i) f_{\rho_c|c}(a|i) f_{\rho_{cd}|\rho_c,c}(b|a,i)$ and $p_c(i)$ is the probability mass function for $c = i$.

On one hand, since ρ_i is the product of two independent exponential random variables, ρ_i ($i \in \{1, \cdots, N_r\}$) are i.i.d. with the distribution given in [72]. Hence, it is easy to see that $p_c(i) = N_r^{-1}$ and $f_{\rho_c|c}(a|i) = f_{\rho_c|c}(a|j)$ ($\forall i, j \in \{1, \cdots, N_r\}$). In addition, similar to Eq. (5.135), using ρ_1 to represent ρ_i ($i \in \{1, \cdots, N_r\}$) with the same distribution, the conditional PDF of $f_{\rho_c|c}(a|i)$ has

$$f_{\rho_c|c}(a|i) = \sum_{i=1}^{N_r} p_c(i) f_{\rho_c|c}(a|i) = f_{\rho_c}(a) \tag{5.148}$$

$$= N_r(F_{\rho_1}(a))^{N_r-1} f_{\rho_1}(a) = 2N_r K_0(2\sqrt{a}) \left[1 - 2\sqrt{a}K_1(2\sqrt{a})\right]^{N_r-1}. \tag{5.149}$$

On the other hand, since ρ_{si} and ρ_{id} are i.i.d. random variables, and $\rho_i = \rho_{si}\rho_{id}$, we have

$$f_{\rho_{cd}|\rho_c,c}(b|a,i) = f_{\rho_{1d}|\rho_1}(b|a) = \frac{f_{\rho_1,\rho_{1d}}(a,b)}{f_{\rho_1}(a)} = \frac{e^{-b-\frac{a}{b}}}{b f_{\rho_1}(a)}, \ \forall i \in \{1, \cdots, N_r\}. \tag{5.150}$$

Therefore, the joint PDF in Eq. (5.146) is given by

$$f_{\rho_c,\rho_{cd}}(a,b) = \frac{N_r}{b} e^{-b-\frac{a}{b}} [1 - 2\sqrt{a} K_1(2\sqrt{a})]^{N_r-1}. \tag{5.151}$$

Because $f_\beta(\beta)$ at $\beta \to 0^+$ is of our concern, now we bring Eq. (5.151) into Eq. (5.146), substitute $a = \beta(b + C^{-1})$ and further split the integration interval as

$$\begin{aligned} f_\beta(\beta) &= \frac{N_r e^{-\beta}}{\sqrt{1+\beta^2}} \left(\int_0^\eta + \int_\eta^\infty \right) \frac{b + C^{-1}}{b e^{b+\frac{\beta}{bC}}} \\ &\quad \left[1 - 2\sqrt{\beta(b+C^{-1})} K_1 \left(2\sqrt{\beta(b+C^{-1})} \right) \right]^{N_r-1} db \qquad (5.152) \\ &\triangleq \frac{N_r e^{-\beta}}{\sqrt{1+\beta^2}} \left(I_0^\eta + I_\eta^\infty \right), \qquad (5.153) \end{aligned}$$

where $\eta = C^{-1}(\beta^{\delta-1} - 1) > 0$ for $0 < \delta < 1$ and $\beta < 1$.

Since the first integral I_0^η in Eq. (5.153) integrates from 0 to η, it can be further bounded by

$$I_0^\eta < \left[1 - 2\sqrt{\epsilon} K_1(2\sqrt{\epsilon}) \right]^{N_r-1} \int_0^\eta \frac{b + C^{-1}}{b e^{b+\frac{\beta}{bC}}} db, \tag{5.154}$$

where $\epsilon = \beta(\eta + C^{-1}) = C^{-1}\beta^\delta$. Because of Eq. (5.141) and [33, 3.471.9], the asymptotic bound on I_0^η is

$$\begin{aligned} \lim_{\beta\to 0^+} I_0^\eta &< \lim_{\beta\to 0^+} \frac{2\delta^{N_r-1}}{C^{N_r-1}} \beta^{\delta(N_r-1)} (\ln \beta^{-1})^{N_r-1} \left[\frac{1}{C} K_0 \left(2\sqrt{\frac{\beta}{C}} \right) + 2\sqrt{\frac{\beta}{C}} K_1 \left(2\sqrt{\frac{\beta}{C}} \right) \right] \\ &= \lim_{\beta\to 0^+} \frac{\delta^{N_r-1}}{C^{N_r}} \beta^{\delta(N_r-1)} (\ln \beta^{-1})^{N_r}. \qquad (5.155) \end{aligned}$$

Since (5.155) is valid for any $0 < \delta < 1$, when $\delta \to 1^-$, the above inequality indicates that

$$I_0^\eta = \frac{1}{C^{N_r}} \beta^{N_r-1} (\ln \beta^{-1})^{N_r} + o(\beta^{N_r-1} (\ln \beta^{-1})^{N_r}), \text{ for } \beta \to 0^+. \tag{5.156}$$

Meanwhile, the integration interval in I_η^∞ ranges from η to ∞, in which we have $(b + C^{-1})/b < (1 - \beta^{1-\delta})^{-1}$, $1 - 2\sqrt{\beta(b+C^{-1})} K_1(2\sqrt{\beta(b+C^{-1})}) \le 1$, and $e^{-\frac{\beta}{bC}} \le 1$. Therefore, for $\beta \to 0^+$,

$$I_\eta^\infty < (1 - \beta^{1-\delta})^{-1} \int_\eta^\infty e^{-b} db \doteq e^{-\beta^{\delta-1}} = o(\beta^{N_r-1} (\ln \beta^{-1})^{N_r}). \tag{5.157}$$

In summary, by substituting Eqs. (5.155) and (5.157) into Eq. (5.153), the PDF of β at $\beta \to 0^+$ is shown to be the same with Eq. (5.143). Accordingly, due to Theorem 5.3, the 1H-CSI selection with the fixed-gain AF relaying can achieve the same asymptotic error performance with the 2H-CSI selection scheme.

5.5.4.5 Simulation Results

In Figure 5.13, the average SER P_e versus average SNR $\bar{\gamma}$ curves are plotted for both the 1H-CSI and the 2H-CSI single-relay selection schemes with the fixed gain $\alpha_i = (1+\bar{\gamma}^{-1})^{-1}$. QPSK modulation ($\kappa_1 = 2$ and $\kappa_2 = 1$) and flat Rayleigh fading channels with unit variance are adopted. In addition, ideal channel state information is assumed available at the destination: both h_i and h_{si} are known for the 2H-CSI selection, while the 1H-CSI selection only requires h_i ($i \in \{1, \cdots, N_r\}$). The examples of $N_r = 2$, 3 and 4 relay nodes are illustrated in Figure 5.13, in which the 1H-CSI selection is shown to achieve the same SER performance with the 2H-CSI selection. The corresponding theoretical bounds given by (5.92) with the parameters in Eq. (5.144) are also plotted. The results validate that Theorem 5.3 gives tight bounds for the asymptotic error performance. Moreover, with the fixed-gain AF relaying, both the 2H-CSI and the 1H-CSI single-relay selection schemes can achieve the diversity gain function $G_f = \bar{\gamma}^{-N_r}(\ln \bar{\gamma})^{N_r}$, which makes the 1H-CSI selection with fixed-gain relays favored due to its implementation merits.

Moreover, the SER curves for the instantaneous PSF and fixed PSF are compared in Figure 5.14. The diversity performance of these PSFs and selection schemes has been evaluated above and is summarized in Table 5.2. With the instantaneous PSF, 2H-CSI selection is shown to achieve the optimal SER performance with the diversity order $G_d = N_r$, while 1H-CSI selection only generates $G_d = 1$. For comparison, the fixed PSF not only is easy to implement because of the needlessness of the 2H CSI at both the relay and the destination, but also achieves the near-optimal SER

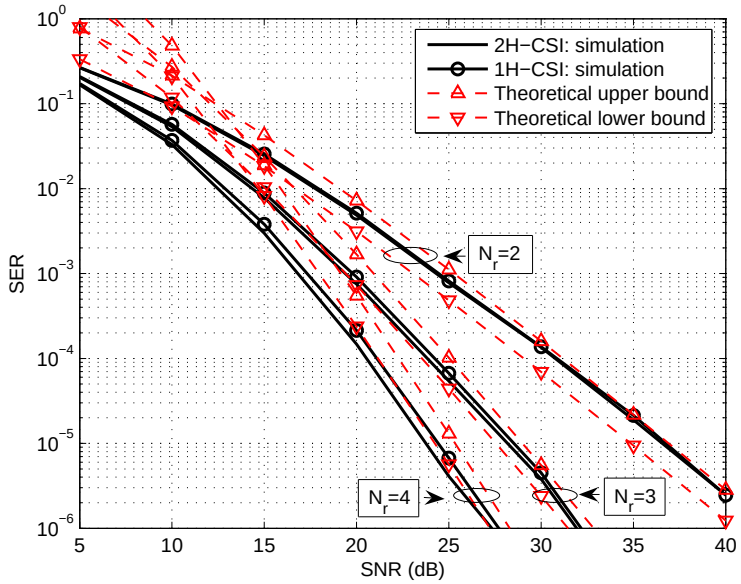

Figure 5.13: SER versus SNR curves for 1H-CSI and 2H-CSI selection schemes with $\alpha_{1,i} = (1 + \bar{\gamma}^{-1})^{-1}$; $N_r = 2$, 3 and 4 relay nodes are used; the theoretical upper and lower bounds are also drawn.

Table 5.2: The diversity performance of single-relay selection schemes ($\bar{\gamma} \to \infty$).

Selection\PSF	Instantaneous	Fixed
2H-CSI	$\bar{\gamma}^{-N_r}$	$\bar{\gamma}^{-N_r}(\ln \bar{\gamma})^{N_r}$
1H-CSI	$\bar{\gamma}^{-1}$	$\bar{\gamma}^{-N_r}(\ln \bar{\gamma})^{N_r}$

performance by collecting the diversity gain function and the diversity order of $G_d = N_r$ asymptotically.

Last but not least, the multi-relay selection schemes can be adopted to further improve the coding gain [42], where more than one relay node can be selected to cooperate in the second time slot simultaneously. Details are omitted and examples of generalized 2H-CSI and 1H-CSI multi-relay selection schemes are illustrated in Figure 5.15 to validate the performance.

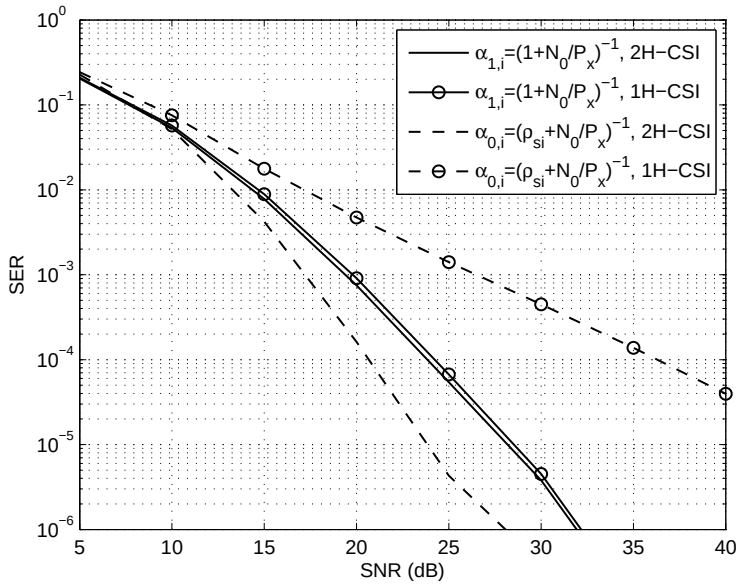

Figure 5.14: SER versus SNR curves for 1H-CSI and 2H-CSI selection schemes with the instantaneous PSF $\alpha_{0,i}$ as well as the fixed PSF $\alpha_{1,i}$; $N_r = 3$ relay nodes are used.

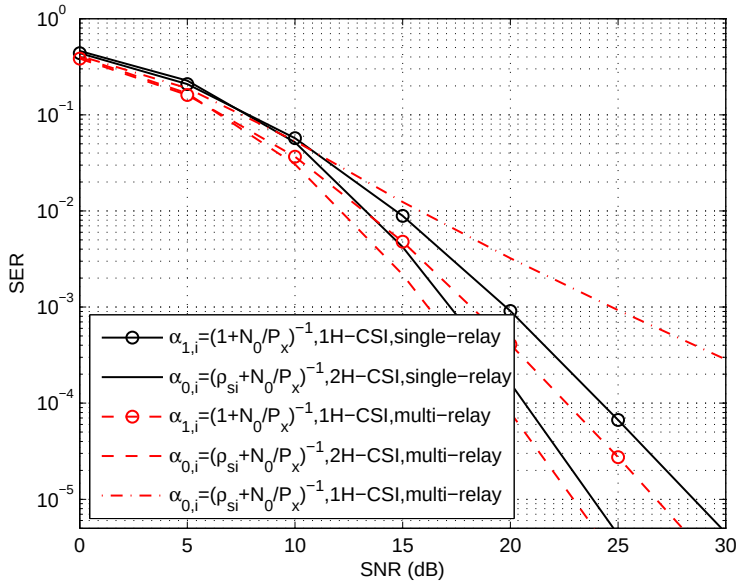

Figure 5.15: SER versus SNR curves for both the single-relay selection and multi-relay selection schemes; $N_r = 3$ relay nodes are used.

5.6 Conclusions

In this chapter, error performance and some practical issues in amplify-and-forward cooperative networks are studied.

Basic design criteria for generalized AF strategies are provided to guarantee full cooperative diversity order for both 2H-MRC and 1H-MRC destinations. Based on these guidelines, an intentional peak power limit strategy is proposed for the practical two-hop relay network where the relay nodes are peak power constrained and have bounded power scaling factors. It can achieve full cooperative diversity with simplified relay and destination nodes.

To improve spectral efficiency, relay selection schemes are also studied. First, a general theorem relating the diversity gain function with the PDF of the instantaneous SNR around the origin is presented, providing an easy way to evaluate the asymptotic error performance of general wireless communication systems. With the help of the proposed theory, the error performance of relay selection schemes in cooperative networks is analyzed. It reveals that, unlike the instantaneous gain, the fixed-gain relays enable the 1H-CSI selection to achieve the same asymptotic SER with the 2H-CSI selection scheme.

The results make AF strategies more attractive to practical cooperative networks.

CHAPTER VI

CONCLUSIONS

6.1 Contributions

In this dissertation, we have studied the power efficiency and transmission reliability issues in peak power constrained wireless communication systems. The main research results are summarized in the following list:

- The EVM optimization PAR reduction method was proposed for OFDM systems.
- The tradeoff between power efficiency and in-band distortions was lower bounded and established a way to compare the PAR reduction methods in OFDM systems.
- The MCPTS PAR reduction method was proposed for OFDM-FDMA systems.
- Joint MCPTS and power allocation schemes were proposed to improve the average error performance in OFDM-FDMA systems.
- It was demonstrated how full antenna diversity order can be collected without receiver-side modification in peak power constrained SIMO-OFDM systems.
- It was established how linear equalizers could obtain full antenna diversity order with the proposed joint MRC and clipping mitigation method.
- General design criteria were established for AF cooperative networks to achieve full cooperative diversity orders with 2H-MRC or 1H-MRC.
- Intentional peak power limit AF relaying strategy was proposed for low-complexity and full-diversity peak power constrained cooperative networks.

- A general theorem was established to relate the asymptotic error rate (measured by diversity gain function and coding gain) only with the PDF of instantaneous SNR at the origin.

- The diversity performance of relay selection schemes was studied.

6.2 Suggestions for Future Research

The following is a list of interesting research topics that can be pursued as an extension of this dissertation:

- Low-complexity optimization algorithms, e.g., the minimum-spanning circle method [56, 65, 66], are in need of achieving good, albeit sub-optimal, PAR reduction performance.

- Design low-complexity receivers for peak power constrained MIMO-OFDM systems to collect both spatial and multipath diversity.

- Design high-spectral-efficient cooperative networks that have low-complexity transceivers. For example, precoding in cooperative networks can achieve high spectral efficiency [27]. However, ML equalizers are required to achieve full diversity orders in precoded cooperative networks. It can be shown that linear equalizers can only collect diversity order of $\frac{1}{2}$, while lattice-reduction aided equalizers [70] achieve diversity order of 1. How to achieve full diversity order and high spectral efficiency with linear equalizers remains an open question.

REFERENCES

[1] *EN300744: Digital Video Broadcasting (DVB): Framing Structure, Channel Coding and Modulation for Digital Terrestrial Television.* Eur. Telecommun. Standards Inst. (ETSI), Sophia Antipolis, France, 1997.

[2] *Wireless LAN Medium Access Control (MAC) and Physical Layer (PHY) Specifications: High-Speed Physical Layer in the 5 GHz Band.* IEEE Std. 802.11a, Sept. 1999.

[3] *IEEE Standard for Local and Metropolitan Area Networks Part 16: Air Interface for Fixed Broadband Wireless Access Systems.* IEEE Std. 802.16-2004 (Revision of IEEE Std. 802.16-2001), 2004.

[4] *Draft Standard for Local and Metropolitan Area Networks: Standard Air Interface for Mobile Broadband Wireless Access Systems Supporting Vehicular Mobility.* IEEE Std. P802.20-2007, 2007.

[5] Abramowitz, M. and Stegun, I. A., eds., *Handbook of Mathematical Functions.* New York: Dover, 10th ed., 1972.

[6] Aggarwal, A. and Meng, T. H., "Minimizing the peak-to-average power ratio of OFDM signals using convex optimization," *IEEE Trans. on Signal Process.*, vol. 54, pp. 3099–3110, Aug. 2006.

[7] Andreoli, S., McClure, H. G., Banelli, P., and Cacopardi, S., "Digital linearizer for RF amplifiers," *IEEE Trans. on Broadcast.*, vol. 43, pp. 12–19, Mar. 1997.

[8] Anghel, P. A. and Kaveh, M., "Exact symbol error probability of a cooperative network in a Rayleigh-fading environment," *IEEE Trans. on Wireless Commun.*, vol. 3, pp. 1416–1421, Sept. 2004.

[9] Anghel, P. A., Leus, G., and Kaveh, M., "Distributed space-time cooperative systems with regenerative relays," *IEEE Trans. on Wireless Commun.*, vol. 5, pp. 3130–3141, Nov. 2006.

[10] Armstrong, J., "Peak-to-average power reduction for OFDM by repeated clipping and frequency domain filtering," *Electronics Letters*, vol. 38, pp. 246–247, Feb. 2002.

[11] Bauml, R. W., Fischer, R. F. H., and Huber, J. B., "Reducing the peak-to-average power ratio of multicarrier modulation by selected mapping," *Electronics Letters*, vol. 32, pp. 2056–2057, Oct. 1996.

[12] Baxley, R. J., Zhao, C., and Zhou, G. T., "Constrained clipping for crest factor reduction in OFDM," *IEEE Trans. on Broadcast.*, vol. 52, pp. 570–575, Dec. 2006.

[13] Baxley, R. J., "Analyzing selected mapping for peak-to-average power reduction in OFDM," Master's thesis, Georgia Institute of Technology, June 2005.

[14] Bittner, S., Zillmann, P., and Fettweis, G., "Iterative correction of clipped and filtered spatially multiplexed OFDM signals," in *Proc. IEEE Vehicular Technology Conference (VTC) Spring*, (Singapore), pp. 953–957, May 2008.

[15] Bletsas, A., Khisti, A., Reed, D. P., and Lippman, A., "A simple cooperative diversity method based on network path selection," *IEEE J. Sel. Areas Commun.*, vol. 24, pp. 659–672, Mar. 2006.

[16] Boyd, S. and Vandenberghe, L., *Convex Optimization*. Cambridge, UK: Cambridge Univ. Press, Mar. 2004.

[17] Chang, R. W., "Synthesis of band-limited orthogonal signals for multichannel data transmission," *Bell Sys. Tech. Journal*, vol. 45, 1966.

[18] Choi, G., Zhang, W., and Ma, X., "Designing diversity-enabled power profiles for wireless relay networks," submitted to *IEEE Trans. on Inf. Theory*, Mar. 2009.

[19] Cimini, L. J., "Analysis and simulation of a digital mobile channel using orthogonal frequency division multiplexing," *IEEE Trans. on Commun.*, vol. 33, pp. 665–675, Mar. 1985.

[20] Costa, E., Midrio, M., and Pupolin, S., "Impact of amplifier nonlinearities on OFDM transmission system performance," *IEEE Commun. Lett.*, vol. 3, pp. 37–39, Feb. 1999.

[21] Cripps, S. C., *RF Power Amplifiers for Wireless Communications*. Norwood, MA: Artech House, 1999.

[22] Cui, T., Gao, F., Ho, T., and Nallanathan, A., "Distributed space-time coding for two-way wireless relay networks," *IEEE Trans. on Signal Process.*, vol. 57, pp. 658–671, Feb. 2009.

[23] D'Andrea, A. N., Lottici, V., and Reggiannini, R., "RF power amplifier linearization through amplitude and phase predistortion," *IEEE Trans. on Commun.*, vol. 44, pp. 1477–1484, Nov. 1996.

[24] Davis, J. A. and Jedwab, J., "Peak-to-mean power control in OFDM, golay complementary sequences, and Reed-Muller codes," *IEEE Trans. on Inf. Theory*, vol. 45, pp. 2397–2417, Nov. 1999.

[25] Declercq, D. and Giannakis, G. B., "Recovering clipped OFDM symbols with Bayesian inference," in *Proc. IEEE International Conference on Acoustics, Speech, and Signal Processing (ICASSP)*, vol. 1, (Istanbul, Turkey), pp. 157–160, June 2000.

[26] Ding, L., Zhou, G. T., Morgan, D. R., Ma, Z., Kenney, J. S., Kim, J., and Giardina, C. R., "A robust digital baseband predistorter constructed using memory polynomials," *IEEE Trans. on Commun.*, vol. 52, pp. 159–165, Jan. 2004.

[27] Ding, Y., Zhang, J.-K., and Wong, K. M., "The amplify-and-forward half-duplex cooperative: Pairwise error probability and precoder design," *IEEE Trans. on Signal Process.*, vol. 55, pp. 605–617, Feb. 2007.

[28] Ekstrom, H., Furuskar, A., Karlsson, J., Meyer, M., Parkvall, S., Torsner, J., and Wahlqvist, M., "Technical solutions for the 3G long-term evolution," *IEEE Commun. Mag.*, vol. 44, pp. 38–45, Mar. 2006.

[29] Farhadi, G. and Beaulieu, N. C., "On the performance of amplify-and-forward cooperative links with fixed gain relays," *IEEE Trans. on Wireless Commun.*, vol. 7, pp. 1851–1856, May 2008.

[30] Foschini, G. J. and Gans, M. J., "On limits of wireless communication in a fading environment when using multiple antennas," *Wireless Pers. Commun.*, vol. 6, pp. 311–335, Mar. 1998.

[31] Gatzianas, M. A., Georgiadis, L. G., and Karagiannidis, G. K., "Optimal relay control in power-constrained dual-hop transmissions over arbitrary fading channels," in *Proc. IEEE International Conference on Communications (ICC)*, (Istanbul, Turkey), pp. 4543–4548, June 2006.

[32] Goldsmith, A., *Wireless Communications*. Cambridge University Press, 2005.

[33] Gradshteyn, I. S. and Ryzhik, I. M., *Table of Integrals, Series, and Products*. Academic Press, 5th ed., 1994.

[34] Greville, T. N. E., "Note on the generalized inverse of a matrix product," *SIAM Review*, vol. 8, pp. 518–521, Oct. 1966.

[35] Han, S. H. and Lee, J. H., "An overview of peak-to-average power ratio reduction techniques for multicarrier transmission," *IEEE Wireless Commun. Mag.*, vol. 12, pp. 56–65, Apr. 2005.

[36] Hasna, M. and Alouini, M. S., "End-to-end performance of transmission systems with relays over Rayleigh-fading channels," *IEEE Trans. on Wireless Commun.*, vol. 2, pp. 1126–1131, Nov. 2003.

[37] Hasna, M. and Alouini, M. S., "Optimal power allocation for relayed transmissions over Rayleigh-fading channels," *IEEE Trans. on Wireless Commun.*, vol. 3, pp. 1999–2004, Nov. 2004.

[38] Hasna, M. and Alouini, M. S., "A performance study of dual-hop transmissions with fixed gain relay," *IEEE Trans. on Wireless Commun.*, vol. 3, pp. 1963–1968, Nov. 2004.

[39] Janani, M., Hedayat, A., Hunter, T. E., and Nosratinia, A., "Coded cooperation in wireless communications: Space-time transmission and iterative decoding," *IEEE Trans. on Signal Process.*, vol. 52, pp. 362–371, Feb. 2004.

[40] Jiang, T. and Wu, Y., "An overview: Peak-to-average power ratio reduction techniques for OFDM signals," *IEEE Trans. on Broadcast.*, vol. 54, pp. 257–268, June 2008.

[41] Jing, Y. and Hassibi, B., "Distributed space-time coding in wireless relay networks," *IEEE Trans. on Wireless Commun.*, vol. 5, pp. 3524–3536, Dec. 2006.

[42] Jing, Y. and Jafarkhani, H., "Single and multiple relay selection schemes and their achievable diversity orders," *IEEE Trans. on Wireless Commun.*, vol. 8, pp. 1414–1423, Mar. 2009.

[43] Kennedy, J., Eberhard, R. C., and Shi, Y., *Swarm Intelligence*. San Francisco, CA: Morgan Kaufmann Publishers, 2001.

[44] Krongold, B. S. and Jones, D. L., "PAR reduction in OFDM via active constellation extension," *IEEE Trans. on Broadcast.*, vol. 49, pp. 258–268, Sept. 2003.

[45] Krongold, B. S. and Jones, D. L., "An active-set approach for OFDM PAR reduction via tone reservation," *IEEE Trans. on Signal Process.*, vol. 52, pp. 495–509, Feb. 2004.

[46] Kwon, U.-K., Kim, D., Kim, K., and Im, G.-H., "Amplitude clipping and iterative reconstruction of STBC/SFBC-OFDM signals," *IEEE Signal Process. Lett.*, vol. 14, pp. 808–811, Nov. 2007.

[47] Kwon, U.-K., Kim, D., and Im, G.-H., "Amplitude clipping and iterative reconstruction of MIMO-OFDM signals with optimum equalization," *IEEE Trans. on Wireless Commun.*, vol. 8, pp. 268–277, Jan. 2009.

[48] Laneman, J. N., Tse, D. N. C., and Wornell, G. W., "Cooperative diversity in wireless networks: Efficient protocols and outage behavior," *IEEE Trans. on Inf. Theory*, vol. 50, pp. 3062–3080, Dec. 2004.

[49] Laneman, J. N. and Wornell, G. W., "Energy-efficient antenna sharing and relaying for wireless networks," in *Proc. IEEE Wireless Communications and Networking Conference (WCNC)*, vol. 1, (Chicago, IL), pp. 7–12, Sept. 2000.

[50] Lawrey, E. and Kikkert, C. J., "Peak to average power ratio reduction of OFDM signals using peak reduction carriers," in *Proc. Fifth International Symposium on Signal Processing and Its Applications (ISSPA)*, vol. 2, (Brisbane QPD, Australia), pp. 737–740, Aug. 1999.

[51] Li, H., Kwon, D. H., Chen, D., and Chiu, Y., "A fast digital predistortion algorithm for radio-frequency power amplifier linearization with loop delay compensation," *IEEE J. Sel. Topics in Signal Process.*, vol. 3, pp. 374–383, June 2009.

[52] Li, Y., Cimini, L. J., J., and Sollenberger, N. R., "Robust channel estimation for OFDM systems with rapid dispersive fading channels," *IEEE Trans. on Commun.*, vol. 46, pp. 902–915, July 1998.

[53] Li, Y., "Pilot-symbol-aided channel estimation for OFDM in wireless systems," *IEEE Trans. on Veh. Technol.*, vol. 49, pp. 1207–1215, July 2000.

[54] Litsyn, S. and Shpunt, A., "A balancing method for PMEPR reduction in OFDM signals," *IEEE Trans. on Commun.*, vol. 55, pp. 683–691, Apr. 2007.

[55] Liu, Q., Baxley, R. J., Ma, X., and Zhou, G. T., "Diversity-enabled and power-efficient transceiver designs for peak-power-limited SIMO-OFDM systems," *EURASIP J. Advances in Signal Process.*, Feb. 2010. revised.

[56] Liu, Q., Baxley, R. J., Ma, X., and Zhou, G. T., "Optimizing free subcarrier index to minimize peak-to-average power ratio for OFDM systems," in *Proc. IEEE International Conference on Acoustics, Speech and Signal Processing (ICASSP)*, (Dallas, TX), Mar. 2010.

[57] Liu, Q., Ma, X., and Zhou, G. T., "A general diversity gain function and its application in AF cooperative networks," submitted to *IEEE Trans. on Signal Process.*, Apr. 2010.

[58] Liu, Q., Zhang, W., and Ma, X., "Practical and general amplify-and-forward designs for cooperative networks," in *Proc. IEEE International Conference on Computer Communications (INFOCOM)*, (San Diego, CA), Mar. 2010.

[59] Liu, Q., Zhang, W., Ma, X., and Zhou, G. T., "Designing peak power constrained amplify-and-forward relay networks with cooperative diversity," submitted to *IEEE Trans. on Signal Process.*, Sept. 2009.

[60] Liu, Q., Zhang, W., Ma, X., and Zhou, G. T., "A practical amplify-and-forward relaying strategy with an intentional peak power limit," in *Proc. IEEE*

International Conference on Acoustics, Speech and Signal Processing (ICASSP), (Dallas, TX), Mar. 2010.

[61] Liu, Q., Baxley, R. J., Ma, X., and Zhou, G. T., "Error vector magnitude optimization for OFDM systems with a deterministic peak-to-average power ratio constraint," *IEEE J. Sel. Topics in Signal Process.*, vol. 3, pp. 418–429, June 2009.

[62] Liu, Q., Baxley, R. J., Ma, X., and Tong Zhou, G., "Error vector magnitude optimization for OFDM systems with a deterministic peak-to-average power ratio constraint," in *Proc. 42nd Annual Conference on Information Sciences and Systems (CISS)*, (Princeton, NJ), pp. 101–104, Mar. 2008.

[63] Liu, Q., Baxley, R. J., Ma, X., and Zhou, G. T., "On the PTS method and BER-minimizing power allocation of the multi-channel OFDM system," in *Proc. IEEE International Conference on Acoustics, Speech and Signal Processing (ICASSP)*, (Taipei), pp. 2585–2588, Apr. 2009.

[64] Liu, Q., Baxley, R. J., and Zhou, G. T., "Free subcarrier optimization for peak-to-average power ratio minimization in OFDM systems," in *Proc. IEEE International Conference on Acoustics, Speech and Signal Processing (ICASSP)*, (Las Vegas, NV), pp. 3073–3076, Mar. 2008.

[65] Liu, Q., Baxley, R. J., Ma, X., and Zhou, G. T., "Peak reduction for multiplexed asynchronous OFDM-FDMA," in *Proc. IEEE Military Communications (MILCOM)*, Nov. 2009.

[66] Liu, S., Zeng, Y., and Hu, B., "Minimum spanning circle method for using spare subcarriers in PAPR reduction of OFDM systems," *IEEE Signal Process. Lett.*, vol. 15, pp. 513–516, June 2008.

[67] Liu, Z., Xin, Y., and Giannakis, G. B., "Linear constellation precoding for OFDM with maximum multipath diversity and coding gains," *IEEE Trans. on Commun.*, vol. 51, pp. 416–427, Mar. 2003.

[68] Lu, J., Tjhung, T. T., and Chai, C. C., "Error probability performance of L-branch diversity reception of MQAM in Rayleigh fading," *IEEE Trans. on Commun.*, vol. 46, pp. 179–181, Feb. 1998.

[69] Ma, J., Orlik, P., Zhang, J., Kuze, T., Iura, H., and Li, G. Y., "Static power allocation in two-hop MIMO amplify-and-forward relay systems," in *Proc. IEEE Vehicular Technology Conference (VTC)*, (Barcelona, Spain), pp. 1–5, Apr. 2009.

[70] Ma, X., Zhang, W., and Swami, A., "Lattice-reduction aided equalization for OFDM systems," *IEEE Trans. on Wireless Commun.*, vol. 8, pp. 1608–1613, Apr. 2009.

[71] Ma, X. and Zhang, W., "Fundamental limits of linear equalizers: Diversity, capacity, and complexity," *IEEE Trans. on Inf. Theory*, vol. 54, pp. 3442–3456, Aug. 2008.

[72] Malik, H. J. and Trudel, R., "Probability density function of the product and quotient of two correlated exponential random variables," *Canad. Math. Bull.*, vol. 29, pp. 413–418, Dec. 1986.

[73] Muller, S. H. and Huber, J. B., "OFDM with reduced peak-to-average power ratio by optimum combination of partial transmit sequences," *Electronics Letters*, vol. 33, pp. 368–369, Feb. 1997.

[74] Negi, R. and Cioffi, J., "Pilot tone selection for channel estimation in a mobile OFDM system," *IEEE Trans. on Consum. Electron.*, vol. 44, pp. 1122–1128, Sept. 1998.

[75] Nocedal, J. and Wright, S., *Numerical Optimization*. New York: Springer, Apr. 2000.

[76] Ochiai, H., "Performance analysis of peak power and band-limited OFDM system with linear scaling," *IEEE Trans. on Wireless Commun.*, vol. 2, pp. 1055–1065, Sept. 2003.

[77] Ochiai, H. and Imai, H., "Performance analysis of deliberately clipped OFDM signals," *IEEE Trans. on Commun.*, vol. 50, pp. 89–101, Jan. 2002.

[78] Pacific Monolithics, *The PM2105 RFIC Power Amplifier in Linear Mode for PHS/PCN Applications*, 2000.

[79] Peng, F. and Ryan, W. E., "New approaches to clipped OFDM channels: modeling and receiver design," in *Proc. IEEE Global Telecommunications Conference (GLOBECOM)*, vol. 3, (St. Louis, MO), Nov. 2005.

[80] Peng, F. and Ryan, W. E., "On the capacity of clipped OFDM channels," in *Proc. IEEE International Symposium on Information Theory (ISIT)*, (Seattle, WA), pp. 1866–1870, July 2006.

[81] Peng, F. and Ryan, W. E., "MLSD bounds and receiver designs for clipped OFDM channels," *IEEE Trans. on Wireless Commun.*, vol. 7, pp. 3568–3578, Sept. 2008.

[82] Popovic, D. and Popovic, Z., "Multibeam antennas with polarization and angle diversity," *IEEE Trans. on Antennas Propag.*, vol. 50, pp. 651–657, May 2002.

[83] Proakis, J. G., *Digital Communications*. New York, NY: McGraw-Hill, 4th ed., 2001.

[84] Qian, H., Raich, R., and Zhou, G. T., "Optimization of SNDR in the presence of amplitude limited nonlinearity and multipath fading," in *Conference Record of the Thirty-Eighth Asilomar Conference on Signals, Systems and Computers*, vol. 1, (Pacific Grove, CA), pp. 712–716, Nov. 2004.

[85] Raich, R., Qian, H., and Zhou, G. T., "Optimization of SNDR for amplitude-limited nonlinearities," *IEEE Trans. on Commun.*, vol. 53, pp. 1964–1972, Nov. 2005.

[86] Rankov, B. and Wittneben, A., "Spectral efficient protocols for half-duplex fading relay channels," *IEEE J. Sel. Areas Commun.*, vol. 25, pp. 379–389, Feb. 2007.

[87] Ribeiro, A., Cai, X., and Giannakis, G. B., "Symbol error probabilities for general cooperative links," *IEEE Trans. on Wireless Commun.*, vol. 4, pp. 1264–1273, May 2005.

[88] Rowe, H. E., "Memoryless nonlinearities with Gaussian inputs: Elementary results," *Bell Syst. Tech. J.*, vol. 61, pp. 1519–1525, Sept. 1982.

[89] Saltzberg, B., "Performance of an efficient parallel data transmission system," *IEEE Trans. on Commun.*, vol. 15, pp. 805–811, Sept. 1967.

[90] Savazzi, S. and Spagnolini, U., "Design criteria of two-hop based wireless networks with non-regenerative relays in arbitrary fading channels," *IEEE Trans. on Commun.*, vol. 57, p. 5, May 2009.

[91] Schenk, T., *RF Imperfections in High-Rate Wireless Systems*. Springer, Feb. 2008.

[92] Sendonaris, A., Erkip, E., and Aazhang, B., "User cooperation diversity – Part I: System description," *IEEE Trans. on Commun.*, vol. 51, pp. 1927–1938, Nov. 2003.

[93] Shimizu, R., "On a lack of memory property of the exponential distribution," *Ann. Inst. Statist. Math.*, vol. 31, pp. 309–313, Dec. 1979.

[94] Shin, O.-S., Chan, A. M. andKung, H. T., and Tarokh, V., "Design of an OFDM cooperative space-time diversity system," *IEEE Trans. on Veh. Technol.*, vol. 56, pp. 2203–2215, July 2007.

[95] Stanojev, I., Simeone, O., Bar-Ness, Y., and You, C., "Performance of multi-relay collaborative hybrid-ARQ protocols over fading channels," *IEEE Commun. Lett.*, vol. 10, pp. 522–524, July 2006.

[96] Stuber, G. L., *Principles of Mobile Communication*. Kluwei Academic Publishers, 2nd ed., 2001.

[97] Stuber, G. L., Barry, J. R., McLaughlin, S. W., Li, Y., Ingram, M. A., and Pratt, T. G., "Broadband MIMO-OFDM wireless communications," *Proc. IEEE*, vol. 92, pp. 271–294, Feb. 2004.

[98] Tarighat, A., Bagheri, R., and Sayed, A. H., "Compensation schemes and performance analysis of IQ imbalances in OFDM receivers," *IEEE Trans. on Signal Process.*, vol. 53, pp. 3257–3268, Aug. 2005.

[99] Tarokh, V., Seshadri, N., and Calderbank, A. R., "Space-time codes for high data rate wireless communication: Performance criterion and code construction," *IEEE Trans. on Inf. Theory*, vol. 44, pp. 744–765, Mar. 1998.

[100] Tellado, J., *Multicarrier Modulation with Low PAR: Applications to DSL and Wireless*. Norwell, MA: Kluwer, Sept. 2000.

[101] Tellado, J., Hoo, L. M. C., and Cioffi, J. M., "Maximum-likelihood detection of nonlinearly distorted multicarrier symbols by iterative decoding," *IEEE Trans. on Commun.*, vol. 51, pp. 218–228, Feb. 2003.

[102] Tse, D. and Viswanath, P., *Fundamentals of Wireless Communications*. Cambridge, 2005.

[103] Tubbax, J., Come, B., Van der Perre, L., Donnay, S., Engels, M., Man, H. D., and Moonen, M., "Compensation of IQ imbalance and phase noise in OFDM systems," *IEEE Trans. on Wireless Commun.*, vol. 4, pp. 872–877, May 2005.

[104] Wang, A. Y. and Sodini, C. G., "On the energy efficiency of wireless transceivers," in *Proc. IEEE International Conference on Communications (ICC)*, vol. 8, pp. 3783–3788, June 2006.

[105] Wang, T., Cano, A., Giannakis, G. B., and Lenamen, J. N., "High-performance cooperative demodulation with decode-and-forward relays," *IEEE Trans. on Commun.*, vol. 55, pp. 1427–1438, July 2007.

[106] Wang, T., Wang, R., and Giannakis, G. B., "Smart regenerative relays for link-adaptive cooperative communications," *IEEE Trans. on Commun.*, vol. 56, pp. 1950–1960, Nov. 2008.

[107] Wang, Z. and Giannakis, G. B., "A simple and general parameterization quantifying performance in fading channels," *IEEE Trans. on Commun.*, vol. 51, pp. 1389–1398, Aug. 2003.

[108] Weinstein, S. B. and Ebert, P. M., "Data transmission by frequency-division multiplexing using the discrete Fourier transform," *IEEE Trans. on Commun.*, vol. 19, pp. 628–634, Feb. 1971.

[109] Woo, Y. Y., Kim, J., Yi, J., Hong, S., Kim, I., Moon, J., and Kim, B., "Adaptive digital feedback predistortion technique for linearizing power amplifiers," *IEEE Trans. on Microw. Theory Tech.*, vol. 55, pp. 932–940, May 2007.

[110] Zhao, C., Baxley, R. J., and Zhou, G. T., "Peak-to-average power ratio and power efficiency considerations in MIMO-OFDM systems," *IEEE Commun. Lett.*, vol. 12, pp. 268–270, Apr. 2008.

[111] Zimmerman, M. S. and Kirsch, A. L., "The AN/GSC-10 (KATHRYN) variable rate data modem for HF radio," *IEEE Trans. on Commun.*, vol. 15, pp. 197–203, Jan. 1967.

[112] Zimmermann, E., Herhold, P., and Fettweis, G., "On the performance of cooperative diversity protocols in practical wireless systems," in *Proc. IEEE Vehicular Technology Conference (VTC)*, vol. 4, (Orlando, FL), pp. 2212–2216, Oct. 2003.

[113] Zou, Q., Tarighat, A., and Sayed, A., "Joint compensation of IQ imbalance and phase noise in OFDM wireless systems," *IEEE Trans. on Commun.*, vol. 57, pp. 404–414, Feb. 2009.

VITA

Qijia Liu was born in Taiyuan, China on May 29, 1982. He received the Bachelor of Engineering and the Master of Science degrees in 2004 and 2007, respectively, both in Electrical Engineering from Tsinghua University, Beijing, China. Since January 2007, he has been with the School of Electrical and Computer Engineering, Georgia Institute of Technology, where he is working towards the Ph.D. degree in Electrical Engineering.

His general research interests are in the areas of signal processing and communications. His current research interests mainly include multicarrier communications, distributed signal processing, detection and estimation theories, and optimizations.